PHYSICAL REVIEW D **92,** 054034 (2015)

Bottomonium mesons and strategies for their observation

Stephen Godfrey* and Kenneth Moats

Ottawa-Carleton Institute for Physics, Department of Physics, Carleton University, Ottawa, Canada K1S 5B6

(Received 16 July 2015; published 28 September 2015)

The B-factories and Large Hadron Collider experiments have demonstrated the ability to observe and measure the properties of bottomonium mesons. In order to discover missing states it is useful to know their properties to develop a successful search strategy. To this end we calculate the masses and decay properties of excited bottomonium states. We use the relativized quark model to calculate the masses and wave functions and the $^3P_0$ quark-pair creation model to calculate decay widths to open bottom. We also summarize results for radiative transitions, annihilation decays, hadronic transitions and production cross sections which are used to develop strategies to find these states. We find that the $b\bar{b}$ system has a rich spectroscopy that we expect to be substantially extended by the LHC and e^+e^- experiments in the near future. Some of the most promising possibilities at the LHC are observing the $\chi_{b(1,2)}(3P)$, $\chi_{b(1,2)}(4P)$ and $\eta_b(3S)$ states in $\gamma\mu^+\mu^-$ final states that proceed via radiative transitions through $\Upsilon(nS)$ intermediate states and 1^3D_J and 2^3D_J into $\gamma\gamma\mu^+\mu^-$ final states proceeding via $1^3P_J \to 1^3S_1$ and $2^3P_J \to 2^3S_1$ intermediate states respectively. Some of the most interesting possibilities in e^+e^- collisions are studying the 1^3D_J states via 4γ cascades starting with the $\Upsilon(3S)$ and the 3^3P_J states in $\gamma\gamma\mu^+\mu^-$ final states starting with the $\Upsilon(4S)$ and proceeding via $\Upsilon(nS)$ intermediate states. Completing the bottomonium spectrum is an important validation of lattice QCD calculations and a test of our understanding of bottomonium states in the context of the quark model.

DOI: 10.1103/PhysRevD.92.054034 PACS numbers: 12.39.Pn, 13.25.-k, 13.25.Gv, 14.40.Pq

I. INTRODUCTION

The Large Hadron Collider experiments have demonstrated that they can discover some of the missing bottomonium states. In fact, the first new particle discovered at the LHC was a $3P$ bottomonium state [1,2]. The Belle II experiment at SuperKEKB will also offer the possibility of studying excited bottomonium states [3]. At the same time, lattice QCD calculations of bottomonium properties have advanced considerably in recent years [4–7] so it is important to expand our experimental knowledge of bottomonium states to test these calculations. With this motivation, we calculate properties of bottomonium mesons to suggest experimental strategies to observe missing states. The observation of these states is a crucial test of lattice QCD calculations and will also test the various models of hadron properties. Some recent reviews of bottomonium spectroscopy are Refs. [8–10].

We use the relativized quark model to calculate the masses and wave functions [11]. The mass predictions for this model are given in Sec. II. The wave functions are used to calculate radiative transitions between states, to calculate annihilation decays, and to estimate hadronic transitions as described in Secs. III–V respectively. The strong decay widths to open bottom are described in Sec. VI and are calculated using the $^3P_0$ model [12,13] with simple harmonic oscillator (SHO) wave functions with the oscillator parameters, β, found by fitting the SHO wave function rms radii to those of the corresponding relativized quark model wave functions. This approach has proven to be a useful phenomenological tool for calculating hadron properties which has helped us to understand the observed spectra [14–18]. Additional details of the $^3P_0$ model are given in the Appendix, primarily so that the various conventions are written down explicitly so that the interested reader is able to reproduce our results.

We combine our results for the various decay modes to produce branching ratios (BRs) for each of the bottomonium states we study. The purpose of this paper is to suggest strategies to find some of the missing bottomonium states in pp collisions at the LHC and in e^+e^- collisions at SuperKEKB. The final missing input is an estimate of production rates for bottomonium states in pp and e^+e^- collisions. This is described in Sec. VII. We combine the cross sections with the expected integrated luminosities and various BRs to estimate the number of events expected for the production of bottomonium states with decays to various final states. This is the main result of the paper, to identify which of the missing bottomonium states are most likely to be observed and the most promising signal to find them. However, there are many experimental issues that could alter our conclusions so we hope that the interested reader can use the information in this paper as a starting point to study other potentially useful experimental

*godfrey@physics.carleton.ca

signatures that we might have missed. In the final section we summarize the most promising signatures.

II. SPECTROSCOPY

We calculate the bottomonium mass spectrum using the relativized quark model [11]. This model assumes a relativistic kinetic energy term and the potential incorporates a Lorentz vector one-gluon-exchange interaction with a QCD motivated running coupling constant, $\alpha_s(r)$, and a Lorentz scalar linear confining interaction. The details of this model, including the parameters, can be found in Ref. [11] (see also Refs. [19–22]). This is typical of most such models which are based on some variant of the Coulomb plus linear potential expected from QCD and often include some relativistic effects. The relativized quark model has been reasonably successful in describing most known mesons and is a useful template against which to identify newly found states. However in recent years, starting with the discovery of the $D_{sJ}(2317)$ [23–25] and $X(3872)$ states [26], an increasing number of states have been observed that do not fit into this picture [27–30] pointing to the need to include physics which has hitherto been neglected such as coupled channel effects [31]. As a consequence of neglecting coupled channel effects and the crudeness of the relativization procedure we do not expect the mass predictions to be accurate to better than ~10–20 MeV.

The bottomonium mass predictions for this model are shown in Fig. 1. These are also listed in Tables I–II along with known experimental masses and the effective SHO wave function parameters, β. These, along with the masses and effective β's for the B meson states, listed in Table III, are used in the calculations of the open bottom strong decay widths as described in Sec. VI. We note that the 1^1P_1 and 1^3P_1 B meson states mix to form the physical $1P_1$ and $1P_1'$ states, as defined in Table III, with a singlet-triplet mixing angle of $\theta_{1P} = -30.3°$ for $b\bar{q}$ ordering.

If available, the experimental masses are used as input in our calculations rather than the predicted masses. When the mass of only one meson in a multiplet has been measured, we shift our input masses for the remaining states using the measured mass and the predicted splittings. Specifically, to obtain the $\eta_b(n^1S_0)$ masses (for $n = 3, 4, 5, 6$) we subtracted the predicted $n^3S_1 - n^1S_0$ splitting from the measured $\Upsilon(n^3S_1)$ mass [32]. For the $\chi_b(3P)$ states, we calculated the predicted mass differences with respect to the $\chi_{b1}(3^3P_1)$ state and subtracted them from the observed $\chi_{b1}(3^3P_1)$ mass recently measured by LHCb [33]. We used a similar procedure for the $\Upsilon(1D)$ mesons [32] as well as for the currently unobserved $1P$ B mesons [32] listed in Table III.

III. RADIATIVE TRANSITIONS

Radiative transitions of excited bottomonium states are of interest for a number of reasons. First, they probe the internal structure of the states and provide a strong test of the predictions of the various models. Moreover, for the purposes of this paper they provide a means of accessing $b\bar{b}$ states with different quantum numbers. Observation of the photons emitted in radiative transitions between different $b\bar{b}$ states was in fact how the $3P$ $b\bar{b}$ state was observed by the ATLAS Collaboration [1,2] and subsequently by LHCb

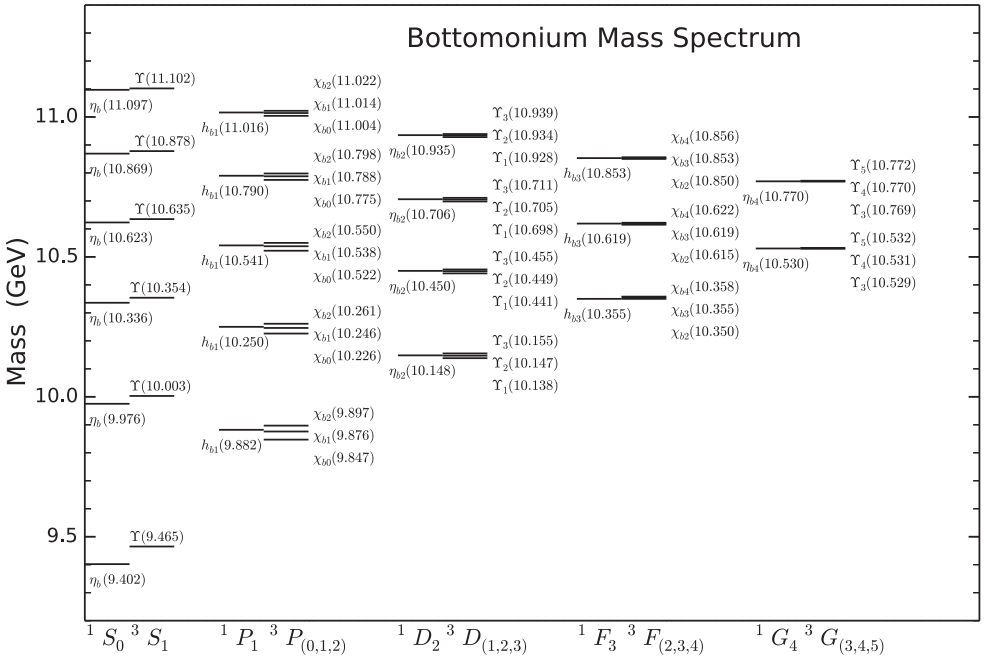

FIG. 1. The $b\bar{b}$ mass spectrum as predicted by the relativized quark model [11].

TABLE I. Masses and effective harmonic oscillator parameter values (β) for S-, P- and D-wave bottomonium mesons.

Meson	M_{theo} (MeV)	M_{exp} (MeV)	β (GeV)
$\Upsilon(1^3S_1)$	9465	9460.30 ± 0.26[a]	1.157
$\eta_b(1^1S_0)$	9402	9398.0 ± 3.2[a]	1.269
$\Upsilon(2^3S_1)$	10003	10023.26 ± 0.31[a]	0.819
$\eta_b(2^1S_0)$	9976	$9999.0 \pm 3.5^{+2.8}_{-1.9}$[a]	0.854
$\Upsilon(3^3S_1)$	10354	10355.2 ± 0.5[a]	0.698
$\eta_b(3^1S_0)$	10336	10337[b]	0.719
$\Upsilon(4^3S_1)$	10635	10579.4 ± 1.2[a]	0.638
$\eta_b(4^1S_0)$	10623	10567[b]	0.654
$\Upsilon(5^3S_1)$	10878	10876 ± 11[a]	0.600
$\eta_b(5^1S_0)$	10869	10867[b]	0.615
$\Upsilon(6^3S_1)$	11102	11019 ± 8[a]	0.578
$\eta_b(6^1S_0)$	11097	11014[b]	0.593
$\chi_{b2}(1^3P_2)$	9897	$9912.21 \pm 0.26 \pm 0.31$[a]	0.858
$\chi_{b1}(1^3P_1)$	9876	$9892.78 \pm 0.26 \pm 0.31$[a]	0.889
$\chi_{b0}(1^3P_0)$	9847	$9859.44 \pm 0.42 \pm 0.31$[a]	0.932
$h_b(1^1P_1)$	9882	9899.3 ± 1.0[a]	0.880
$\chi_{b2}(2^3P_2)$	10261	$10268.65 \pm 0.22 \pm 0.50$[a]	0.711
$\chi_{b1}(2^3P_1)$	10246	$10255.46 \pm 0.22 \pm 0.50$[a]	0.725
$\chi_{b0}(2^3P_0)$	10226	$10232.5 \pm 0.4 \pm 0.5$[a]	0.742
$h_b(2^1P_1)$	10250	$10259.8 \pm 0.5 \pm 1.1$[a]	0.721
$\chi_{b2}(3^3P_2)$	10550	10528[b]	0.640
$\chi_{b1}(3^3P_1)$	10538	$10515.7^{+2.2+1.5}_{-3.9-2.1}$[c]	0.649
$\chi_{b0}(3^3P_0)$	10522	10500[b]	0.660
$h_b(3^1P_1)$	10541	10519[b]	0.649
$\chi_{b2}(4^3P_2)$	10798	N/A	0.598
$\chi_{b1}(4^3P_1)$	10788	N/A	0.605
$\chi_{b0}(4^3P_0)$	10775	N/A	0.613
$h_b(4^1P_1)$	10790	N/A	0.603
$\chi_{b2}(5^3P_2)$	11022	N/A	0.570
$\chi_{b1}(5^3P_1)$	11014	N/A	0.576
$\chi_{b0}(5^3P_0)$	11004	N/A	0.585
$h_b(5^1P_1)$	11016	N/A	0.575
$\Upsilon_3(1^3D_3)$	10155	10172[b]	0.752
$\Upsilon_2(1^3D_2)$	10147	10163.7 ± 1.4[a]	0.763
$\Upsilon_1(1^3D_1)$	10138	10155[b]	0.776
$\eta_{b2}(1^1D_2)$	10148	10165[b]	0.761
$\Upsilon_3(2^3D_3)$	10455	N/A	0.660
$\Upsilon_2(2^3D_2)$	10449	N/A	0.666
$\Upsilon_1(2^3D_1)$	10441	N/A	0.672
$\eta_{b2}(2^1D_2)$	10450	N/A	0.665
$\Upsilon_3(3^3D_3)$	10711	N/A	0.609
$\Upsilon_2(3^3D_2)$	10705	N/A	0.613
$\Upsilon_1(3^3D_1)$	10698	N/A	0.618
$\eta_{b2}(3^1D_2)$	10706	N/A	0.612
$\Upsilon_3(4^3D_3)$	10939	N/A	0.577
$\Upsilon_2(4^3D_2)$	10934	N/A	0.580
$\Upsilon_1(4^3D_1)$	10928	N/A	0.583
$\eta_{b2}(4^1D_2)$	10935	N/A	0.579

[a]Measured mass from Particle Data Group [32].
[b]Using predicted multiplet mass splittings with measured mass as described in Sec. II.
[c]Measured mass from LHCb [33].

TABLE II. Masses and effective harmonic oscillator parameter values (β) for F- and G-wave bottomonium mesons.

Meson	M_{theo} (MeV)	M_{exp} (MeV)	β (GeV)
$\chi_{b4}(1^3F_4)$	10358	N/A	0.693
$\chi_{b3}(1^3F_3)$	10355	N/A	0.698
$\chi_{b2}(1^3F_2)$	10350	N/A	0.704
$h_{b3}(1^1F_3)$	10355	N/A	0.698
$\chi_{b4}(2^3F_4)$	10622	N/A	0.626
$\chi_{b3}(2^3F_3)$	10619	N/A	0.630
$\chi_{b2}(2^3F_2)$	10615	N/A	0.633
$h_{b3}(2^1F_3)$	10619	N/A	0.629
$\chi_{b4}(3^3F_4)$	10856	N/A	0.587
$\chi_{b3}(3^3F_3)$	10853	N/A	0.590
$\chi_{b2}(3^3F_2)$	10850	N/A	0.592
$h_{b3}(3^1F_3)$	10853	N/A	0.589
$\Upsilon_5(1^3G_5)$	10532	N/A	0.653
$\Upsilon_4(1^3G_4)$	10531	N/A	0.656
$\Upsilon_3(1^3G_3)$	10529	N/A	0.660
$\eta_{b4}(1^1G_4)$	10530	N/A	0.656
$\Upsilon_5(2^3G_5)$	10772	N/A	0.602
$\Upsilon_4(2^3G_4)$	10770	N/A	0.604
$\Upsilon_3(2^3G_3)$	10769	N/A	0.606
$\eta_{b4}(2^1G_4)$	10770	N/A	0.604

[33,34]. E1 radiative partial widths of bottomonium are typically $\mathcal{O}(1$–$10)$ keV so they can represent a significant BR for $b\bar{b}$ states that are relatively narrow. As we will see, a large number of $b\bar{b}$ states fall into this category. With the high statistics available at the LHC it should be possible to observe some of the missing $b\bar{b}$ states with a well-constrained search strategy. Likewise, SuperKEKB can provide large event samples of the $\Upsilon(3S)$ and $\Upsilon(4S)$ and possibly the $\Upsilon(5S)$ and $\Upsilon(6S)$ which could be used to identify radially excited P- and D-wave and other high L states. e^+e^- collisions at SuperKEKB could also produce the $\Upsilon(1^3D_1)$ and $\Upsilon(2^3D_1)$ directly which could be observed by Belle II in decay chains involving radiative transitions.

We calculate the E1 radiative partial widths using [35]

$$\Gamma(n^{2S+1}L_J \to n'^{2S+1}L'_{J'} + \gamma) = \frac{4\alpha e_b^2 k_\gamma^3}{3} C_{fi}\delta_{L,L'\pm1}|\langle\psi_f|r|\psi_i\rangle|^2 \quad (1)$$

where the angular momentum matrix element is given by

$$C_{fi} = \max(L,L')(2J'+1)\begin{Bmatrix} J & 1 & J' \\ L' & S & L \end{Bmatrix}, \quad (2)$$

and $\{\cdots\}$ is a 6-j symbol, $e_b = -1/3$ is the b-quark charge in units of $|e|$, α is the fine-structure constant, k_γ is the photon energy and $\langle\psi_f|r|\psi_i\rangle$ is the transition matrix

TABLE III. Masses and effective β values for B mesons used in the calculations of bottomonium strong decay widths. The physical $1P_1{}'$ and $1P_1$ states are mixtures of 1^1P_1 and 1^3P_1 with singlet-triplet mixing angle $\theta_{1P} = -30.3°$ for $b\bar{q}$ ordering. Where two values of β are listed, the first (second) value is for the singlet (triplet) state.

Meson	State	M_{theo} (MeV)	M_{exp} (MeV)	β (GeV)
$B^{\pm}$	1^1S_0	5312	5279.26 ± 0.17[a]	0.580
B^0	1^1S_0	5312	5279.58 ± 0.17[a]	0.580
B^*	1^3S_1	5371	5325.2 ± 0.4[a]	0.542
$B(1^3P_0)$	1^3P_0	5756	5702[b]	0.536
$B(1P_1)$	$\cos\theta_{1P}(1^1P_1) + \sin\theta_{1P}(1^3P_1)$	5777	5723.5 ± 2.0[a]	0.499, 0.511
$B(1P_1')$	$-\sin\theta_{1P}(1^1P_1) + \cos\theta_{1P}(1^3P_1)$	5784	5730[b]	0.499, 0.511
$B(1^3P_2)$	1^3P_2	5797	5743 ± 5[a]	0.472
B_s	1^1S_0	5394	5366.77 ± 0.24[a]	0.636
B_s^*	1^3S_1	5450	$5415.4^{+2.4}_{-2.1}$[a]	0.595

[a]Measured mass from Particle Data Group [32].
[b]Input mass from predicted mass splittings, as described in Sec. II.

element from the initial state ψ_i to the final state ψ_f. For these initial and final states, we use the relativized quark model wave functions [11]. The E1 radiative widths are given in Tables IV–XXIII along with the matrix elements so that the interested reader can reproduce our results. The initial and final state masses are also listed in these tables where Particle Data Group (PDG) [32] masses are used when the masses are known. For unobserved states the masses are taken from the predicted values in Tables I–II except when a member of a multiplet has been observed. In this latter case the mass used was obtained using the procedure described in Sec. II.

An interesting observation is that the E1 transitions $3S \to 1P$ are highly suppressed relative to other E1 transitions [37] (see Ref. [10] for a detailed discussion). Grant and Rosner [38] showed this to be a general property of E1 transitions, that E1 transitions between states that differ by two radial nodes are highly suppressed relative to the dominant E1 transitions and are in fact zero for the three-dimensional harmonic oscillator. As a consequence, these radiative transitions are particularly sensitive to relativistic corrections [10]. We found that this pattern was also apparent for similar transitions of the type $|n, l\rangle \to |n-2, l \pm 1\rangle$ such as $5S \to 3P$, $3P \to 1D$, $4P \to 2S$, $4D \to 2P$, $3D \to 1F$ etc.

M1 transition rates are typically weaker than E1 rates. Nevertheless they have been useful in observing spin-singlet states that are difficult to observe in other ways [39,40]. The M1 radiative partial widths are evaluated using [41]

$$\Gamma(n^{2S+1}L_J \to n'^{2S'+1}L_{J'} + \gamma) = \frac{4\alpha e_b^2 k_\gamma^3}{3m_b^2}\frac{2J'+1}{2L+1}\delta_{S,S'\pm 1}|\langle\psi_f|j_0(kr/2)|\psi_i\rangle|^2 \quad (3)$$

where $j_0(x)$ is the spherical Bessel function and the other factors have been defined above. As with the E1 transitions, we use the relativized quark model wave functions [11] for the initial and final states.

The partial widths and branching ratios for the M1 radiative transitions are listed in Tables IV–XXIII as appropriate. For comparison, other calculations of $b\bar{b}$ radiative transitions can be found in Refs. [35,42–46].

IV. ANNIHILATION DECAYS

Annihilation decays into gluons and light quarks make significant contributions to the total widths of some $b\bar{b}$ resonances. In addition, annihilation decays into leptons or photons can be useful for the production and identification of some bottomonium states. For example, the vector mesons are produced in e^+e^- collisions through their couplings to e^+e^-. Annihilation decay rates have been studied extensively using perturbative QCD (pQCD) methods [41,47–59]. The relevant formulas for S- and P-wave states including first-order QCD corrections (when they are known) are summarized in Ref. [53]. Expressions for D- and F-wave decays are given in Refs. [56,57] and Refs. [55,58] respectively. The expression for ${}^3D_1 \to e^+e^-$ including the QCD correction comes from Ref. [59]. Ackleh and Barnes [54] give a general expression for singlet decays to two gluons. A general property of annihilation decays is that the decay amplitude for a state with orbital angular momentum l goes like $R^{(l)}/m_Q^{2l+2}$ where $R^{(l)}$ is the lth derivative of the radial wave function. $R^{(l)}$ is typically $\mathcal{O}(1)$ so for bottom quark masses the magnitude of the annihilation decay widths decreases rapidly as the orbital angular momentum of the bottomonium state increases. Expressions for the decay widths including first-order QCD corrections when known are summarized in Table XXIV. To obtain our numerical results for these partial widths we take the number of light quarks to be $n_f = 4$; assumed $m_b = 4.977$ GeV, $\alpha_s \approx 0.18$ (with some weak mass dependence); and used the wave

TABLE IV. Partial widths and branching ratios for strong and electromagnetic decays and transitions for the $1S$ and $2S$ bottomonium states. The state's mass is given in GeV and is listed below the state's name in column 1. Column 4, labeled $\mathcal{M}$, gives the matrix element appropriate to the particular decay; for S-wave annihilation decays $\mathcal{M}$ designates $\Psi(0) = R(0)/\sqrt{4\pi}$ representing the wave function at the origin and for radiative transitions the E1 or M1 matrix elements are $\langle\psi_f|r|\psi_i\rangle$ (GeV^{-1}) and $\langle\psi_f|j_0(kr/2)|\psi_i\rangle$ respectively. Details of the calculations are given in the text.

				Predicted		Measured	
Initial state	Final state	M_f (GeV)	$\mathcal{M}$	Width (keV)	BR (%)	Width (keV)	BR (%)
$\Upsilon(1^3S_1)$ 9.460[a]	$\ell^+\ell^-$		0.793	1.44	2.71	1.34 ± 0.04	2.48 ± 0.05[a]
	ggg		0.793	47.6	89.6	44.1 ± 1.1	81.7 ± 0.7[a]
	γgg		0.793	1.2	2.3	1.2 ± 0.3	2.2 ± 0.6[a]
	$\gamma\gamma\gamma$		0.793	1.7×10^{-5}	3.2×10^{-5}		
	$\eta_b(1^1S_0)\gamma$	9.398[a]	0.9947	0.010	0.019		
	Total			53.1	100	54.02 ± 1.25[a]	
$\eta_b(1^1S_0)$ 9.398[a]	gg		1.081	16.6 MeV	~100		
	$\gamma\gamma$		1.081	0.94	0.0057		
	Total			16.6 MeV	100	$10.8^{+6.0}_{-4.2}$ MeV[a]	
$\Upsilon(2^3S_1)$ 10.023[a]	$\ell^+\ell^-$		0.597	0.73	1.8	0.62 ± 0.06	1.93 ± 0.17
	ggg		0.597	26.3	65.4	18.8 ± 1.6	58.8 ± 1.2
	γgg		0.597	0.68	1.7	2.81 ± 0.42	8.8 ± 1.1
	$\gamma\gamma\gamma$		0.597	9.8×10^{-6}	2.4×10^{-5}		
	$\chi_{b2}(1^3P_2)\gamma$	9.912[a]	−1.524	1.88	4.67	2.29 ± 0.22	7.15 ± 0.35[a]
	$\chi_{b1}(1^3P_1)\gamma$	9.893[a]	−1.440	1.63	4.05	2.21 ± 0.22	6.9 ± 0.4[a]
	$\chi_{b0}(1^3P_0)\gamma$	9.859[a]	−1.330	0.91	2.3	1.22 ± 0.16	3.8 ± 0.4[a]
	$\eta_b(2^1S_0)\gamma$	9.999[a]	0.9924	5.9×10^{-4}	1.5×10^{-3}		
	$\eta_b(1^1S_0)\gamma$	9.398[a]	0.0913	0.081	0.20	0.012 ± 0.004	$(3.9 \pm 1.5) \times 10^{-2}$[a]
	$\Upsilon(1^3S_1)\pi\pi$			8.46[a]	21.0	8.46 ± 0.71	26.45 ± 0.48[a]
	Total			40.2	100	31.98 ± 2.63	
$\eta_b(2^1S_0)$ 9.999[a]	gg		0.718	7.2 MeV	~100		
	$\gamma\gamma$		0.718	0.41	5.7×10^{-3}		
	$h_b(1^1P_1)\gamma$	9.899[a]	−1.526	2.48	0.034		
	$\Upsilon(1^3S_1)\gamma$	9.460	−0.0610	0.068	9.4×10^{-4}		
	$\eta_b(1^1S_0)\pi\pi$			12.4	0.17		
	Total			7.2 MeV	100	<24 MeV[a]	

[a]PDG Ref. [32].

functions found using the model of Ref. [11] as described in Sec. II.

Considerable uncertainties arise in these expressions from the model dependence of the wave functions and possible relativistic and QCD radiative corrections (see for example the discussion in Ref. [11]). One example is that the logarithm evident in some of these formulas is evaluated at a rather arbitrarily chosen scale, and that the pQCD radiative corrections to these processes are often found to be large, but are prescription dependent and so are numerically unreliable. As a consequence, these formulas should be regarded as estimates of the partial widths for these annihilation processes rather than precise predictions. The numerical results for partial widths for the annihilation processes are included in Tables IV–XXII.

V. HADRONIC TRANSITIONS

Hadronic transitions between quarkonium levels are needed to estimate branching ratios and potentially offer useful signatures for some missing bottomonium states. There have been numerous theoretical estimates of hadronic transitions over the years [60–73]. In some cases the estimates disagree by orders of magnitude [64]. Hadronic transitions are typically described as a two-step process in which the gluons are first emitted from the heavy quarks and then recombine into light quarks. A multipole expansion of the color gauge field is employed to describe the emission process where the intermediate color octet quarkonium state is typically modeled by some sort of quarkonium hybrid wave function [61,73]. An uncertainty in predictions arises from how the rehadronization step is estimated. To some extent this latter uncertainty can be reduced by employing the multipole expansion of the color gauge fields developed by Yan and collaborators [60–63] together with the Wigner-Eckart theorem to estimate the E1-E1 transition rates [60].

In addition to E1-E1 transitions such as $^3S_1 \to {}^3S_1\pi\pi$, there will be other transitions such as $^3S_1 \to {}^3S_1 + \eta$, which

TABLE V. Partial widths and branching ratios for strong and electromagnetic decays and transitions for the $3S$ states. See the caption to Table IV for further details.

				Predicted		Measured	
Initial state	Final state	M_f (GeV)	$\mathcal{M}$	Width (keV)	BR (%)	Width (keV)	BR (%)
$\Upsilon(3^3S_1)$	$\ell^+\ell^-$		0.523	0.53	1.8	0.44 ± 0.06	2.18 ± 0.21
10.355[a]	ggg		0.523	19.8	67.9	7.25 ± 0.84	35.7 ± 2.6
	γgg		0.523	0.52	1.8	0.20 ± 0.04	0.97 ± 0.18
	$\gamma\gamma\gamma$		0.523	7.6×10^{-6}	2.6×10^{-5}		
	$\chi_{b2}(2^3P_2)\gamma$	10.269[a]	−2.446	2.30	7.90	2.66 ± 0.40	13.1 ± 1.6[a]
	$\chi_{b1}(2^3P_1)\gamma$	10.255[a]	−2.326	1.91	6.56	2.56 ± 0.34	12.6 ± 1.2[a]
	$\chi_{b0}(2^3P_0)\gamma$	10.232[a]	−2.169	1.03	3.54	1.20 ± 0.16	5.9 ± 0.6[a]
	$\chi_{b2}(1^3P_2)\gamma$	9.912[a]	0.096	0.45	1.5	0.20 ± 0.03	0.99 ± 0.13[a]
	$\chi_{b1}(1^3P_1)\gamma$	9.893[a]	0.039	0.05	0.2	0.018 ± 0.010	0.09 ± 0.05[a]
	$\chi_{b0}(1^3P_0)\gamma$	9.859[a]	−0.028	0.01	0.03	0.055 ± 0.010	0.27 ± 0.04[a]
	$\eta_b(3^1S_0)\gamma$	10.337[a]	0.9920	2.5×10^{-4}	8.6×10^{-4}		
	$\eta_b(2^1S_0)\gamma$	9.999[a]	0.1003	0.19	0.65	<0.12	<0.062 at 90% C.L.[a]
	$\eta_b(1^1S_0)\gamma$	9.398[a]	0.0427	0.060	0.20	0.01 ± 0.002	0.051 ± 0.007[a]
	$\Upsilon(1^3S_1)\pi\pi$			1.34[a]	4.60	1.335 ± 0.125	6.57 ± 0.15[a]
	$\Upsilon(2^3S_1)\pi\pi$			0.95[a]	3.3	0.949 ± 0.098	4.67 ± 0.23[a]
	Total			29.1	100	20.32 ± 1.85	
$\eta_b(3^1S_0)$	gg		0.601	4.9 MeV	∼100		
10.337[b]	$\gamma\gamma$		0.601	0.29	5.9×10^{-3}		
	$h_b(2^1P_1)\gamma$	10.260[a]	−2.461	2.96	0.060		
	$h_b(1^1P_1)\gamma$	9.899[a]	0.1235	1.3	0.026		
	$\Upsilon(2^3S_1)\gamma$	10.023[a]	−0.0484	9.1×10^{-3}	1.8×10^{-4}		
	$\Upsilon(1^3S_1)\gamma$	9.460[a]	−0.031	0.074	1.5×10^{-3}		
	$\eta_b(1^1S_0)\pi\pi$			1.70 ± 0.12	3.5×10^{-2}		
	$\eta_b(2^1S_0)\pi\pi$			1.16 ± 0.10	2.4×10^{-2}		
	Total			4.9 MeV	100		

[a]PDG Ref. [32].
[b]Using predicted $3^3S_1 - 3^1S_0$ splitting and measured 3^3S_1 mass.

goes via M1-M1 and E1-M2 multipoles and spin-flip transitions such as ${}^3S_1 \to {}^1P_1\pi\pi$, which goes via E1-M1 [61]. These transitions are suppressed by inverse powers of the quark masses and are expected to be small compared to the E1-E1 and electromagnetic transitions. As a consequence, we will neglect them in our estimates of branching ratios. We note, however, that in certain situations they have provided a pathway to otherwise difficult-to-observe states such as the h_c and h_b [74,75] and have played an important role in these states' discoveries [76,77]. Another example of a higher multipole transition is $\chi_{b1,b2}(2P) \to \omega\Upsilon(1S)$ [78] which proceeds via three E1 gluons although it turns out that this particular example has a larger branching ratio than the $2P \to 1P + \pi\pi$ transition [32].

The differential rate for E1-E1 transitions from an initial quarkonium state Φ' to the final quarkonium state Φ, and a system of light hadrons, h, is given by the expression [60,61]

$$\frac{d\Gamma}{d\mathcal{M}^2}[\Phi' \to \Phi + h] = (2J+1)\sum_{k=0}^{2} \begin{Bmatrix} k & \ell' & \ell \\ s & J & J' \end{Bmatrix}^2 A_k(\ell', \ell) \quad (4)$$

where ℓ', ℓ are the orbital angular momentum and J', J are the total angular momentum of the initial and final states respectively; s is the spin of the $Q\bar{Q}$ pair; $\mathcal{M}^2$ is the invariant mass squared of the light hadron system; and $A_k(\ell', \ell)$ are the reduced matrix elements. For the convenience of the reader we give the expressions for the transition rates in terms of the reduced matrix elements in Table XXV. The magnitudes of the $A_k(\ell', \ell)$ are model dependent with a large variation in their estimates. The $A_k(\ell', \ell)$ are a product of a phase space factor, overlap integrals with the intermediate hybrid wave function and a fitted constant. There is a large variation in the predicted reduced rates. For example, for the transition $1^3D_1 \to 1^3S_1 + \pi\pi$, estimates for $A_2(2, 0)$ differ by almost 3 orders of magnitude [61,64,71,72]. In an attempt to minimize the theoretical uncertainty we estimate the reduced matrix elements by rescaling measured transition rates by phase space factors and interquark separation expectation values. While imperfect, we hope that this approach captures the essential features of the reduced matrix elements and gives a reasonable order of magnitude estimate of the partial widths. In the soft-pion limit the A_1 contributions are suppressed so, as is the usual practice, we

TABLE VI. Partial widths and branching ratios for strong and electromagnetic decays and transitions and OZI allowed strong decays for the $4S$ and $5S$ bottomonium states. Details of the OZI allowed decay amplitudes are described in the Appendix. See the caption to Table IV for further details.

				Predicted		Measured	
Initial state	Final state	M_f (GeV)	$\mathcal{M}$	Width (keV)	BR (%)	Width (keV)	BR (%)
$\Upsilon(4^3S_1)$ 10.579[a]	$\ell^+\ell^-$		0.459	0.39	1.8×10^{-3}	0.32 ± 0.04[a]	$(1.57\pm0.08)\times10^{-3}$[a]
	ggg		0.459	15.1	0.0686		
	γgg		0.459	0.40	1.8×10^{-3}		
	$\gamma\gamma\gamma$		0.459	6.0×10^{-6}	2.7×10^{-8}		
	$\chi_{b2}(3^3P_2)\gamma$	10.528[d]	−3.223	0.82	3.7×10^{-3}		
	$\chi_{b1}(3^3P_1)\gamma$	10.516[d]	−3.072	0.84	3.8×10^{-3}		
	$\chi_{b0}(3^3P_0)\gamma$	10.500[d]	−2.869	0.48	2.2×10^{-3}		
	$\Upsilon(1^3S_1)\pi^+\pi^-$			1.66[b]	7.54×10^{-3}	1.66 ± 0.24[b]	$(8.1\pm0.6)\times10^{-3}$[a]
	$\Upsilon(2^3S_1)\pi^+\pi^-$			1.76[b]	8.00×10^{-3}	1.76 ± 0.34[b]	$(8.6\pm1.3)\times10^{-3}$[a]
	BB			22.0 MeV	∼100		>96 at 95% C.L.[a]
	Total			22.0 MeV	100	20.5 ± 2.5 MeV[a]	
$\eta_b(4^1S_0)$ 10.567[c]	gg		0.500	3.4 MeV	∼100		
	$\gamma\gamma$		0.500	0.20	5.9×10^{-3}		
	$h_b(3^1P_1)\gamma$	10.519[d]	−3.238	1.24	3.6×10^{-2}		
	$\eta_b(1^1S_0)\pi^+\pi^-$			2.03 ± 0.29	6.0×10^{-2}		
	$\eta_b(2^1S_0)\pi^+\pi^-$			1.90 ± 0.36	5.6×10^{-2}		
	Total			3.4 MeV	100		
$\Upsilon(5^3S_1)$ 10.876[a]	$\ell^+\ell^-$		0.432	0.33	1.2×10^{-3}	0.31 ± 0.23[a]	$(5.6\pm3.1)\times10^{-4}$[a]
	ggg		0.432	13.1	4.78×10^{-2}		
	$\chi_{b2}(4^3P_2)\gamma$	10.798	−3.908	4.3	1.6×10^{-2}		
	$\chi_{b1}(4^3P_1)\gamma$	10.788	−3.724	3.4	1.2×10^{-2}		
	$\chi_{b0}(4^3P_0)\gamma$	10.775	−3.483	1.5	5.5×10^{-3}		
	$\chi_{b2}(3^3P_2)\gamma$	10.528[d]	0.131	0.42	1.5×10^{-3}		
	$\chi_{b1}(3^3P_1)\gamma$	10.516[d]	0.0020	6.2×10^{-5}	2.3×10^{-7}		
	$\chi_{b0}(3^3P_0)\gamma$	10.500[d]	−0.156	0.15	5.5×10^{-4}		
	BB			5.35 MeV	19.5	3.0 ± 1.6 MeV[b]	5.5 ± 1.0[a]
	BB^*			16.6 MeV	60.6	7.5 ± 3.9 MeV[b]	13.7 ± 1.6[a]
	B^*B^*			2.42 MeV	8.83	21 ± 11 MeV[b]	38.1 ± 3.4[a]
	B_sB_s			0.157 MeV	0.573	0.3 ± 0.3 MeV[b]	0.5 ± 0.5[a]
	$B_sB_s^*$			0.833 MeV	3.04	0.74 ± 0.42 MeV[b]	1.35 ± 0.32[a]
	$B_s^*B_s^*$			2.00 MeV	7.30	9.7 ± 5.1 MeV[b]	17.6 ± 2.7[a]
	Total			27.4 MeV	100	55 ± 28 MeV[a]	
$\eta_b(5^1S_0)$ 10.867[c]	gg		0.464	2.9 MeV	13		
	$\gamma\gamma$		0.464	0.17	7.4×10^{-4}		
	$h_b(4^1P_1)\gamma$	10.790	3.925	7.5	3.3×10^{-2}		
	$h_b(3^1P_1)\gamma$	10.519[d]	0.162	1.1	4.8×10^{-3}		
	BB^*			13.1 MeV	57.0		
	B^*B^*			0.914 MeV	3.97		
	$B_sB_s^*$			0.559 MeV	2.43		
	$B_s^*B_s^*$			5.49 MeV	23.9		
	Total			23.0 MeV	100		

[a]From PDG Ref. [32].
[b]Found by combining the PDG BR with the PDG total widths for the $\Upsilon(4^3S_1)$ or $\Upsilon(5^3S_1)$ [32] as appropriate.
[c]Using predicted $n^3S_1-n^1S_0$ splitting and measured n^3S_1 mass.
[d]3^3P_1 from LHCb [33] and 3^3P_2, 3^3P_0 and 3^1P_1 using predicted splittings with 3^3P_1 measured mass.

will take $A_1(\ell',\ell)=0$ [60] (see also Ref. [79]) so that in practice only $A_0(\ell',\ell)$ and/or $A_2(\ell',\ell)$ will contribute to a given transition. The A_0 and A_2 amplitudes have phase space integrals of the form [61]

$$G=\frac{3}{4}\frac{M_f}{M_i}\pi^3\int dM^2_{\pi\pi}K\left(1-\frac{4m_\pi^2}{M^2_{\pi\pi}}\right)^{1/2}(M^2_{\pi\pi}-2m_\pi^2)^2 \quad (5)$$

and

TABLE VII. Partial widths and branching ratios for strong and electromagnetic decays and transitions and OZI allowed strong decays for the $6S$ states. Details of the OZI allowed decay amplitudes are described in the Appendix. See the caption to Table IV for further details.

				Predicted		Measured	
Initial state	Final state	M_f	$\mathcal{M}$	Width (keV)	BR (%)	Width (keV)	BR (%)
$\Upsilon(6^3S_1)$	$\ell^+\ell^-$		0.396	0.27	8.0×10^{-4}	0.13 ± 0.05[a]	$(1.6 \pm 0.5) \times 10^{-4}$[a]
11.019[a]	ggg		0.396	11.0	0.0324		
	$\chi_{b2}(5^3P_2)\gamma$	11.022		Below threshold			
	$\chi_{b1}(5^3P_1)\gamma$	11.014	−4.282	8.3×10^{-4}	2.4×10^{-6}		
	$\chi_{b0}(5^3P_0)\gamma$	11.004	−3.992	6.4×10^{-3}	1.9×10^{-5}		
	$\chi_{b2}(4^3P_2)\gamma$	10.798	0.116	8.5×10^{-2}	2.5×10^{-4}		
	$\chi_{b1}(4^3P_1)\gamma$	10.788	−0.054	0.012	3.5×10^{-5}		
	$\chi_{b0}(4^3P_0)\gamma$	10.775	−0.244	0.1	3×10^{-4}		
	$\chi_{b2}(3^3P_2)\gamma$	10.528[c]	0.089	0.53	1.6×10^{-3}		
	$\chi_{b1}(3^3P_1)\gamma$	10.516[c]	0.100	0.43	1.3×10^{-3}		
	$\chi_{b0}(3^3P_0)\gamma$	10.500[c]	0.115	0.21	6.2×10^{-4}		
	BB			1.32 MeV	3.89		
	BB^*			7.59 MeV	22.4		
	$BB(1P_1)$			7.81 MeV	23.0		
	$BB(1P_1')$			10.8 MeV	31.8		
	B^*B^*			5.89 MeV	17.4		
	B_sB_s			1.31	3.86×10^{-3}		
	$B_sB_s^*$			0.136 MeV	0.401		
	$B_s^*B_s^*$			0.310 MeV	0.914		
	Total			33.9 MeV	100	79 ± 16 MeV[a]	
$\eta_b(6^1S_0)$	gg		0.410	2.2 MeV	16		
11.014[b]	$\gamma\gamma$		0.410	0.14	1.0×10^{-3}		
	$h_b(5^1P_1)\gamma$	11.016		Below threshold			
	$h_b(4^1P_1)\gamma$	10.790	0.136	0.22	1.6×10^{-3}		
	$h_b(3^1P_1)\gamma$	10.519[c]	0.123	1.8	1.3×10^{-2}		
	BB^*			8.98 MeV	66.0		
	$BB(1^3P_0)$			0.745 MeV	5.48		
	B^*B^*			1.14 MeV	8.38		
	$B_sB_s^*$			0.420 MeV	3.09		
	$B_s^*B_s^*$			0.156 MeV	1.15		
	Total			13.6 MeV	100		

[a]From PDG Ref. [32].
[b]Using predicted $n^3S_1 - n^1S_0$ splitting and measured n^3S_1 mass.
[c]3^3P_1 from LHCb [33] and 3^3P_2, 3^3P_0 and 3^1P_1 using predicted splittings with 3^3P_1 measured mass.

$$H = \frac{1}{20}\frac{M_f}{M_i}\pi^3 \int dM_{\pi\pi}^2 K \left(1 - \frac{4m_\pi^2}{M_{\pi\pi}^2}\right)^{1/2} \times \left[(M_{\pi\pi}^2 - 4m_\pi^2)^2\left(1 + \frac{2}{3}\frac{K^2}{M_{\pi\pi}^2}\right) + \frac{K^2}{15M_{\pi\pi}^4}(M_{\pi\pi}^4 + 2m_\pi^2 M_{\pi\pi}^2 + 6m_\pi^4)\right] \quad (6)$$

respectively where

$$K = \frac{1}{2M_i}[(M_i + M_f)^2 - M_{\pi\pi}^2]^{1/2}[(M_i - M_f)^2 - M_{\pi\pi}^2]^{1/2}. \quad (7)$$

The amplitudes for E1-E1 transitions depend quadratically on the interquark separation so the scaling law between decay rates for two $b\bar{b}$ states is given by [60]

$$\frac{\Gamma(\Phi_1)}{\Gamma(\Phi_2)} = \frac{\langle r^2(\Phi_1)\rangle^2}{\langle r^2(\Phi_2)\rangle^2}. \quad (8)$$

Because each set of transitions uses different experimental input we will give details of how we rescale the $A_k(\ell', \ell)$ sector by sector in the following subsections and give the predicted partial widths in the summary tables.

A. $n'^1S_0 \to n^1S_0 + \pi\pi$

The $n'^1S_0 \to n^1S_0 + \pi\pi$ partial widths are found by rescaling the measured $n'^3S_1 \to n^3S_1 + \pi\pi$ partial

TABLE VIII. Partial widths and branching ratios for strong and electromagnetic decays and transitions for the $1P$ states. For P-wave annihilation decays $\mathcal{M}$ designates $R'(0)$, the first derivative of the radial wave function at the origin. See the caption to Table IV for further details.

Initial state	Final state	M_f (GeV)	$\mathcal{M}$	Predicted Width (keV)	Predicted BR (%)	Measured BR (%)
$\chi_{b2}(1^3P_2)$ 9.912[a]	gg		1.318	147	81.7	
	$\gamma\gamma$		1.318	9.3×10^{-3}	5.2×10^{-3}	
	$\Upsilon(1^3S_1)\gamma$	9.460	1.028	32.8	18.2	19.1 ± 1.2[a]
	$h_b(1^1P_1)\gamma$	9.899	1.000	9.6×10^{-5}	5.3×10^{-5}	
	Total			180	100	
$\chi_{b1}(1^3P_1)$ 9.893[a]	$q\bar{q}+g$		1.700	67	70	
	$\Upsilon(1^3S_1)\gamma$	9.460	1.040	29.5	31	33.9 ± 2.2[a]
	Total			96	100	
$\chi_{b0}(1^3P_0)$ 9.859[a]	gg		2.255	2.6 MeV	~100	
	$\gamma\gamma$		2.255	0.15	5.8×10^{-3}	
	$\Upsilon(1^3S_1)\gamma$	9.460	1.050	23.8	0.92	1.76 ± 0.35[a]
	Total			2.6 MeV	100	
$h_b(1^1P_1)$ 9.899[a]	ggg		1.583	37	51	
	$\eta_b(1^1S_0)\gamma$	9.398	0.922	35.7	49	49^{+8}_{-7}[a]
	$\chi_{b1}(1^3P_1)\gamma$	9.893	1.000	1.0×10^{-5}	1.4×10^{-5}	
	$\chi_{b0}(1^3P_0)\gamma$	9.859	0.998	8.9×10^{-4}	1.2×10^{-5}	
	Total			73	100	

[a]From PDG Ref. [32].

widths [32]. The $n'S \to nS + \pi\pi$ transitions are described by $A_0(0,0)$ amplitudes so that $\Gamma(n'^1S_0 \to n^1S_0 + \pi\pi)$ are given by

$$\Gamma(n'^1S_0) = \frac{\langle r^2(n'^1S_0)\rangle^2}{\langle r^2(n'^3S_1)\rangle^2} \times \frac{G(n'^1S_0 \to n^1S_0\pi\pi)}{G(n'^3S_1 \to n^3S_1\pi\pi)} \times \Gamma(n'^3S_1). \quad (9)$$

The hadronic transition partial widths for the n'^1S_0 states are given in Tables IV–VI for $n' = 2, 3, 4$.

We do not make predictions for the $\eta_b(5S)$ state as the measured hadronic transition rates for the $\Upsilon(5S)$ are anomalously large and inconsistent with other transitions between S-waves [80]. This has resulted in speculation that the $\Upsilon(5S)$ is mixed with a hybrid state leading to its anomalously large hadronic transition rates [81], contains a sizable tetraquark component [82,83] or is the consequence of $B^{(*)}\bar{B}^{(*)}$ rescattering [84]. See also Refs. [3,9]. It could also be the result of a large overlap with the intermediate states. This subject needs a separate more detailed study which lies outside the present work. We also do not include hadronic transitions for the $6S$ states as there are no measurements of hadronic transitions originating from the 6^3S_1 state and in any case, the total widths for the $6S$ states are quite large so that the BRs for hadronic transitions would be rather small.

B. $n'P_J \to nP_J + \pi\pi$

All $n'P_J \to nP_J + \pi\pi$ transitions can be expressed in terms of $A_0(1,1)$ and $A_2(1,1)$ where we have taken $A_1(1,1) = 0$. The expressions relating the various partial widths in terms of these reduced amplitudes are summarized in Table XXV. We can obtain $A_0(1,1)$ and $A_2(1,1)$ from the measured values for $\Gamma(2^3P_2 \to 1^3P_2 + \pi\pi)$ and $\Gamma(2^3P_1 \to 1^3P_1 + \pi\pi)$. These partial widths were obtained by first finding the total widths for the $\chi_{b2}(2P)$ and $\chi_{b1}(2P)$ using the measured BRs from the PDG [32] with our predicted partial widths for E1 transitions for $\chi_{b2(1)}(2P) \to \gamma\Upsilon(2S)$ and $\chi_{b2(1)}(2P) \to \gamma\Upsilon(1S)$. We obtain $\Gamma(\chi_{b2}) = 122 \pm 11$ keV and $\Gamma(\chi_{b1}) = 62.6 \pm 4.0$ keV. Combining with the measured hadronic BRs we find $\Gamma(2^3P_2 \to 1^3P_2 + \pi\pi) = 0.62 \pm 0.12$ keV and $\Gamma(2^3P_1 \to 1^3P_1 + \pi\pi) = 0.57 \pm 0.09$ keV leading to $A_2(1,1) = 1.5$ keV and $A_0(1,1) = 1.335$ keV. We neglected the small differences in phase space between the χ_{b1} and χ_{b2} transitions and remind the reader that model dependence has been introduced into these results by using model predictions for the radiative transition partial widths. For example, using the E1 partial width predictions from Kwong and Rosner [35] results in slightly different total widths and hadronic transition partial widths. Using these values for A_0 and A_2 with Eq. (4) we obtain the hadronic transition partial widths for $2P \to 1P$ transitions given in Table IX. A note of caution is that A_0 and A_2 are sensitive to small variations in the input values of the partial widths so

TABLE IX. Partial widths and branching ratios for strong and electromagnetic decays and transitions for the $2P$ states. For P-wave annihilation decays $\mathcal{M}$ designates $R'(0)$, the first derivative of the radial wave function at the origin. See the caption to Table IV for further details.

Initial state	Final state	M_f (GeV)	$\mathcal{M}$	Predicted Width (keV)	Predicted BR (%)	Measured BR (%)
$\chi_{b2}(2^3P_2)$ 10.269[a]	gg		1.528	207	89.0	
	$\gamma\gamma$		1.528	1.2×10^{-2}	5.2×10^{-3}	
	$\Upsilon(2^3S_1)\gamma$	10.023	1.667	14.3	6.15	10.6 ± 2.6[a]
	$\Upsilon(1^3S_1)\gamma$	9.460	0.224	8.4	3.6	7.0 ± 0.7[a]
	$\Upsilon_3(1^3D_3)\gamma$	10.172	−1.684	1.5	0.65	
	$\Upsilon_2(1^3D_2)\gamma$	10.164	−1.625	0.3	0.1	
	$\Upsilon_1(1^3D_1)\gamma$	10.154	−1.561	0.03	0.01	
	$h_b(2^1P_1)\gamma$	10.260	1.000	2.8×10^{-5}	1.2×10^{-5}	
	$h_b(1^1P_1)\gamma$	9.899	−0.011	2.4×10^{-4}	1.0×10^{-4}	
	$\chi_{b2}(1^3P_2)\pi\pi$			0.62 ± 0.12[b]	0.27	0.51 ± 0.09[a]
	$\chi_{b1}(1^3P_1)\pi\pi$			0.23	0.10	
	$\chi_{b0}(1^3P_0)\pi\pi$			0.10	0.043	
	Total			232.5	100	
$\chi_{b1}(2^3P_1)$ 10.255[a]	$q\bar{q}+g$		1.857	96	82	
	$\Upsilon(2^3S_1)\gamma$	10.023	1.749	13.3	11.3	19.9 ± 1.9[a]
	$\Upsilon(1^3S_1)\gamma$	9.460	0.184	5.5	4.7	9.2 ± 0.8[a]
	$\Upsilon_2(1^3D_2)\gamma$	10.164	−1.701	1.2	1.0	
	$\Upsilon_1(1^3D_1)\gamma$	10.154	−1.639	0.5	0.4	
	$h_b(1^1P_1)\gamma$	9.899	−0.035	2.2×10^{-3}	1.9×10^{-3}	
	$\chi_{b2}(1^3P_2)\pi\pi$			0.38	0.32	
	$\chi_{b1}(1^3P_1)\pi\pi$			0.57 ± 0.09[b]	0.48	0.91 ± 0.13[a]
	$\chi_{b0}(1^3P_0)\pi\pi$			∼0	∼0	
	Total			117	100	
$\chi_{b0}(2^3P_0)$ 10.232[a]	gg		2.290	2.6 MeV	∼100	
	$\gamma\gamma$		2.290	0.15	5.7×10^{-3}	
	$\Upsilon(2^3S_1)\gamma$	10.023	1.842	10.9	0.42	4.6 ± 2.1[a]
	$\Upsilon(1^3S_1)\gamma$	9.460	0.130	2.5	9.6×10^{-2}	0.9 ± 0.6[a]
	$\Upsilon_1(1^3D_1)\gamma$	10.154	−1.731	1.0	3.8×10^{-2}	
	$h_b(1^1P_1)\gamma$	9.899	−0.079	9.7×10^{-3}	3.7×10^{-4}	
	$\chi_{b2}(1^3P_2)\pi\pi$			0.5	2×10^{-2}	
	$\chi_{b1}(1^3P_1)\pi\pi$			∼0	∼0	
	$\chi_{b0}(1^3P_0)\pi\pi$			0.44	1.7×10^{-2}	
	Total			2.6 MeV	100	
$h_b(2^1P_1)$ 10.260[a]	ggg		1.758	54	64	
	$\eta_b(2^1S_0)\gamma$	9.999	1.510	14.1	17	48 ± 13[a]
	$\eta_b(1^1S_0)\gamma$	9.398	0.252	13.0	15	22 ± 5[a]
	$\eta_{b2}(1^1D_2)\gamma$	10.165	−1.689	1.7	2.0	
	$\chi_{b2}(1^3P_2)\gamma$	9.912	−0.027	2.2×10^{-3}	2.6×10^{-3}	
	$\chi_{b1}(1^3P_1)\gamma$	9.893	−0.023	1.1×10^{-3}	1.3×10^{-3}	
	$\chi_{b0}(1^3P_0)\gamma$	9.859	0.019	3.2×10^{-4}	3.8×10^{-4}	
	$h_b(1^1P_1)\pi\pi$			0.94	1.1	
	Total			84	100	

[a]From PDG Ref. [32].
[b]Input, see text.

given the experimental errors on the input values, the predictions should only be regarded as rough estimates.

There are no measured BRs for $3P$ hadronic transitions that can be used as input for other $3P$ transitions. Furthermore, as pointed out by Kuang and Yan [61], hadronic transitions are dependent on intermediate states with complicated cancellations contributing to the amplitudes so that predictions are rather model dependent. To try to take into account the structure dependence of the amplitudes we make the assumption that once phase space

TABLE X. Partial widths and branching ratios for strong and electromagnetic decays and transitions for the $3P$ states. For P-wave annihilation decays $\mathcal{M}$ designates $R'(0)$, the first derivative of the radial wave function at the origin. See the caption to Table IV for further details.

Initial state	Final state	M_f (GeV)	$\mathcal{M}$	Width (keV)	BR (%)
$\chi_{b2}(3^3P_2)$ 10.528[b]	gg		1.584	227	91.9
	$\gamma\gamma$		1.584	1.3×10^{-2}	5.3×10^{-3}
	$\Upsilon(3^3S_1)\gamma$	10.355	2.255	9.3	3.8
	$\Upsilon(2^3S_1)\gamma$	10.023	0.323	4.5	1.8
	$\Upsilon(1^3S_1)\gamma$	9.460	0.086	2.8	1.1
	$\Upsilon_3(2^3D_3)\gamma$	10.455	−2.568	1.5	0.61
	$\Upsilon_2(2^3D_2)\gamma$	10.449	−2.482	0.32	0.13
	$\Upsilon_1(2^3D_1)\gamma$	10.441	−2.389	0.027	0.011
	$\Upsilon_3(1^3D_3)\gamma$	10.172	0.042	0.046	0.019
	$\chi_{b2}(1^3P_2)\pi\pi$			0.68	0.28
	$\chi_{b1}(1^3P_1)\pi\pi$			0.52	0.21
	$\chi_{b0}(1^3P_0)\pi\pi$			0.24	0.10
	Total			247	100
$\chi_{b1}(3^3P_1)$ 10.516[a]	$q\bar{q}+g$		1.814	101	86.3
	$\Upsilon(3^3S_1)\gamma$	10.355	2.388	8.4	7.2
	$\Upsilon(2^3S_1)\gamma$	10.023	0.278	3.1	2.6
	$\Upsilon(1^3S_1)\gamma$	9.460	0.061	1.3	1.1
	$\Upsilon_2(2^3D_2)\gamma$	10.449	−2.595	1.1	0.94
	$\Upsilon_1(2^3D_1)\gamma$	10.441	−2.506	0.47	0.40
	$\Upsilon_2(1^3D_2)\gamma$	10.164	0.060	0.080	0.068
	$\Upsilon_1(1^3D_1)\gamma$	10.154	0.029	7.0×10^{-3}	6.0×10^{-3}
	$\chi_{b2}(1^3P_2)\pi\pi$			0.88	0.75
	$\chi_{b1}(1^3P_1)\pi\pi$			0.56	0.48
	$\chi_{b0}(1^3P_0)\pi\pi$			∼0	∼0
	Total			117	100
$\chi_{b0}(3^3P_0)$ 10.500[b]	gg		2.104	2.2 MeV	∼100
	$\gamma\gamma$		2.104	0.13	5.9×10^{-3}
	$\Upsilon(3^3S_1)\gamma$	10.355	2.537	6.9	0.31
	$\Upsilon(2^3S_1)\gamma$	10.023	0.213	1.7	0.077
	$\Upsilon(1^3S_1)\gamma$	9.460	0.029	0.3	0.01
	$\Upsilon_1(2^3D_1)\gamma$	10.441	−2.637	1.0	0.045
	$\Upsilon_1(1^3D_1)\gamma$	10.154	0.084	0.20	0.0091
	$\chi_{b2}(1^3P_2)\pi\pi$			1.2	0.054
	$\chi_{b1}(1^3P_1)\pi\pi$			∼0	∼0
	$\chi_{b0}(1^3P_0)\pi\pi$			0.27	0.012
	Total			2.2 MeV	100
$h_b(3^1P_1)$ 10.519[b]	ggg		1.749	59	71
	$\eta_b(3^1S_0)\gamma$	10.337	2.047	8.9	11
	$\eta_b(2^1S_0)\gamma$	9.999	0.418	8.2	9.9
	$\eta_b(1^1S_0)\gamma$	9.398	0.091	3.6	4.3
	$\eta_{b2}(2^1D_2)\gamma$	10.450	−2.579	1.6	1.9
	$\eta_{b2}(1^1D_2)\gamma$	10.165	0.052	0.081	0.098
	$\chi_{b2}(1^3P_2)\gamma$	9.912	−0.032	1.4×10^{-2}	1.7×10^{-2}
	$\chi_{b1}(1^3P_1)\gamma$	9.893	−0.031	9.3×10^{-3}	1.1×10^{-2}
	$\chi_{b0}(1^3P_0)\gamma$	9.859	−0.016	9.8×10^{-4}	1.2×10^{-3}
	$h_b(1^1P_1)\pi\pi$			1.4	1.7
	Total			83	100

[a]From LHCb Ref. [33].
[b]Using the predicted $3P$ splittings with the measured 3^3P_1 mass.

TABLE XI. Partial widths and branching ratios for strong and electromagnetic decays and transitions and OZI allowed strong decays for the $4P$ states. For P-wave annihilation decays $\mathcal{M}$ designates $R'(0)$, the first derivative of the radial wave function at the origin. Details of the OZI allowed decay amplitudes are described in the Appendix. See the caption to Table IV for further details.

Initial state	Final state	M_f (GeV)	$\mathcal{M}$	Width (keV)	BR (%)
$\chi_{b2}(4^3P_2)$	gg		1.646	248	0.569
10.798	$\gamma\gamma$		1.646	1.5×10^{-2}	3.4×10^{-5}
	$\Upsilon(4^3S_1)\gamma$	10.579	2.765	28.1	6.44×10^{-2}
	$\Upsilon(3^3S_1)\gamma$	10.355	0.427	5.4	1.2×10^{-2}
	$\Upsilon(2^3S_1)\gamma$	10.023	0.063	0.59	1.4×10^{-3}
	$\Upsilon(1^3S_1)\gamma$	9.460	0.056	2.2	5.0×10^{-3}
	$\Upsilon_3(3^3D_3)\gamma$	10.711	−3.310	4.3	9.9×10^{-3}
	$\Upsilon_2(3^3D_2)\gamma$	10.705	−3.202	0.88	2.0×10^{-3}
	$\Upsilon_1(3^3D_1)\gamma$	10.698	−3.084	0.68	1.6×10^{-3}
	BB			8.74 MeV	20.0
	BB^*			28.1 MeV	64.4
	B^*B^*			5.05 MeV	11.6
	B_sB_s			0.593 MeV	1.36
	$B_sB_s^*$			0.833 MeV	1.91
	Total			43.6 MeV	100
$\chi_{b1}(4^3P_1)$	$q\bar{q}+g$		1.849	110	0.36
10.788	$\Upsilon(4^3S_1)\gamma$	10.579	2.942	27.7	9.17×10^{-2}
	$\Upsilon(3^3S_1)\gamma$	10.355	0.373	3.8	1.3×10^{-2}
	$\Upsilon(2^3S_1)\gamma$	10.023	0.035	0.18	6.0×10^{-4}
	$\Upsilon(1^3S_1)\gamma$	9.460	0.038	1.0	3.3×10^{-3}
	$\Upsilon_2(3^3D_2)\gamma$	10.705	−3.345	3.4	1.1×10^{-2}
	$\Upsilon_1(3^3D_1)\gamma$	10.698	−3.234	1.4	4.6×10^{-3}
	BB^*			20.6 MeV	68.3
	B^*B^*			0.478 MeV	1.58
	$B_sB_s^*$			8.93 MeV	29.6
	Total			30.2 MeV	100
$\chi_{b0}(4^3P_0)$	gg		2.079	2.1 MeV	6.1
10.775	$\gamma\gamma$		2.079	0.13	3.8×10^{-4}
	$\Upsilon(4^3S_1)\gamma$	10.579	3.139	26.0	7.54×10^{-2}
	$\Upsilon(3^3S_1)\gamma$	10.355	0.295	2.2	6.4×10^{-3}
	$\Upsilon(2^3S_1)\gamma$	10.023	−0.001	9×10^{-5}	3×10^{-7}
	$\Upsilon(1^3S_1)\gamma$	9.460	0.017	0.21	6.1×10^{-4}
	$\Upsilon_1(3^3D_1)\gamma$	10.698	−3.397	3.8	1.1×10^{-2}
	BB			20.0 MeV	58.0
	B^*B^*			12.2 MeV	35.4
	B_sB_s			0.129 MeV	0.374
	Total			34.5 MeV	100
$h_b(4^1P_1)$	ggg		1.790	64	0.16
10.790	$\eta_b(4^1S_0)\gamma$	10.567	2.808	24.4	6.07×10^{-2}
	$\eta_b(3^1S_0)\gamma$	10.337	0.587	10.8	2.69×10^{-2}
	$\eta_b(2^1S_0)\gamma$	9.999	0.055	0.48	1.2×10^{-3}
	$\eta_b(1^1S_0)\gamma$	9.398	0.052	2.1	5.2×10^{-3}
	$\eta_{b2}(3^1D_2)\gamma$	10.790	−3.325	4.7	1.2×10^{-2}
	BB^*			31.8 MeV	79.1
	B^*B^*			4.09 MeV	10.2
	$B_sB_s^*$			4.18 MeV	10.4
	Total			40.2 MeV	100

TABLE XII. Partial widths and branching ratios for strong and electromagnetic transitions and OZI allowed strong decays for the 5^3P_2 and 5^3P_1 states. Details of the OZI allowed decay amplitudes are described in the Appendix. See the caption to Table IV for further details.

Initial state	Final state	M_f (GeV)	$\mathcal{M}$	Width (keV)	BR (%)
$\chi_{b2}(5^3P_2)$ 11.022	$\Upsilon(5^3S_1)\gamma$	10.876	3.232	11.5	2.06×10^{-2}
	$\Upsilon(4^3S_1)\gamma$	10.579	0.595	10.4	1.86×10^{-2}
	$\Upsilon(3^3S_1)\gamma$	10.355	0.024	0.06	1×10^{-4}
	$\Upsilon(2^3S_1)\gamma$	10.023	0.067	1.4	2.5×10^{-3}
	$\Upsilon(1^3S_1)\gamma$	9.460	0.042	1.9	3.4×10^{-3}
	$\Upsilon_3(4^3D_3)\gamma$	10.939	−3.955	5.4	9.7×10^{-3}
	$\Upsilon_2(4^3D_2)\gamma$	10.934	−3.828	1.1	2.0×10^{-3}
	$\Upsilon_1(4^3D_1)\gamma$	10.928	−3.685	0.08	1×10^{-4}
	BB			0.456 MeV	0.816
	BB^*			2.71 MeV	4.85
	$BB(1P_1)$			4.72 MeV	8.44
	$BB(1P_1')$			15.8 MeV	28.3
	B^*B^*			31.3 MeV	56.0
	B_sB_s			0.154 MeV	0.275
	$B_sB_s^*$			0.130 MeV	0.232
	$B_s^*B_s^*$			0.618 MeV	1.10
	Total			55.9 MeV	100
$\chi_{b1}(5^3P_1)$ 11.014	$\Upsilon(5^3S_1)\gamma$	10.876	3.439	11.0	1.75×10^{-2}
	$\Upsilon(4^3S_1)\gamma$	10.579	0.534	8.0	1.3×10^{-2}
	$\Upsilon(3^3S_1)\gamma$	10.355	−0.006	2.8×10^{-3}	4.4×10^{-6}
	$\Upsilon(2^3S_1)\gamma$	10.023	0.052	0.83	1.3×10^{-3}
	$\Upsilon(1^3S_1)\gamma$	9.460	0.029	0.90	1.4×10^{-3}
	$\Upsilon_2(4^3D_2)\gamma$	10.934	−3.990	4.4	7.0×10^{-3}
	$\Upsilon_1(4^3D_1)\gamma$	10.928	−3.857	1.7	2.7×10^{-3}
	BB^*			16.7 MeV	26.5
	$BB(^3P_0)$			0.306	4.86×10^{-4}
	$BB(1P_1)$			13.5 MeV	21.4
	$BB(1P_1')$			6.82 MeV	10.8
	B^*B^*			25.1 MeV	39.8
	$B_sB_s^*$			21.5	3.41×10^{-2}
	$B_s^*B_s^*$			0.614 MeV	0.975
	Total			63.0 MeV	100

and scaling factors [as in Eq. (8)] are factored out, the ratios of amplitudes will be approximately the same for transitions between states with the same number of nodes in the initial and final states, i.e.,

$$\frac{A'(3P\to 1P)}{A'(2P\to 1P)}\sim\frac{A'(3S\to 1S)}{A'(2S\to 1S)} \tag{10}$$

where the A''s have factored out the phase space and scaling factors in the amplitude. Thus, we will relate the $3P\to 1P$ partial widths to measured $2P\to 1P$ partial widths by rescaling the phase space, the $b\bar{b}$ separation factors and using the relationship between amplitudes outlined in Eq. (10). We understand that this is far from rigorous but hope that it captures the gross features of the transition and will give us an order of magnitude estimate of the transitions that can at least tell us if the transition is big or small and how significant its contribution to the total width will be. With this prescription we obtain $A_0(3P\to 1P)=0.68\,\text{keV}$ and $A_2(3P\to 1P)=4.94$ keV. The resulting estimates for the $3P\to 1P$ hadronic transitions are given in Table X. To obtain these results we used spin averaged P-wave masses for the phase space factors given all the other uncertainties in these estimates. If we do not include the $\langle r^2\rangle$ rescaling factors, the partial widths increase by 45%, which is another reminder that these estimates should be regarded as educated guesses that hopefully get the order of magnitude right.

C. $1D_J\to 1S+\pi\pi$ and $2D_J\to 1D+\pi\pi$

The *BABAR* collaboration measured $\text{BR}(1^3D_2\to\Upsilon(1S)+\pi^+\pi^-)=(0.66\pm0.16)\%$ [36]. It should be noted that *BABAR* used the predicted partial widths for $\chi_{bJ'}\to\gamma\Upsilon(1^3D_J)$ from Ref. [35] as input to obtain this value. Combining this measured BR with the remaining 1^3D_2

TABLE XIII. Partial widths and branching ratios for strong and electromagnetic transitions and OZI allowed strong decays for the 5^3P_0 and 5^1P_1 states. Details of the OZI allowed decay amplitudes are described in the Appendix. See the caption to Table IV for further details.

Initial state	Final state	M_f (GeV)	$\mathcal{M}$	Width (keV)	BR (%)
$\chi_{b0}(5^3P_0)$	$\Upsilon(5^3S_1)\gamma$	10.876	3.668	10.0	1.86×10^{-2}
11.004	$\Upsilon(4^3S_1)\gamma$	10.579	0.446	5.2	9.6×10^{-3}
	$\Upsilon(3^3S_1)\gamma$	10.355	−0.043	0.16	3.0×10^{-4}
	$\Upsilon(2^3S_1)\gamma$	10.023	0.035	0.36	6.7×10^{-4}
	$\Upsilon(1^3S_1)\gamma$	9.460	0.014	0.22	4.1×10^{-4}
	$\Upsilon_1(4^3D_1)\gamma$	10.928	−4.038	5.1	9.5×10^{-3}
	BB			4.52 MeV	8.38
	$BB(1P_1)$			7.16 MeV	13.3
	B^*B^*			40.3 MeV	74.8
	B_sB_s			0.166 MeV	0.308
	$B_s^*B_s^*$			1.71 MeV	3.17
	Total			53.9 MeV	100
$h_b(5^1P_1)$	$\eta_b(5^1S_0)\gamma$	10.867	2.900	9.8	2.1×10^{-2}
11.016	$\eta_b(4^1S_0)\gamma$	10.567	0.824	20.8	4.54×10^{-2}
	$\eta_b(3^1S_0)\gamma$	10.337	−0.003	9.7×10^{-4}	2.1×10^{-6}
	$\eta_b(2^1S_0)\gamma$	9.999	0.030	0.29	6.3×10^{-4}
	$\eta_b(1^1S_0)\gamma$	9.398	0.042	2.2	4.8×10^{-3}
	$\eta_{b2}(4^1D_2)\gamma$	10.790	−3.967	6.0	1.3×10^{-2}
	BB^*			11.7 MeV	25.5
	$BB(1^3P_0)$			6.81 MeV	14.9
	$BB(1P_1)$			0.412	9.00×10^{-4}
	$BB(1P_1')$			0.689	1.50×10^{-3}
	B^*B^*			26.4 MeV	57.6
	$B_sB_s^*$			55.8	0.122
	$B_s^*B_s^*$			0.670 MeV	1.46
	Total			45.8 MeV	100

partial decay widths given in Table XIV we obtain $\Gamma(1^3D_2 \to \Upsilon(1S) + \pi^+\pi^-) = 0.169 \pm 0.045$ keV. For comparison, using the predictions for the 1^3D_2 decays from Ref. [35] we obtain the hadronic width $\Gamma = 0.186 \pm 0.047$ keV. Prior to the *BABAR* measurement, predictions for this transition varied from 0.07 keV to 24 keV [61,64,71,72]. Using the partial width value $\Gamma = 0.169 \pm 0.045$ keV as input we obtain $A_2(2,0) = 0.845$ keV which we use along with phase space [Eq. (6)] and $\langle r^2 \rangle$ rescaling factors [Eq. (8)] to obtain the $1D \to 1S\pi\pi$ transitions given in Table XIV. For comparison we include the measurements for the 1^3D_1 and 1^3D_3 transitions from Ref. [36] which are less certain than those for the 1^3D_2 transitions.

Because we have no data on the $2D$ states we use the same strategy to estimate $2D \to 1D$ transitions as we did in estimating the $3P \to 1P$ transitions. We assume that rescaling an amplitude with the same number of nodes in the initial and final state wave functions will capture the gross features of the complicated overlap integrals with intermediate wave functions. We use the A_0 and A_2 amplitudes from the $2P \to 1P$ transitions as input and rescale the amplitudes using the appropriate phase space factors and $\langle r^2 \rangle$ rescaling factors. This gives $A_0(2,2) = 3.1 \times 10^{-2}$ keV and $A_2(2,2) = 4.6 \times 10^{-5}$ keV. As a check we also estimated A_0 found by rescaling the A_0 amplitude obtained from the $2S \to 1S$ transition where only A_0 contributes and found it to be roughly a factor of 40 smaller than the value obtained from the $2P \to 1P$ transition. This should be kept in mind when assessing the reliability of our predictions. In any case, the partial widths obtained for the $2D \to 1D$ hadronic transitions are sufficiently small (see Table XV) that the large uncertainties will not change our conclusions regarding the $2D$ states.

D. $1F \to 1P + \pi\pi$ and $1G \to 1D + \pi\pi$

We take the same approach as we used to estimate some of the hadronic transition widths given above. We take a measured width, in this case the $1^3D_2 \to \Upsilon(1S)\pi^+\pi^-$, and rescale it using ratios of phase space factors and separation factors to estimate the $1F \to 1P$ and $1G \to 1D$ transitions. We obtain $A_2(1F \to 1P) = 0.027$ keV and $A_2(1G \to 1D) = 1.94 \times 10^{-3}$ keV. These small values are primarily due to the ratio of phase space factors which roughly go like the mass difference to the seventh power. Given that the $1D - 1S$, $1F - 1P$ and $1G - 1D$ mass splittings are

TABLE XIV. Partial widths and branching ratios for strong and electromagnetic decays and transitions for the $1D$ states. For D-wave annihilation decays $\mathcal{M}$ designates $R''(0)$, the second derivative of the radial wave function at the origin. See the caption to Table IV for further details.

Initial state	Final state	M_f (GeV)	$\mathcal{M}$	Predicted Width (keV)	Predicted BR (%)	Measured BR (%)
$\Upsilon_3(1^3D_3)$ 10.172[b]	$\chi_{b2}(1^3P_2)\gamma$	9.912	1.830	24.3	91.0	
	$\eta_{b2}(1^1D_2)\gamma$	10.165	1.000	1.5×10^{-5}	5.6×10^{-5}	
	ggg		0.9923	2.07	7.75	
	$\Upsilon(1^3S_1)\pi^+\pi^-$			0.197	0.738	0.29 ± 0.23 (or < 0.62 at 90% C.L.)[a]
	Total			26.7	100	
$\Upsilon_2(1^3D_2)$ 10.164[a]	$\chi_{b2}(1^3P_2)\gamma$	9.912	1.835	5.6	22	
	$\chi_{b1}(1^3P_1)\gamma$	9.893	1.762	19.2	74.7	
	ggg		1.149	0.69	2.7	
	$\Upsilon(1^3S_1)\pi^+\pi^-$			0.169 ± 0.045[c]	0.658	0.66 ± 0.16[a]
	Total			25.7	100	
$\Upsilon_1(1^3D_1)$ 10.155[b]	$\ell^+\ell^-$			1.38 eV	3.93×10^{-3}	
	$\chi_{b2}(1^3P_2)\gamma$	9.912	1.839	0.56	1.6	
	$\chi_{b1}(1^3P_1)\gamma$	9.893	1.768	9.7	28	
	$\chi_{b0}(1^3P_0)\gamma$	9.859	1.673	16.5	47.1	
	ggg	1.356		8.11	23.1	
	$\Upsilon(1^3S_1)\pi^+\pi^-$			0.140	0.399	0.42 ± 0.29 (or < 0.82 at 90% C.L.)[a]
	Total			35.1	100	
$\eta_{b2}(1^1D_2)$ 10.165[b]	$h_b(1^1P_1)\gamma$	9.899	0.178	24.9	91.5	
	$\eta_b(1^1S_0)\pi^+\pi^-$			0.35	1.3	
	gg		1.130	1.8	6.6	
	Total			27.2	100	

[a]From *BABAR* [36].
[b]Using predicted splittings and 1^3D_2 mass from Ref. [36].
[c]See Sec. IV C for the details of how this was obtained.

~0.69, 0.46 and 0.38 MeV respectively resulting in little available phase space one can understand why the amplitudes are small. We include our estimates for these transitions in Tables XIX and XXII. While the estimates may be crude the point is that we expect these partial widths to be quite small.

VI. STRONG DECAYS

For states above the $B\bar{B}$ threshold, we calculate Okubo-Zweig-Iizuka (OZI) allowed strong decay widths using the $^3P_0$ quark pair creation model [12,13,16,17,85] which proceeds through the production of a light $q\bar{q}$ pair ($q = u, d, s$) followed by separation into $B\bar{B}$ mesons. The $q\bar{q}$ pair is assumed to be produced with vacuum quantum numbers (0^{++}). There are a number of predictions for Υ strong decay widths in the literature using the $^3P_0$ model [86,87] and other models [88], but a complete analysis of their strong decays had yet to be carried out prior to this work. We give details regarding the notation and conventions used in our $^3P_0$ model calculations in the Appendix to make it more transparent for an interested reader to reproduce our results.

We use the meson masses listed in Tables I–III. If available, the measured value, $M_{\rm exp}$, is used as input for calculating the strong decay widths, rather than the predicted value, $M_{\rm theo}$. When the mass of only one meson in a multiplet has been measured, we estimate the input masses for the remaining states following the procedure described at the end of Sec. II.

We use simple harmonic oscillator wave functions with the effective oscillator parameter, β, obtained by equating the rms radius of the harmonic oscillator wave function for the specified (n, l) quantum numbers to the rms radius of the wave functions calculated using the relativized quark model of Ref. [11]. The effective harmonic oscillator wave function parameters found in this way are listed in the final column of Tables I–III. For the constituent quark masses in our calculations of both the meson masses and of the strong decay widths, we use $m_b = 4.977$ GeV, $m_s = 0.419$ GeV, and $m_q = 0.220$ GeV ($q = u, d$). Finally, we use "relativistic phase space" as described in Refs. [16,85] and in the Appendix.

Typical values of the parameters β and γ are found from fits to light meson decays [16,89,90]. The predicted widths are fairly insensitive to the precise values used for β provided γ is appropriately rescaled. However γ can vary as much as 30% and still give reasonable overall fits of light meson decay widths [89,90]. This can result in factor-of-2

TABLE XV. Partial widths and branching ratios for strong and electromagnetic decays and transitions for the $2D$ states. For D-wave annihilation decays $\mathcal{M}$ designates $R''(0)$, the second derivative of the radial wave function at the origin. See the caption to Table IV for further details.

Initial state	Final state	M_f (GeV)	$\mathcal{M}$	Width (keV)	BR (%)
$\Upsilon_3(2^3D_3)$	$\chi_{b2}(2^3P_2)\gamma$	10.269	2.445	16.4	65.1
10.455	$\chi_{b2}(1^3P_2)\gamma$	9.912	0.200	2.6	10.
	$\chi_{b4}(1^3F_4)\gamma$	10.358	−1.798	1.7	6.7
	$\chi_{b3}(1^3F_3)\gamma$	10.355	−1.751	0.16	0.63
	$\chi_{b2}(1^3F_2)\gamma$	10.350	−1.702	5×10^{-3}	2×10^{-2}
	$\eta_{b2}(2^1D_2)\gamma$	10.450	0.999	6.5×10^{-6}	2.6×10^{-5}
	$\eta_{b2}(1^1D_2)\gamma$	10.165	−0.033	1.1×10^{-3}	4.4×10^{-3}
	ggg		1.389	4.3	17
	$\Upsilon_3(1^3D_3)\pi\pi$			7.4×10^{-3}	2.9×10^{-2}
	$\Upsilon_2(1^3D_2)\pi\pi$			1.9×10^{-6}	7.5×10^{-6}
	$\Upsilon_1(1^3D_1)\pi\pi$			1.9×10^{-7}	7.5×10^{-7}
	Total			25.2	100
$\Upsilon_2(2^3D_2)$	$\chi_{b2}(2^3P_2)\gamma$	10.269	2.490	3.8	17
10.449	$\chi_{b1}(2^3P_1)\gamma$	10.255	2.359	12.7	56.2
	$\chi_{b2}(1^3P_2)\gamma$	9.912	0.161	0.4	2
	$\chi_{b1}(1^3P_1)\gamma$	9.893	0.224	2.6	12
	$\chi_{b3}(1^3F_3)\gamma$	10.355	−1.806	1.5	6.6
	$\chi_{b2}(1^3F_2)\gamma$	10.350	−1.758	0.21	0.93
	$\eta_{b2}(1^1D_2)\gamma$	10.165	−0.047	2.1×10^{-3}	9.3×10^{-3}
	ggg		1.568	1.4	6.2
	$\Upsilon_3(1^3D_3)\pi\pi$			2.6×10^{-6}	1.2×10^{-5}
	$\Upsilon_2(1^3D_2)\pi\pi$			7.4×10^{-3}	3.3×10^{-2}
	$\Upsilon_1(1^3D_1)\pi\pi$			2.3×10^{-6}	1.0×10^{-5}
	Total			22.6	100
$\Upsilon_1(2^3D_1)$	$\ell^+\ell^-$			1.99 eV	5.28×10^{-3}
10.441	$\chi_{b2}(2^3P_2)\gamma$	10.269	2.535	0.4	1
	$\chi_{b1}(2^3P_1)\gamma$	10.255	2.409	6.5	17
	$\chi_{b0}(2^3P_0)\gamma$	10.232	2.243	10.6	28.1
	$\chi_{b2}(1^3P_2)\gamma$	9.912	0.118	0.02	0.05
	$\chi_{b1}(1^3P_1)\gamma$	9.893	0.184	0.9	2
	$\chi_{b0}(1^3P_0)\gamma$	9.859	0.260	2.9	7.7
	$\chi_{b2}(1^3F_2)\gamma$	10.350	−1.815	1.6	4.2
	$\eta_{b2}(1^1D_2)\gamma$	10.165	−0.061	3.3×10^{-3}	8.8×10^{-3}
	ggg		1.771	14.8	39.2
	$\Upsilon_3(1^3D_3)\pi\pi$			4.4×10^{-7}	1.2×10^{-6}
	$\Upsilon_2(1^3D_2)\pi\pi$			3.9×10^{-6}	1.0×10^{-5}
	$\Upsilon_1(1^3D_1)\pi\pi$			7.4×10^{-3}	2.0×10^{-2}
	Total			37.7	100
$\eta_{b2}(2^1D_2)$	$h_b(2^1P_1)\gamma$	10.260	2.390	16.5	67.1
10.450	$h_b(1^1P_1)\gamma$	9.899	0.212	3.0	12
	$h_{b3}(1^1F_3)\gamma$	10.355	−1.802	1.8	7.3
	$\Upsilon_3(1^3D_3)\gamma$	10.172	−0.072	6.5×10^{-3}	2.6×10^{-2}
	$\Upsilon_2(1^3D_2)\gamma$	10.164	−0.048	2.2×10^{-3}	8.9×10^{-3}
	$\Upsilon_1(1^3D_1)\gamma$	10.154	−0.046	1.4×10^{-3}	5.7×10^{-3}
	gg		1.530	3.3	13
	$\eta_{b2}(1^1D_2)\pi\pi$			7.4×10^{-3}	3.0×10^{-2}
	Total			24.6	100

TABLE XVI. Partial widths and branching ratios for strong and electromagnetic decays and transitions and OZI allowed decays for the $3D$ states. For D-wave annihilation decays $\mathcal{M}$ designates $R''(0)$, the second derivative of the radial wave function at the origin. Details of the OZI allowed decays amplitudes are described in the Appendix. See the caption to Table IV for further details.

Initial state	Final state	M_f (GeV)	$\mathcal{M}$	Width (keV)	BR (%)
$\Upsilon_3(3^3D_3)$	$\chi_{b2}(3^3P_2)\gamma$	10.528	3.022	23.6	1.19×10^{-2}
10.711	$\chi_{b2}(2^3P_2)\gamma$	10.269	0.265	2.5	1.3×10^{-3}
	$\chi_{b2}(1^3P_2)\gamma$	9.912	0.064	0.82	4.1×10^{-4}
	$\chi_{b4}(2^3F_4)\gamma$	10.622	−2.683	3.0	1.5×10^{-3}
	$\chi_{b3}(2^3F_3)\gamma$	10.619	−2.617	0.27	1.4×10^{-4}
	$\chi_{b2}(2^3F_2)\gamma$	10.615	−2.545	8×10^{-3}	4×10^{-6}
	ggg		1.691	6.6	3.3×10^{-3}
	BB			16.3 MeV	8.23
	BB^*			72.9 MeV	36.8
	B^*B^*			109 MeV	55.0
	Total			198 MeV	100
$\Upsilon_2(3^3D_2)$	$\chi_{b2}(3^3P_2)\gamma$	10.528	3.098	5.6	4.3×10^{-3}
10.705	$\chi_{b1}(3^3P_1)\gamma$	10.516	2.919	18.2	1.41×10^{-2}
	$\chi_{b2}(2^3P_2)\gamma$	10.269	0.218	0.40	3.1×10^{-4}
	$\chi_{b1}(2^3P_1)\gamma$	10.255	0.303	2.5	1.9×10^{-3}
	$\chi_{b2}(1^3P_2)\gamma$	9.912	0.043	0.09	7×10^{-5}
	$\chi_{b1}(1^3P_1)\gamma$	9.893	0.062	0.59	4.6×10^{-4}
	$\chi_{b3}(2^3F_3)\gamma$	10.619	−2.698	2.6	2.0×10^{-3}
	$\chi_{b2}(2^3F_2)\gamma$	10.615	−2.628	0.36	2.8×10^{-4}
	ggg		1.875	2.0	1.6×10^{-3}
	BB^*			52.4 MeV	40.6
	B^*B^*			76.5 MeV	59.3
	Total			128.9 MeV	100
$\Upsilon_1(3^3D_1)$	$\ell^+\ell^-$			2.38 eV	2.30×10^{-6}
10.698	$\chi_{b2}(3^3P_2)\gamma$	10.528	3.174	0.58	5.6×10^{-4}
	$\chi_{b1}(3^3P_1)\gamma$	10.516	3.003	9.5	9.2×10^{-3}
	$\chi_{b0}(3^3P_0)\gamma$	10.500	2.775	14.0	1.35×10^{-2}
	$\chi_{b2}(2^3P_2)\gamma$	10.269	0.165	0.02	2×10^{-5}
	$\chi_{b1}(2^3P_1)\gamma$	10.255	0.256	0.96	9.3×10^{-4}
	$\chi_{b0}(2^3P_0)\gamma$	10.233	0.354	2.8	2.7×10^{-3}
	$\chi_{b0}(1^3P_1)\gamma$	9.893	0.040	0.13	1.3×10^{-4}
	$\chi_{b0}(1^3P_0)\gamma$	9.859	0.069	0.59	5.7×10^{-4}
	$\chi_{b2}(2^3F_2)\gamma$	10.615	−2.712	2.7	2.6×10^{-3}
	$\chi_{b2}(1^3F_2)\gamma$	10.350	0.039	0.39	3.8×10^{-5}
	ggg		2.081	21.2	2.05×10^{-2}
	BB			23.8 MeV	23.0
	BB^*			0.245 MeV	0.236
	B^*B^*			79.5 MeV	76.7
	Total			103.6 MeV	100
$\eta_{b2}(3^1D_2)$	$h_{b1}(3^1P_1)\gamma$	10.519	2.956	24.1	1.43×10^{-2}
10.706	$h_{b1}(2^1P_1)\gamma$	10.260	0.285	2.9	1.7×10^{-3}
	$h_{b1}(1^1P_1)\gamma$	9.899	0.061	0.76	4.5×10^{-4}
	$h_{b3}(2^1F_3)\gamma$	10.619	−2.691	3.1	1.8×10^{-3}
	$h_{b2}(1^1F_2)\gamma$	10.355	0.030	0.02	1×10^{-5}
	gg		1.839	4.7	2.8×10^{-3}
	BB^*			77.8 MeV	46.1
	B^*B^*			90.9 MeV	53.9
	Total			168.7 MeV	100

TABLE XVII. Predicted partial widths and branching ratios for strong and electromagnetic transitions and OZI allowed decays for the 4^3D_3 and 4^3D_2 states. Details of the OZI allowed decay amplitudes are described in the Appendix. See the caption to Table IV for further details.

Initial state	Final state	M_f (GeV)	$\mathcal{M}$	Width (keV)	BR (%)
$\Upsilon_3(4^3D_3)$ 10.939	$\chi_{b2}(4^3P_2)\gamma$	10.798	3.553	15.0	2.59×10^{-2}
	$\chi_{b2}(3^3P_2)\gamma$	10.528	0.322	2.9	5.0×10^{-3}
	$\chi_{b2}(2^3P_2)\gamma$	10.269	0.073	0.63	1.1×10^{-3}
	$\chi_{b2}(1^3P_2)\gamma$	9.912	0.035	0.50	8.6×10^{-4}
	$\chi_{b4}(3^3F_4)\gamma$	10.856	−3.143	3.9	6.7×10^{-3}
	$\chi_{b3}(3^3F_3)\gamma$	10.853	−3.330	0.36	6.2×10^{-4}
	$\chi_{b2}(3^3F_2)\gamma$	10.850	−3.241	0.01	2×10^{-5}
	BB			0.726 MeV	1.25
	BB^*			2.94 MeV	5.07
	B^*B^*			51.5 MeV	88.8
	B_sB_s			0.265 MeV	0.457
	$B_sB_s^*$			0.0827 MeV	0.142
	$B_s^*B_s^*$			2.44 MeV	4.21
	Total			58.0 MeV	100
$\Upsilon_2(4^3D_2)$ 10.934	$\chi_{b2}(4^3P_2)\gamma$	10.798	3.655	3.6	5.6×10^{-3}
	$\chi_{b1}(4^3P_1)\gamma$	10.788	3.428	11.6	1.80×10^{-2}
	$\chi_{b2}(3^3P_2)\gamma$	10.528	0.270	0.50	7.8×10^{-4}
	$\chi_{b1}(3^3P_1)\gamma$	10.516	0.384	3.3	5.1×10^{-3}
	$\chi_{b2}(2^3P_2)\gamma$	10.269	0.048	0.07	1×10^{-4}
	$\chi_{b1}(2^3P_1)\gamma$	10.255	0.061	0.35	5.4×10^{-4}
	$\chi_{b2}(1^3P_2)\gamma$	9.912	0.022	0.05	8×10^{-5}
	$\chi_{b1}(1^3P_1)\gamma$	9.893	0.046	0.68	1.1×10^{-3}
	$\chi_{b3}(3^3F_3)\gamma$	10.853	−3.431	3.6	5.6×10^{-3}
	$\chi_{b2}(3^3F_2)\gamma$	10.850	−3.344	0.47	7.3×10^{-4}
	BB^*			25.7 MeV	40.0
	B^*B^*			36.4 MeV	56.6
	$B_sB_s^*$			0.357 MeV	0.56
	$B_s^*B_s^*$			1.80 MeV	2.80
	Total			64.3 MeV	100

changes to predicted widths, both smaller or larger. In our calculations of D_s meson strong decay widths in [18], we used a value of $\gamma = 0.4$, which has also been found to give a good description of strong decays of charmonium [17]. However, we found that this value underestimated the bottomonium strong decay widths when compared to the PDG values for the $\Upsilon(4S)$, $\Upsilon(5S)$ and $\Upsilon(6S)$ widths. Therefore, we used a value of $\gamma = 0.6$ in our strong decay width calculations in this paper, which was determined by fitting our results to the PDG values in the Υ sector. This scaling of the value of γ in different quarkonia sectors has been studied in [87]. The resulting strong decay widths are listed in Tables VI–XXIII in which we use a more concise notation where BB refers to the $B\bar{B}$ decay mode, BB^* refers to $B\bar{B}^* + \bar{B}B^*$, etc.

We note that our results differ from the recent work of Ferretti and Santopinto [86], in some cases quite substantially. This is primarily due to the values chosen for the harmonic oscillator parameter β (with a corresponding change in the pair creation strength γ). In our calculations we used a value for β found by fitting the rms radius of a harmonic oscillator wave function to the "exact" wave function for each state while Ferretti and Santopinto used a common value for all states. Another reason our results differ is because Ferretti and Santopinto included an additional Gaussian smearing function in their momentum-space wave function overlap to model the nonpointlike nature of the created $q\bar{q}$ pair. As a numerical check of our programs we reproduced their results using their parameters and including the Gaussian smearing function, although we found that the latter had little effect on our results. We believe our approach best describes the properties of individual states but this underlines the importance of experimental input to test models and improve predictions.

VII. SEARCH STRATEGIES

An important motivation for this work is to suggest strategies to observe some of the missing bottomonium

TABLE XVIII. Predicted partial widths and branching ratios for strong and electromagnetic transitions for 4^3D_1 and 4^1D_2 states. Details of the OZI allowed decay amplitudes are described in the Appendix. See the caption to Table IV for further details.

Initial state	Final state	M_f (GeV)	$\mathcal{M}$	Width (keV)	BR (%)
$\Upsilon_1(4^3D_1)$	$\ell^+\ell^-$			2.18 eV	3.04×10^{-6}
10.928	$\chi_{b2}(4^3P_2)\gamma$	10.798	3.756	0.36	5.0×10^{-4}
	$\chi_{b1}(4^3P_1)\gamma$	10.788	3.538	6.1	8.5×10^{-3}
	$\chi_{b0}(4^3P_0)\gamma$	10.775	3.262	9.0	1.2×10^{-2}
	$\chi_{b2}(3^3P_2)\gamma$	10.528	0.210	0.03	4×10^{-5}
	$\chi_{b1}(3^3P_1)\gamma$	10.516	0.331	1.3	1.8×10^{-3}
	$\chi_{b0}(3^3P_0)\gamma$	10.500	0.476	4.0	5.6×10^{-3}
	$\chi_{b2}(2^3P_2)\gamma$	10.269	0.022	1.5×10^{-3}	2.1×10^{-6}
	$\chi_{b1}(2^3P_1)\gamma$	10.255	0.037	0.07	1×10^{-4}
	$\chi_{b0}(2^3P_0)\gamma$	10.233	0.060	0.26	3.6×10^{-4}
	$\chi_{b1}(1^3P_1)\gamma$	9.893	0.033	0.19	2.6×10^{-4}
	$\chi_{b0}(1^3P_0)\gamma$	9.859	0.054	0.75	1.0×10^{-3}
	$\chi_{b2}(3^3F_2)\gamma$	10.850	−3.448	3.6	5.0×10^{-3}
	BB			3.85 MeV	5.36
	BB^*			14.0 MeV	19.5
	B^*B^*			50.6 MeV	70.5
	B_sB_s			0.101 MeV	0.141
	$B_sB_s^*$			0.332 MeV	0.462
	$B_s^*B_s^*$			2.94 MeV	4.09
	Total			71.8 MeV	100
$\eta_{b2}(4^1D_2)$	$h_b(4^1P_1)\gamma$	10.790	3.477	15.6	2.58×10^{-2}
10.935	$h_b(3^1P_1)\gamma$	10.519	0.362	3.8	6.3×10^{-3}
	$h_b(2^1P_1)\gamma$	10.260	0.065	0.51	8.4×10^{-4}
	$h_b(1^1P_1)\gamma$	9.899	0.042	0.75	1.2×10^{-3}
	$h_{b3}(3^1F_3)\gamma$	10.853	−3.423	4.1	6.8×10^{-3}
	BB^*			19.4 MeV	32.1
	B^*B^*			38.9 MeV	64.3
	$B_sB_s^*$			0.239 MeV	0.395
	$B_s^*B_s^*$			1.92 MeV	3.17
	Total			60.5 MeV	100

mesons. While there are similarities between searches at hadron colliders and e^+e^- colliders there are important differences. As a consequence we will consider the two production channels separately.

A. At the large hadron collider

1. Production

An important ingredient needed in discussing searches for the missing bottomonium states at a hadron collider is an estimate of the production rate for the different states [8,91–94]. The production cross sections for the $\Upsilon(nS)$ and χ_{bJ} states are in good agreement with predictions of nonrelativistic QCD (NRQCD) also referred to as the color octet model. However we are interested in higher excitations with both higher principle quantum number and higher orbital angular momentum for which we are not aware of any existing calculations. To estimate production rates we use the NRQCD factorization approach to rescale measured event rates. In the NRQCD factorization approach the cross section goes like [8]

$$\sigma(H) = \sum_n \sigma_n(\Lambda)\langle\mathcal{O}_n^H(\Lambda)\rangle \tag{11}$$

for quarkonium state H and where n denotes the color, spin and angular momentum of the intermediate $b\bar{b}$ pair, $\sigma_n(\Lambda)$ is the perturbative short distance (parton level) cross section and $\langle\mathcal{O}_n^H(\Lambda)\rangle$ is the long distance matrix element (LDME) which includes the color octet $Q\bar{Q}$ pair that evolves into quarkonium. We work with the assumption that the quarkonium state dependence resides primarily in the LDME which goes very roughly like (see Ref. [91])

$$\langle\mathcal{O}(^{2S+1}L_J)\rangle \propto (2J+1)\frac{|R_{nL}^{(\ell)}(0)|^2}{M^{2L+2}} \tag{12}$$

where $R_{nL}^{(\ell)}(0)$ is the ℓth derivative of the wave function at the origin and M is the mass of the state being produced.

TABLE XIX. Predicted partial widths and branching ratios for strong and electromagnetic decays and transitions for $1F$-wave states. For F-wave annihilation decays $\mathcal{M}$ designates $R'''(0)$, the third derivative of the radial wave function at the origin. See the caption to Table IV for further details.

Initial state	Final state	M_f (GeV)	$\mathcal{M}$	Width (keV)	BR (%)
$\chi_{b4}(1^3F_4)$	$\Upsilon_3(1^3D_3)\gamma$	10.172	2.479	18.0	~100
10.358	$\chi_{b2}(1^3P_2)\pi\pi$			3.9×10^{-3}	2.2×10^{-2}
	gg		0.868	0.048	0.27
	Total			18.0	100
$\chi_{b3}(1^3F_3)$	$\Upsilon_3(1^3D_3)\gamma$	10.172	2.482	1.9	10.
10.355	$\Upsilon_2(1^3D_2)\gamma$	10.164	2.442	16.7	89.3
	gg		0.974	0.060	0.32
	$\chi_{b2}(1^3P_2)\pi\pi$			1.3×10^{-3}	7.0×10^{-3}
	$\chi_{b1}(1^3P_1)\pi\pi$			2.6×10^{-3}	1.4×10^{-2}
	Total			18.7	100
$\chi_{b2}(1^3F_2)$	$\Upsilon_3(1^3D_3)\gamma$	10.172	2.485	0.070	0.35
10.350	$\Upsilon_2(1^3D_2)\gamma$	10.164	2.446	2.7	14
	$\Upsilon_1(1^3D_1)\gamma$	10.154	2.402	16.4	82.4
	gg		1.091	0.70	3.5
	$\chi_{b2}(1^3P_2)\pi\pi$			2.6×10^{-4}	1.3×10^{-3}
	$\chi_{b1}(1^3P_1)\pi\pi$			1.8×10^{-3}	9.0×10^{-3}
	$\chi_{b0}(1^3P_0)\pi\pi$			1.8×10^{-3}	9.0×10^{-3}
	Total			19.9	100
$h_{b3}(1^1F_3)$	$\eta_{b2}(1^1D_2)\gamma$	10.165	2.449	18.8	~100
10.355	$h_b(1^1P_1)\pi\pi$			3.9×10^{-3}	2.1×10^{-2}
	Total			18.8	100

There are numerical factors, the operator coefficients of order 1 that have only been computed for the S- and P-wave states [91]. This gives, for example, an additional factor of 3 in the numerator for P-wave states in Eq. (12). We note that at LO, NRQCD predictions are not in good agreement with experiment but at NLO the agreement is much better [8]. Some of the additional factors that contribute to the uncertainty in our crude estimates are not calculating the relative contributions of color singlet and color octet contributions, the neglect of higher-order QCD corrections, the sensitivity of event rates to the p_T cuts used in the analysis, and ignoring the dependence of detector efficiencies on photon energies.

We will base our estimates on LHCb expectations but expect similar estimates for the collider experiments ATLAS and CMS based on the measured event rates for bottomonium production by LHCb [34], ATLAS [95] and CMS [96]. However, there are differences between these experiments as LHCb covers the low p_T region while ATLAS and CMS extend to higher p_T so that the production rates are not expected to be identical [92], only that the general trends are expected to be similar.

To estimate production rates we start with the production rates measured by LHCb for LHC Run I and rescale them using Eq. (12). Further, it is expected that the cross sections will more than double going from 8 TeV to 14 TeV [94] and the total integrated luminosity is expected to be an order of magnitude larger for Run II compared to Run I. LHCb observed $\sim 1.07 \times 10^6$ $\Upsilon(1S)$'s in the $\mu^+\mu^-$ final state for the combined 7 TeV and 8 TeV runs [34]. Taking into account the $\Upsilon(1S) \to \mu^+\mu^-$ BR, roughly 4.3×10^7 $\Upsilon(1S)$'s were produced. Multiplying this value by the expected doubling of the production cross section going to the current 13 TeV center-of-mass energy and the factor of 10 in integrated luminosity leads to 8.6×10^8 $\Upsilon(1S)$'s as our starting point. We rescale this using Eq. (12) and use our estimates for the branching ratios for decay chains to estimate event rates. Our results can easily be rescaled to correct for the actual integrated luminosity.

We find that this crude approach agrees with the LHCb event rates for nS and nP [34] within roughly a factor of 2, in some cases too small and in other cases too large. Considering the crudeness of these estimates and the many factors listed above which were not included we consider this to be acceptable agreement. We want to emphasize before proceeding that we only expect our estimates to be reliable as order of magnitude estimates but this should be sufficient to identify the most promising channels to pursue.

In the following subsections we generally focus on $b\bar{b}$ states below $B\bar{B}$ threshold, as the BRs for decay chains originating from states above $B\bar{B}$ threshold will generally result in too few events to be observable. Likewise, the production cross sections for high L states are suppressed by large powers of masses in the denominator.

TABLE XX. Predicted partial widths and branching ratios for strong decays and electromagnetic transitions for the $2F$-wave states. For F-wave annihilation decays $\mathcal{M}$ designates $R'''(0)$, the third derivative of the radial wave function at the origin. Details of the OZI allowed decay amplitudes are described in the Appendix. See the caption to Table IV for further details.

Initial state	Final state	M_f (GeV)	$\mathcal{M}$	Width (keV)	BR (%)
$\chi_{b4}(2^3F_4)$	$\Upsilon_3(2^3D_3)\gamma$	10.455	3.053	19.6	0.700
10.622	$\Upsilon_3(1^3D_3)\gamma$	10.172	0.191	1.4	5.0×10^{-2}
	$\Upsilon_5(1^3G_5)\gamma$	10.532	−1.886	1.5	5.4×10^{-2}
	$\Upsilon_4(1^3G_4)\gamma$	10.531	−1.848	0.08	3×10^{-3}
	$\Upsilon_3(1^3G_3)\gamma$	10.529	−1.808	1×10^{-3}	4×10^{-5}
	gg		1.455	0.13	4.6×10^{-3}
	BB			2.73 MeV	97.5
	BB^*			0.0462 MeV	1.65
	Total			2.80 MeV	100
$\chi_{b3}(2^3F_3)$	$\Upsilon_3(2^3D_3)\gamma$	10.455	3.084	2.1	1.4×10^{-2}
10.619	$\Upsilon_2(2^3D_2)\gamma$	10.449	3.009	17.9	0.116
	$\Upsilon_3(1^3D_3)\gamma$	10.172	0.156	0.1	6×10^{-4}
	$\Upsilon_2(1^3D_2)\gamma$	10.164	0.199	1.4	9.1×10^{-3}
	$\Upsilon_4(1^3G_4)\gamma$	10.531	−1.892	1.4	9.1×10^{-3}
	$\Upsilon_3(1^3G_3)\gamma$	10.529	−1.852	0.10	6.5×10^{-4}
	gg		1.583	0.16	1.0×10^{-3}
	BB^*			15.4 MeV	∼100
	Total			15.4 MeV	100
$\chi_{b2}(2^3F_2)$	$\Upsilon_3(2^3D_3)\gamma$	10.455	3.114	0.08	9×10^{-5}
10.615	$\Upsilon_2(2^3D_2)\gamma$	10.449	3.042	3.0	3.4×10^{-3}
	$\Upsilon_1(2^3D_1)\gamma$	10.441	2.961	17.5	1.98×10^{-2}
	$\Upsilon_3(1^3D_3)\gamma$	10.172	0.118	2×10^{-3}	2×10^{-6}
	$\Upsilon_2(1^3D_2)\gamma$	10.164	0.163	0.16	1.8×10^{-4}
	$\Upsilon_1(1^3D_1)\gamma$	10.154	0.210	1.6	1.8×10^{-3}
	$\Upsilon_3(1^3G_3)\gamma$	10.529	−1.898	1.4	1.6×10^{-3}
	gg		1.752	1.77	2.00×10^{-3}
	BB			83.4 MeV	94.1
	BB^*			5.20 MeV	5.987
	Total			88.6 MeV	100
$h_{b3}(2^1F_3)$	$\eta_{b2}(2^1D_2)\gamma$	10.450	3.019	19.9	0.169
10.619	$\eta_{b2}(1^1D_2)\gamma$	10.148	0.196	1.6	1.4×10^{-2}
	$\eta_{b4}(1^1G_4)\gamma$	10.530	−1.890	1.5	1.3×10^{-2}
	BB^*			11.8 MeV	∼100
	Total			11.8 MeV	100

We also focus on decay chains involving radiative transitions although hadronic transitions with charged pions often have higher detection efficiencies. However, hadronic transitions are not nearly as well understood as radiative transitions so we were only able to even attempt to estimate a limited number of cases that, as discussed, we could relate to measured transitions. In addition, in many cases of interest, hadronic transitions are expected to be small. Nevertheless, as demonstrated by the study of the $\Upsilon(1^3D_J)$ by the *BABAR* Collaboration [36] and the $h_b(1P)$ and $h_b(2P)$ by the Belle Collaboration [97], hadronic transitions offer another means to find and study bottomonium states. We include a few examples in the tables that follow but they are by no means an exhaustive compilation and we encourage experimentalists to not neglect this decay mode.

2. The 3S and higher excited S-wave states

We start with the S-wave states. Our interest is that they will be produced in large quantities and their decay chains include states we are interested in such as excited P- and D-waves and will therefore add to the statistics for those states. We therefore focus on decay chains that include these states.

The $3S$ decay chains of interest are given in Table XXVI. The estimates for the number of events expected for LHCb are included but we also include a column with estimates for e^+e^- collisions expected by Belle II which we discuss

TABLE XXI. Partial widths and branching ratios for electromagnetic transitions and OZI allowed decays for the $3F$-wave states. Details of the OZI allowed decay amplitudes are described in the Appendix. See the caption to Table IV for further details.

Initial state	Final state	M_f (GeV)	$\mathcal{M}$	Width (keV)	BR (%)
$\chi_{b4}(3^3F_4)$	$\Upsilon_3(2^3D_3)\gamma$	10.711	3.593	17.9	1.87×10^{-2}
10.856	$\Upsilon_3(2^3D_3)\gamma$	10.455	0.256	1.9	2.0×10^{-3}
	$\Upsilon_3(1^3D_3)\gamma$	10.172	0.050	0.34	3.6×10^{-4}
	$\Upsilon_5(2^3G_5)\gamma$	10.772	−2.776	2.6	2.7×10^{-3}
	$\Upsilon_4(2^3G_4)\gamma$	10.771	−2.722	0.14	1.5×10^{-4}
	$\Upsilon_3(2^3G_3)\gamma$	10.769	−2.664	2.2×10^{-3}	2.3×10^{-6}
	BB			2.84 MeV	2.97
	BB^*			0.681 MeV	0.713
	B^*B^*			85.7 MeV	89.7
	B_sB_s			0.733 MeV	0.768
	$B_sB_s^*$			1.14 MeV	1.19
	$B_s^*B_s^*$			4.43 MeV	4.64
	Total			95.5 MeV	100
$\chi_{b3}(3^3F_3)$	$\Upsilon_3(2^3D_3)\gamma$	10.711	3.646	1.9	1.9×10^{-3}
10.853	$\Upsilon_2(2^3D_2)\gamma$	10.705	3.542	16.4	1.62×10^{-2}
	$\Upsilon_3(2^3D_3)\gamma$	10.455	0.214	0.14	1.4×10^{-4}
	$\Upsilon_2(2^3D_2)\gamma$	10.449	0.271	1.9	1.9×10^{-3}
	$\Upsilon_4(2^3G_4)\gamma$	10.771	−2.785	2.4	2.4×10^{-3}
	$\Upsilon_3(2^3G_3)\gamma$	10.709	−2.728	0.17	1.7×10^{-4}
	BB^*			43.8 MeV	43.2
	B^*B^*			52.4 MeV	51.7
	$B_sB_s^*$			3.83 MeV	3.78
	$B_s^*B_s^*$			1.30 MeV	1.28
	Total			101.4 MeV	100
$\chi_{b2}(3^3F_2)$	$\Upsilon_3(3^3D_3)\gamma$	10.711	3.699	0.07	6×10^{-5}
10.850	$\Upsilon_2(3^3D_2)\gamma$	10.705	3.598	2.8	2.6×10^{-3}
	$\Upsilon_1(3^3D_1)\gamma$	10.698	3.487	16.3	1.50×10^{-2}
	$\Upsilon_1(2^3D_1)\gamma$	10.441	0.290	2.1	1.9×10^{-3}
	$\Upsilon_3(2^3G_3)\gamma$	10.769	−2.794	2.5	2.3×10^{-3}
	BB			7.85 MeV	7.21
	BB^*			32.0 MeV	29.4
	B^*B^*			66.0 MeV	60.6
	B_sB_s			0.709	6.51×10^{-4}
	$B_sB_s^*$			2.50 MeV	2.30
	$B_s^*B_s^*$			0.557 MeV	0.511
	Total			108.9 MeV	100
$h_{b3}(3^1F_3)$	$\eta_{b2}(3^1D_2)\gamma$	10.706	3.555	18.2	1.88×10^{-2}
10.853	$\eta_{b2}(2^1D_2)\gamma$	10.450	0.264	2.0	2.1×10^{-3}
	$\eta_{b2}(1^1D_2)\gamma$	10.165	0.053	0.4	4×10^{-4}
	$\eta_{b4}(2^1G_4)\gamma$	10.770	−2.781	2.7	2.8×10^{-3}
	BB^*			33.2 MeV	34.3
	B^*B^*			58.2 MeV	60.2
	$B_sB_s^*$			3.32 MeV	3.43
	$B_s^*B_s^*$			1.93 MeV	2.00
	Total			96.7 MeV	100

in Sec. VII B. What is relevant is that numerous $1D$ states will be produced in this manner and when added to those produced directly and via P-wave initial states will give rise to significant statistics in $2\gamma + \mu^+\mu^-$ final states. In addition, it might be possible to observe the $\eta_b(3S)$ in a $\gamma\mu^+\mu^-$ final state from the $\eta_b(3S) \to \Upsilon(1S)$ M1 transition.

The 4^3S_1 state can decay to $3P$ states which can subsequently decay to $2D$ or $1D$ states, as shown in Table XXVII. The 4^3S_1 is above the $B\bar{B}$ threshold so has a much larger total width than the lower mass S-waves leading to a much smaller BR for radiative transitions. Decay chains to F-waves involve too many transitions

TABLE XXII. Predicted partial widths and branching ratios for strong and electromagnetic transitions for the $1G$-wave states. For G-wave annihilation decays $\mathcal{M}$ designates $R^{(iv)}(0)$, the fourth derivative of the radial wave function at the origin. See the caption to Table IV for further details.

Initial state	Final state	M_f (GeV)	$\mathcal{M}$	Width (keV)	BR (%)
$\Upsilon_5(1^3G_5)$	$\chi_{b4}(1^3F_4)\gamma$	10.358	3.057	23.1	~100
10.532	$\Upsilon_3(1^3D_3)\pi\pi$			2.2×10^{-4}	9.5×10^{-4}
	Total			23.1	100
$\Upsilon_4(1^3G_4)$	$\chi_{b4}(1^3F_4)\gamma$	10.358	3.059	1.4	6.0
10.531	$\chi_{b3}(1^3F_3)\gamma$	10.355	3.032	22.0	94.0
	$\Upsilon_3(1^3D_3)\pi\pi$			4.0×10^{-5}	1.7×10^{-4}
	$\Upsilon_2(1^3D_2)\pi\pi$			1.8×10^{-4}	7.7×10^{-4}
	Total			23.4	100
$\Upsilon_3(1^3G_3)$	$\chi_{b4}(1^3F_4)\gamma$	10.358	3.060	0.028	0.12
10.529	$\chi_{b3}(1^3F_3)\gamma$	10.355	3.034	1.8	7.5
	$\chi_{b2}(1^3F_2)\gamma$	10.350	3.005	22.3	92.4
	$\Upsilon_3(1^3D_3)\pi\pi$			3.1×10^{-6}	1.3×10^{-5}
	$\Upsilon_2(1^3D_2)\pi\pi$			4.6×10^{-5}	1.9×10^{-4}
	$\Upsilon_1(1^3D_1)\pi\pi$			1.7×10^{-4}	7.0×10^{-4}
	Total			24.1	100
$\eta_{b4}(1^1G_4)$	$h_{b3}(1^1F_3)\gamma$	10.355	3.034	23.1	~100
10.530	gg		1.005	2.3×10^{-3}	1.0×10^{-2}
	$\eta_{b2}(1^2D_2)\pi\pi$			2.2×10^{-4}	9.5×10^{-4}
	Total			23.1	100

TABLE XXIII. Predicted partial widths and branching ratios for electromagnetic transitions and OZI allowed strong decays for the $2G$-wave states. Details of the OZI allowed decay amplitudes are described in the Appendix. See the caption to Table IV for further details.

Initial state	Final state	M_f (GeV)	$\mathcal{M}$	Width (keV)	BR (%)
$\Upsilon_5(2^3G_5)$	$\chi_{b4}(2^3F_4)\gamma$	10.622	3.598	20.6	7.20×10^{-3}
10.772	$\chi_{b4}(1^3F_4)\gamma$	10.358	0.186	1.1	3.8×10^{-4}
	BB			25.9 MeV	9.06
	BB^*			42.4 MeV	14.8
	B^*B^*			218 MeV	76.2
	B_sB_s			4.72	1.65×10^{-3}
	Total			286 MeV	100
$\Upsilon_4(2^3G_4)$	$\chi_{b4}(2^3F_4)\gamma$	10.622	3.620	1.3	6.0×10^{-4}
10.770	$\chi_{b3}(2^3F_3)\gamma$	10.619	3.570	19.7	9.1×10^{-3}
	BB^*			116 MeV	53.7
	B^*B^*			100. MeV	46.3
	Total			216 MeV	100
$\Upsilon_3(2^3G_3)$	$\chi_{b4}(2^3F_4)\gamma$	10.622	3.643	0.025	1.6×10^{-5}
10.769	$\chi_{b3}(2^3F_3)\gamma$	10.619	3.593	1.6	1.0×10^{-3}
	$\chi_{b2}(2^3F_2)\gamma$	10.615	3.538	19.8	1.28×10^{-2}
	BB			10.3 MeV	6.68
	BB^*			68.3 MeV	44.3
	B^*B^*			74.8 MeV	48.5
	B_sB_s			0.744 MeV	0.482
	Total			154.2 MeV	100
$\eta_{b4}(2^1G_4)$	$h_{b3}(2^1F_3)\gamma$	10.619	3.573	20.7	9.00×10^{-3}
10.770	BB^*			108 MeV	47.0
	B^*B^*			122 MeV	53.0
	Total			230. MeV	100

TABLE XXIV. Summary of lowest-order expressions and first-order QCD corrections with α_s computed at the mass scale of the decaying state (see Sec. IV for references).

Process	Rate	Correction
$^1S_0 \to gg$	$\frac{8\pi\alpha_s^2}{3m_Q^2}\lvert\Psi(0)\rvert^2$	$(1+\frac{4.4\alpha_s}{\pi})$ (for $b\bar{b}$)
$^1S_0 \to \gamma\gamma$	$\frac{12\pi e_Q^4\alpha^2}{m_Q^2}\lvert\Psi(0)\rvert^2$	$(1-\frac{3.4\alpha_s}{\pi})$
$^3S_1 \to ggg$	$\frac{40(\pi^2-9)\alpha_s^3}{81m_Q^2}\lvert\Psi(0)\rvert^2$	$(1-\frac{4.9\alpha_s}{\pi})$ (for $b\bar{b}$)
$^3S_1 \to \gamma gg$	$\frac{32(\pi^2-9)e_Q^2\alpha\alpha_s^2}{9m_Q^2}\lvert\Psi(0)\rvert^2$	$(1-\frac{7.4\alpha_s}{\pi})$ (for $b\bar{b}$)
$^3S_1 \to \gamma\gamma\gamma$	$\frac{16(\pi^2-9)e_Q^6\alpha^3}{3m_Q^2}\lvert\Psi(0)\rvert^2$	$(1-\frac{12.6\alpha_s}{\pi})$
$^3S_1 \to e^+e^-$	$\frac{16\pi e_Q^2\alpha^2}{M^2}\lvert\Psi(0)\rvert^2$	$(1-\frac{16\alpha_s}{3\pi})$
$^3P_2 \to gg$	$\frac{8\alpha_s^2}{5m_Q^4}\lvert R'_{nP}(0)\rvert^2$	$(1-\frac{0.2\alpha_s}{\pi})$ $(\chi_{b2}(1P))$
		$(1+\frac{0.83\alpha_s}{\pi})$ $(\chi_{b2}(2P))$
		$(1+\frac{1.47\alpha_s}{\pi})$ $(\chi_{b2}(3P))$
		$(1+\frac{1.91\alpha_s}{\pi})$ $(\chi_{b2}(4P))$
$^3P_2 \to \gamma\gamma$	$\frac{36e_Q^4\alpha^2}{5m_Q^4}\lvert R'_{nP}(0)\rvert^2$	$(1-\frac{16\alpha_s}{3\pi})$
$^3P_1 \to q\bar{q}+g$	$\frac{32\alpha_s^3}{9\pi m_Q^4}\lvert R'_{nP}(0)\rvert^2\ln(m_Q\langle R\rangle)$	
$^3P_0 \to gg$	$\frac{6\alpha_s^2}{m_Q^4}\lvert R'_{nP}(0)\rvert^2$	$(1+\frac{9.9\alpha_s}{\pi})$ $(\chi_{b0}(1P))$
		$(1+\frac{10.2\alpha_s}{\pi})$ $(\chi_{b0}(2P))$
		$(1+\frac{10.3\alpha_s}{\pi})$ $(\chi_{b0}(3P))$
		$(1+\frac{10.5\alpha_s}{\pi})$ $(\chi_{b0}(4P))$
$^3P_0 \to \gamma\gamma$	$\frac{27e_Q^4\alpha^2}{m_Q^4}\lvert R'_{nP}(0)\rvert^2$	$(1+\frac{0.2\alpha_s}{\pi})$
$^1P_1 \to ggg$	$\frac{20\alpha_s^3}{9\pi m_Q^4}\lvert R'_{nP}(0)\rvert^2\ln(m_Q\langle R\rangle)$	
$^3D_3 \to ggg$	$\frac{40\alpha_s^3}{9\pi m_Q^6}\lvert R''_{nD}(0)\rvert^2\ln(4m_Q\langle R\rangle)$	
$^3D_2 \to ggg$	$\frac{10\alpha_s^3}{9\pi m_Q^6}\lvert R''_{nD}(0)\rvert^2\ln(4m_Q\langle R\rangle)$	
$^3D_1 \to ggg$	$\frac{760\alpha_s^3}{81\pi m_Q^6}\lvert R''_{nD}(0)\rvert^2\ln(4m_Q\langle R\rangle)$	
$^3D_1 \to e^+e^-$	$\frac{200e_Q^2\alpha^2}{M^6}\lvert R''_{nD}(0)\rvert^2$	$(1-\frac{16\alpha_s}{3\pi})$
$^1D_2 \to gg$	$\frac{2\alpha_s^2}{3\pi m_Q^6}\lvert R''_{nD}(0)\rvert^2$	
$^3F_4 \to gg$	$\frac{20\alpha_s^2}{27m_Q^8}\lvert R'''_{nF}(0)\rvert^2$	
$^3F_3 \to gg$	$\frac{20\alpha_s^2}{27m_Q^8}\lvert R'''_{nF}(0)\rvert^2$	
$^3F_2 \to gg$	$\frac{919\alpha_s^2}{135m_Q^8}\lvert R'''_{nF}(0)\rvert^2$	
$^1G_4 \to gg$	$\frac{2\alpha_s^2}{3\pi m_Q^{10}}\lvert R^{iv}_{nG}(0)\rvert^2$	

making them difficult to reconstruct so we do not include them in our tables. We also include decay chains which might be of interest for e^+e^- studies but would result in insufficient statistics to be relevant to hadron collider studies. We do not include the 4^1S_0 state as the decay chains have too small combined BR to be observed.

For the 5^3S_1, the BRs to the 4^3P_J states are $\mathcal{O}(10^{-4})$ and the BRs of the 4^3P_J are $\lesssim 10^{-4}$ so this product BR is quite small. When we include BRs to interesting states such as the 3^3D_J states the product BRs are likely to be far too small to be observable. The BRs to the 3^3P_J states are comparable to the $4S \to 3P$ transitions, $\mathcal{O}(10^{-5})$ so it might be possible to see $3P$ states starting from the 5^3S_1. It is not likely that the $2D$ and $1D$ states can be

TABLE XXV. Expressions for hadronic transitions in terms of the reduced amplitudes $A_k(\ell',\ell)$. Note that reduced amplitudes are dependent on the initial and final states. Because the A_1 contributions are suppressed we follow the usual practice and will take $A_1(\ell',\ell)=0$ although we include them in the table. The details on how we obtain numerical estimates for amplitudes are described in the text.

Process	Expression
$^3S_1 \to {}^3S_1+\pi\pi$	$A_0(0,0)$
$^1S_0 \to {}^1S_0+\pi\pi$	$A_0(0,0)$
$^3P_2 \to {}^3P_2+\pi\pi$	$\frac{1}{3}A_0(1,1)+\frac{1}{4}A_1(1,1)+\frac{7}{60}A_2(1,1)$
$^3P_2 \to {}^3P_1+\pi\pi$	$\frac{1}{12}A_1(1,1)+\frac{3}{20}A_2(1,1)$
$^3P_2 \to {}^3P_0+\pi\pi$	$\frac{1}{15}A_2(1,1)$
$^3P_1 \to {}^3P_2+\pi\pi$	$\frac{5}{36}A_1(1,1)+\frac{1}{4}A_2(1,1)$
$^3P_1 \to {}^3P_1+\pi\pi$	$\frac{1}{3}A_0(1,1)+\frac{1}{12}A_1(1,1)+\frac{1}{12}A_2(1,1)$
$^3P_1 \to {}^3P_0+\pi\pi$	$\frac{1}{9}A_1(1,1)$
$^3P_0 \to {}^3P_2+\pi\pi$	$\frac{1}{3}A_2(1,1)$
$^3P_0 \to {}^3P_1+\pi\pi$	$\frac{1}{3}A_1(1,1)$
$^3P_0 \to {}^3P_0+\pi\pi$	$\frac{1}{3}A_0(1,1)$
$^1P_1 \to {}^1P_1+\pi\pi$	$\frac{1}{3}A_0(1,1)+\frac{1}{3}A_1(1,1)+\frac{1}{3}A_2(1,1)$
$^3D_3 \to {}^3D_3+\pi\pi$	$\frac{1}{5}A_0(2,2)+\frac{8}{45}A_1(2,2)+\frac{24}{175}A_2(2,2)$
$^3D_3 \to {}^3D_2+\pi\pi$	$\frac{1}{45}A_1(2,2)+\frac{2}{35}A_2(2,2)$
$^3D_3 \to {}^3D_1+\pi\pi$	$\frac{1}{175}A_2(2,2)$
$^3D_2 \to {}^3D_3+\pi\pi$	$\frac{7}{225}A_1(2,2)+\frac{2}{25}A_2(2,2)$
$^3D_2 \to {}^3D_2+\pi\pi$	$\frac{1}{5}A_0(2,2)+\frac{5}{36}A_1(2,2)+\frac{1}{20}A_2(2,2)$
$^3D_2 \to {}^3D_1+\pi\pi$	$\frac{3}{100}A_1(2,2)+\frac{7}{100}A_2(2,2)$
$^3D_1 \to {}^3D_3+\pi\pi$	$\frac{1}{75}A_2(2,2)$
$^3D_1 \to {}^3D_2+\pi\pi$	$\frac{1}{20}A_1(2,2)+\frac{7}{60}A_2(2,2)$
$^3D_1 \to {}^3D_1+\pi\pi$	$\frac{1}{5}A_0(2,2)+\frac{3}{20}A_1(2,2)+\frac{7}{100}A_2(2,2)$
$^1D_2 \to {}^1D_2+\pi\pi$	$\frac{1}{5}A_0(2,2)+\frac{1}{5}A_1(2,2)+\frac{1}{5}A_2(2,2)$
$^3D_3 \to {}^3S_1+\pi\pi$	$\frac{1}{5}A_2(2,0)$
$^3D_2 \to {}^3S_1+\pi\pi$	$\frac{1}{5}A_2(2,0)$
$^3D_1 \to {}^3S_1+\pi\pi$	$\frac{1}{5}A_2(2,0)$
$^1D_2 \to {}^1S_0+\pi\pi$	$\frac{1}{5}A_2(2,0)$
$^3F_4 \to {}^3P_2+\pi\pi$	$\frac{1}{7}A_2(3,1)$
$^3F_3 \to {}^3P_2+\pi\pi$	$\frac{1}{21}A_2(3,1)$
$^3F_3 \to {}^3P_1+\pi\pi$	$\frac{2}{21}A_2(3,1)$
$^3F_2 \to {}^3P_2+\pi\pi$	$\frac{1}{105}A_2(3,1)$
$^3F_2 \to {}^3P_1+\pi\pi$	$\frac{1}{15}A_2(3,1)$
$^3F_2 \to {}^3P_0+\pi\pi$	$\frac{1}{15}A_2(3,1)$
$^1F_3 \to {}^1P_1+\pi\pi$	$\frac{1}{7}A_2(3,1)$
$^3G_5 \to {}^3D_3+\pi\pi$	$\frac{1}{9}A_2(4,2)$
$^3G_4 \to {}^3D_3+\pi\pi$	$\frac{1}{54}A_2(4,2)$
$^3G_4 \to {}^3D_2+\pi\pi$	$\frac{5}{54}A_2(4,2)$
$^3G_3 \to {}^3D_3+\pi\pi$	$\frac{1}{630}A_2(4,2)$
$^3G_3 \to {}^3D_2+\pi\pi$	$\frac{1}{42}A_2(4,2)$
$^3G_3 \to {}^3D_1+\pi\pi$	$\frac{3}{35}A_2(4,2)$
$^1G_4 \to {}^1D_2+\pi\pi$	$\frac{1}{9}A_2(4,2)$

TABLE XXVI. The $3S$ decay chains, branching ratios and event estimates for LHCb Run II and Belle II. The numbers of events in the pp column are based on producing 3.1×10^8 $\Upsilon(3S)$'s and 1.4×10^8 $\eta_b(3S)$'s as described in the text while those in the e^+e^- column are based on 10^9 $\Upsilon(3S)$'s assuming 250 fb^{-1} integrated luminosity. The BR for each step in the decay chain is shown above the corresponding arrow, and for radiative transitions, the photon energy in keV is indicated in brackets.

Parent	Decay chain	Combined BR	Events pp	Events e^+e^-
3^3S_1	$\overset{13.1\%}{\to} 2^3P_2\gamma(86.2) \overset{1.2\%}{\to} 1^3D_3\gamma(96.5) \overset{91.0\%}{\to} 1^3P_2\gamma(256.0) \overset{19.1\%}{\to} 1^3S_1\gamma(441.6) \overset{2.48\%}{\to} \mu^+\mu^-$	6.8×10^{-6}	2100	6800
	$\overset{13.1\%}{\to} 2^3P_2\gamma(86.2) \overset{0.2\%}{\to} 1^3D_2\gamma(104.4) \overset{22\%}{\to} 1^3P_2\gamma(248.4) \overset{19.1\%}{\to} 1^3S_1\gamma(441.6) \overset{2.48\%}{\to} \mu^+\mu^-$	2.7×10^{-7}	84	270
	$\overset{13.1\%}{\to} 2^3P_2\gamma(86.2) \overset{0.2\%}{\to} 1^3D_2\gamma(104.4) \overset{74.7\%}{\to} 1^3P_1\gamma(267.3) \overset{33.9\%}{\to} 1^3S_1\gamma(423.0) \overset{2.48\%}{\to} \mu^+\mu^-$	1.6×10^{-6}	500	1600
	$\overset{13.1\%}{\to} 2^3P_2\gamma(86.2) \overset{0.02\%}{\to} 1^3D_1\gamma(78.0) \overset{1.6\%}{\to} 1^3P_2\gamma(239.1) \overset{19.1\%}{\to} 1^3S_1\gamma(441.6) \overset{2.48\%}{\to} \mu^+\mu^-$	2.0×10^{-9}	0.6	2
	$\overset{13.1\%}{\to} 2^3P_2\gamma(86.2) \overset{0.02\%}{\to} 1^3D_1\gamma(78.0) \overset{28\%}{\to} 1^3P_1\gamma(258.0) \overset{33.9\%}{\to} 1^3S_1\gamma(423.0) \overset{2.48\%}{\to} \mu^+\mu^-$	6.2×10^{-8}	19	62
	$\overset{13.1\%}{\to} 2^3P_2\gamma(86.2) \overset{0.02\%}{\to} 1^3D_1\gamma(78.0) \overset{47.1\%}{\to} 1^3P_0\gamma(290.5) \overset{1.76\%}{\to} 1^3S_1\gamma(391.1) \overset{2.48\%}{\to} \mu^+\mu^-$	5.4×10^{-9}	2	5
	$\overset{13.1\%}{\to} 2^3P_2\gamma(86.2) \overset{0.02\%}{\to} 1^3D_1\gamma(78.0) \overset{0.00393\%}{\to} \mu^+\mu^-$	1.0×10^{-9}	0.3	1
	$\overset{12.6\%}{\to} 2^3P_1\gamma(99.3) \overset{1.9\%}{\to} 1^3D_2\gamma(91.3) \overset{22\%}{\to} 1^3P_2\gamma(248.4) \overset{19.1\%}{\to} 1^3S_1\gamma(441.6) \overset{2.48\%}{\to} \mu^+\mu^-$	2.5×10^{-6}	780	2500
	$\overset{12.6\%}{\to} 2^3P_1\gamma(99.3) \overset{1.9\%}{\to} 1^3D_2\gamma(91.3) \overset{74.7\%}{\to} 1^3P_1\gamma(267.3) \overset{33.9\%}{\to} 1^3S_1\gamma(423.0) \overset{2.48\%}{\to} \mu^+\mu^-$	1.5×10^{-5}	4650	15,000
	$\overset{12.6\%}{\to} 2^3P_1\gamma(99.3) \overset{0.80\%}{\to} 1^3D_1\gamma(100.8) \overset{1.6\%}{\to} 1^3P_2\gamma(239.1) \overset{19.1\%}{\to} 1^3S_1\gamma(441.6) \overset{2.48\%}{\to} \mu^+\mu^-$	7.6×10^{-8}	24	76
	$\overset{12.6\%}{\to} 2^3P_1\gamma(99.3) \overset{0.80\%}{\to} 1^3D_1\gamma(100.8) \overset{28\%}{\to} 1^3P_1\gamma(258.0) \overset{33.9\%}{\to} 1^3S_1\gamma(423.0) \overset{2.48\%}{\to} \mu^+\mu^-$	2.4×10^{-6}	740	2400
	$\overset{12.6\%}{\to} 2^3P_1\gamma(99.3) \overset{0.80\%}{\to} 1^3D_1\gamma(100.8) \overset{47.1\%}{\to} 1^3P_0\gamma(290.5) \overset{1.76\%}{\to} 1^3S_1\gamma(391.1) \overset{2.48\%}{\to} \mu^+\mu^-$	2.1×10^{-7}	65	210
	$\overset{5.9\%}{\to} 2^3P_0\gamma(122.0) \overset{0.4\%}{\to} 1^3D_1\gamma(78.0) \overset{1.6\%}{\to} 1^3P_2\gamma(239.1) \overset{19.1\%}{\to} 1^3S_1\gamma(441.6) \overset{2.48\%}{\to} \mu^+\mu^-$	1.8×10^{-8}	6	18
	$\overset{5.9\%}{\to} 2^3P_0\gamma(122.0) \overset{0.4\%}{\to} 1^3D_1\gamma(78.0) \overset{28\%}{\to} 1^3P_1\gamma(258.0) \overset{33.9\%}{\to} 1^3S_1\gamma(423.0) \overset{2.48\%}{\to} \mu^+\mu^-$	5.6×10^{-7}	170	560
	$\overset{5.9\%}{\to} 2^3P_0\gamma(122.0) \overset{0.4\%}{\to} 1^3D_1\gamma(78.0) \overset{47.1\%}{\to} 1^3P_0\gamma(290.5) \overset{1.76\%}{\to} 1^3S_1\gamma(391.1) \overset{2.48\%}{\to} \mu^+\mu^-$	4.8×10^{-8}	15	48
3^1S_0	$\overset{1.8\times10^{-6}}{\to} 2^3S_1\gamma(309.2) \overset{1.93\%}{\to} \mu^+\mu^-$	3.4×10^{-8}	5	NA
	$\overset{1.5\times10^{-5}}{\to} 1^3S_1\gamma(840.0) \overset{2.48\%}{\to} \mu^+\mu^-$	3.7×10^{-7}	52	NA

observed in decay chains originating from the 5^3S_1. We arrive at similar conclusions for the 6^3S_1 and conclude that the only possible states that might be observed are the 3^3P_J states.

3. The 2P states

The $2P$ states are of course well known. We include them as they can decay to the $1D$ states and hence contribute to the $1D$ event rates which was the discovery channel for the 1^3D_2 state [98] (see also Ref. [99]). We only include event chains relevant to these final states which we list in Table XXVIII. In an attempt to reduce the theoretical uncertainties in the $2P \to 1D$ BRs, rather than using the predictions for total widths and BRs in Table IX we estimate the $\chi_{bJ}(2P)$ total widths using the PDG values [32] for the BRs for the $2P \to 2S + \gamma$ and $2P \to 1S + \gamma$ transitions together with our predictions for these partial widths as was described in Sec. V B. The values for $\Gamma(2^3P_2)$ and $\Gamma(2^3P_1)$ were given there. Similarly we find $\Gamma(2^3P_0) = 247 \pm 93$ keV. Combining these total widths with the partial widths for $2P \to 1D$ transitions given in Table IX, $\Gamma(2^3P_2 \to 1^3D_{3,2,1}) = 1.5$, 0.3 and 0.03 keV respectively, we obtain the corresponding BRs of 1.2%, 0.2% and 0.02%. Likewise $\Gamma(2^3P_1 \to 1^3D_{2,1}) = 1.2$ and 0.5 keV give the corresponding BRs 1.9% and 0.80%, and $\Gamma(2^3P_0 \to 1^3D_1) = 1.0$ keV has BR = 0.4%. There is uncertainty in these estimates as can be seen by comparing the PDG values [32] we used in our estimates to recent *BABAR* measurements [100] and by comparing our predictions for the partial widths to those of Kwong and Rosner [35]. Nevertheless these estimates are sufficient for estimating the $2P \to 1D + \gamma$ BRs and the resulting event rates for the purposes of identifying promising channels. The important point is that in all cases, significant numbers of bottomonium D-waves will be produced from P-wave production and decay which will improve the statistics from those that are produced directly.

4. The 3P states

The observation of the $\chi_b(3P)$ by the ATLAS Collaboration [1] through its radiative transitions to $\Upsilon(1S)$ and $\Upsilon(2S)$ with $\Upsilon(1S, 2S) \to \mu^+\mu^-$ was the first new particle discovered at the LHC. This decay chain represents a clean experimental signature with the two final state muons a clean signal to trigger on. The $\chi_b(3P)$ was confirmed by the D0 Collaboration [101] and by the LHCb Collaboration [33,34]. Further, LHCb identified the state as the $\chi_{b1}(3P)$ with mass $10515.7^{+2.2}_{-3.9}(\text{stat})^{+1.5}_{-2.1}(\text{syst})$ MeV/c^2 [33]. Using the approach outlined above we calculate for

TABLE XXVII. 4^3S_1 decay chains, branching ratios and event estimates for LHCb Run II and Belle II. The numbers of events in the pp column are based on producing 2.3×10^8 $\Upsilon(4S)$s as described in the text while those in the e^+e^- column are based on 10^{10} $\Upsilon(4S)$'s assuming $10\,\mathrm{ab}^{-1}$ integrated luminosity. The BRs for the hadronic transitions were taken from the PDG [32].

Parent	Decay chain	Combined BR	Events pp	Events e^+e^-
4^3S_1	$\xrightarrow{1.57\times10^{-5}} \mu^+\mu^-$	1.6×10^{-5}	3680	1.6×10^5
	$\xrightarrow{3.7\times10^{-5}} 3^3P_2\gamma(50.8) \xrightarrow{3.8\%} 3^3S_1\ \gamma(171.6) \xrightarrow{2.18\%} \mu^+\mu^-$	3.1×10^{-8}	7	310
	$\xrightarrow{3.7\times10^{-5}} 3^3P_2\gamma(50.8) \xrightarrow{1.8\%} 2^3S_1\ \gamma(492.9) \xrightarrow{1.93\%} \mu^+\mu^-$	1.3×10^{-8}	3	130
	$\xrightarrow{3.7\times10^{-5}} 3^3P_2\gamma(50.8) \xrightarrow{1.1\%} 1^3S_1\ \gamma(1013.8) \xrightarrow{2.48\%} \mu^+\mu^-$	1.0×10^{-8}	2	100
	$\xrightarrow{3.7\times10^{-5}} 3^3P_2\gamma(50.8) \xrightarrow{3.8\%} 3^3S_1\ \gamma(171.6) \xrightarrow{2.82\%} 2^3S_1\pi^+\pi^- \xrightarrow{1.93\%} \mu^+\mu^-$	7.7×10^{-10}	0.2	8
	$\xrightarrow{3.7\times10^{-5}} 3^3P_2\gamma(50.8) \xrightarrow{3.8\%} 3^3S_1\ \gamma(171.6) \xrightarrow{4.37\%} 1^3S_1\pi^+\pi^- \xrightarrow{2.48\%} \mu^+\mu^-$	1.5×10^{-9}	0.3	15
	$\xrightarrow{3.7\times10^{-5}} 3^3P_2\gamma(50.8) \xrightarrow{1.8\%} 2^3S_1\ \gamma(492.9) \xrightarrow{17.85\%} 1^3S_1\pi^+\pi^- \xrightarrow{2.48\%} \mu^+\mu^-$	2.9×10^{-9}	0.7	29
	$\xrightarrow{3.7\times10^{-5}} 3^3P_2\gamma(50.8) \xrightarrow{0.61\%} 2^3D_3\ \gamma(72.7) \xrightarrow{65.1\%} 2^3P_2\gamma(185.0) \xrightarrow{10.6\%} 2^3S_1\gamma(242.5) \xrightarrow{1.93\%} \mu^+\mu^-$	3.0×10^{-10}	0.07	3
	$\xrightarrow{3.7\times10^{-5}} 3^3P_2\gamma(50.8) \xrightarrow{0.61\%} 2^3D_3\ \gamma(72.7) \xrightarrow{65.1\%} 2^3P_2\gamma(185.0) \xrightarrow{7.0\%} 1^3S_1\gamma(776.5) \xrightarrow{2.48\%} \mu^+\mu^-$	2.6×10^{-10}	0.06	3
	$\xrightarrow{3.7\times10^{-5}} 3^3P_2\gamma(50.8) \xrightarrow{0.61\%} 2^3D_3\ \gamma(72.7) \xrightarrow{10\%} 1^3P_2\gamma(529.0) \xrightarrow{19.1\%} 1^3S_1\gamma(441.6) \xrightarrow{2.48\%} \mu^+\mu^-$	1.1×10^{-10}	0.03	1
	$\xrightarrow{3.7\times10^{-5}} 3^3P_2\gamma(50.8) \xrightarrow{0.61\%} 2^3D_3\ \gamma(72.7) \xrightarrow{6.7\%} 1^3F_4\gamma(96.7)$ $\xrightarrow{100\%} 1^3D_3\gamma(200.9) \xrightarrow{91.0\%} 1^3P_2\gamma(256.0) \xrightarrow{19.1\%} 1^3S_1\gamma(441.6) \xrightarrow{2.48\%} \mu^+\mu^-$	6.5×10^{-11}	0.01	0.6
	$\xrightarrow{3.7\times10^{-5}} 3^3P_2\gamma(50.8) \xrightarrow{0.019\%} 1^3D_3\gamma(350.0) \xrightarrow{91.0\%} 1^3P_2\gamma(256.0) \xrightarrow{19.1\%} 1^3S_1\gamma(441.6) \xrightarrow{2.48\%} \mu^+\mu^-$	3.0×10^{-11}	...	0.3
	$\xrightarrow{3.7\times10^{-5}} 3^3P_2\gamma(50.8) \xrightarrow{0.13\%} 2^3D_2\ \gamma(78.7) \xrightarrow{56.2\%} 2^3P_1\gamma(191.6) \xrightarrow{19.9\%} 2^3S_1\gamma(229.6) \xrightarrow{1.93\%} \mu^+\mu^-$	1.0×10^{-10}	0.02	1
	$\xrightarrow{3.8\times10^{-5}} 3^3P_1\gamma(62.8) \xrightarrow{7.2\%} 3^3S_1\ \gamma(159.8) \xrightarrow{2.18\%} \mu^+\mu^-$	6.1×10^{-8}	15	610
	$\xrightarrow{3.8\times10^{-5}} 3^3P_1\gamma(62.8) \xrightarrow{2.6\%} 2^3S_1\ \gamma(481.4) \xrightarrow{1.93\%} \mu^+\mu^-$	1.9×10^{-8}	4	190
	$\xrightarrow{3.8\times10^{-5}} 3^3P_1\gamma(62.8) \xrightarrow{1.1\%} 1^3S_1\ \gamma(1003.0) \xrightarrow{2.48\%} \mu^+\mu^-$	1.0×10^{-8}	2	100
	$\xrightarrow{3.8\times10^{-5}} 3^3P_1\gamma(62.8) \xrightarrow{7.2\%} 3^3S_1\ \gamma(159.8) \xrightarrow{2.82\%} 2^3S_1\pi^+\pi^- \xrightarrow{1.93\%} \mu^+\mu^-$	1.5×10^{-9}	0.3	15
	$\xrightarrow{3.8\times10^{-5}} 3^3P_1\gamma(62.8) \xrightarrow{7.2\%} 3^3S_1\ \gamma(159.8) \xrightarrow{4.37\%} 1^3S_1\pi^+\pi^- \xrightarrow{2.48\%} \mu^+\mu^-$	3.0×10^{-9}	0.7	30
	$\xrightarrow{3.8\times10^{-5}} 3^3P_1\gamma(62.8) \xrightarrow{2.6\%} 2^3S_1\ \gamma(481.4) \xrightarrow{17.85\%} 1^3S_1\pi^+\pi^- \xrightarrow{2.48\%} \mu^+\mu^-$	4.4×10^{-9}	1	44
	$\xrightarrow{3.8\times10^{-5}} 3^3P_1\gamma(62.8) \xrightarrow{0.94\%} 2^3D_2\ \gamma(66.8) \xrightarrow{17\%} 2^3P_2\gamma(178.6) \xrightarrow{10.6\%} 2^3S_1\gamma(242.5) \xrightarrow{1.93\%} \mu^+\mu^-$	1.2×10^{-10}	0.03	1
	$\xrightarrow{3.8\times10^{-5}} 3^3P_1\gamma(62.8) \xrightarrow{0.94\%} 2^3D_2\ \gamma(66.8) \xrightarrow{17\%} 2^3P_2\gamma(178.6) \xrightarrow{7.0\%} 1^3S_1\gamma(776.5) \xrightarrow{2.48\%} \mu^+\mu^-$	1.0×10^{-10}	0.02	1
	$\xrightarrow{3.8\times10^{-5}} 3^3P_1\gamma(62.8) \xrightarrow{0.94\%} 2^3D_2\ \gamma(66.8) \xrightarrow{56.2\%} 2^3P_1\gamma(191.6) \xrightarrow{19.9\%} 2^3S_1\gamma(229.6) \xrightarrow{1.93\%} \mu^+\mu^-$	7.7×10^{-10}	0.2	8
	$\xrightarrow{3.8\times10^{-5}} 3^3P_1\gamma(62.8) \xrightarrow{0.94\%} 2^3D_2\ \gamma(66.8) \xrightarrow{56.2\%} 2^3P_1\gamma(191.6) \xrightarrow{9.2\%} 1^3S_1\gamma(764.3) \xrightarrow{2.48\%} \mu^+\mu^-$	4.6×10^{-10}	0.1	5
	$\xrightarrow{3.8\times10^{-5}} 3^3P_1\gamma(62.8) \xrightarrow{0.94\%} 2^3D_2\ \gamma(66.8) \xrightarrow{12\%} 1^3P_1\gamma(541.2) \xrightarrow{33.9\%} 1^3S_1\gamma(423.0) \xrightarrow{2.48\%} \mu^+\mu^-$	3.6×10^{-10}	0.08	4
	$\xrightarrow{3.8\times10^{-5}} 3^3P_1\gamma(62.8) \xrightarrow{0.40\%} 2^3D_1\ \gamma(74.7) \xrightarrow{17\%} 2^3P_1\gamma(183.9) \xrightarrow{19.9\%} 2^3S_1\gamma(229.6) \xrightarrow{1.93\%} \mu^+\mu^-$	9.9×10^{-11}	0.02	1
	$\xrightarrow{3.8\times10^{-5}} 3^3P_1\gamma(62.8) \xrightarrow{0.40\%} 2^3D_1\ \gamma(74.7) \xrightarrow{28.1\%} 2^3P_0\gamma(206.4) \xrightarrow{0.9\%} 1^3S_1\gamma(743.1) \xrightarrow{2.48\%} \mu^+\mu^-$	9.5×10^{-12}	...	0.1
	$\xrightarrow{2.2\times10^{-5}} 3^3P_0\gamma(78.7) \xrightarrow{0.31\%} 3^3S_1\ \gamma(144.0) \xrightarrow{2.18\%} \mu^+\mu^-$	1.5×10^{-9}	0.3	15
	$\xrightarrow{2.2\times10^{-5}} 3^3P_0\gamma(78.7) \xrightarrow{0.077\%} 2^3S_1\ \gamma(466.2) \xrightarrow{1.93\%} \mu^+\mu^-$	3.3×10^{-10}	0.08	3
	$\xrightarrow{2.2\times10^{-5}} 3^3P_0\gamma(78.7) \xrightarrow{0.01\%} 1^3S_1\ \gamma(1003.0) \xrightarrow{2.48\%} \mu^+\mu^-$	5.5×10^{-11}	0.01	0.6
	$\xrightarrow{2.2\times10^{-5}} 3^3P_0\gamma(78.7) \xrightarrow{0.31\%} 3^3S_1\ \gamma(144.0) \xrightarrow{2.82\%} 2^3S_1\pi^+\pi^- \xrightarrow{1.93\%} \mu^+\mu^-$	3.7×10^{-11}	...	0.4
	$\xrightarrow{2.2\times10^{-5}} 3^3P_0\gamma(78.7) \xrightarrow{0.31\%} 3^3S_1\ \gamma(144.0) \xrightarrow{4.37\%} 1^3S_1\pi^+\pi^- \xrightarrow{2.48\%} \mu^+\mu^-$	7.4×10^{-11}	0.02	1
	$\xrightarrow{2.2\times10^{-5}} 3^3P_0\gamma(78.7) \xrightarrow{0.077\%} 2^3S_1\ \gamma(466.2) \xrightarrow{17.85\%} 1^3S_1\pi^+\pi^- \xrightarrow{2.48\%} \mu^+\mu^-$	7.5×10^{-11}	0.02	1
	$\xrightarrow{2.2\times10^{-5}} 3^3P_0\gamma(78.7) \xrightarrow{0.045\%} 2^3D_1\gamma(58.8) \xrightarrow{17\%} 2^3P_1\gamma(183.9) \xrightarrow{19.9\%} 2^3S_1\gamma(229.6) \xrightarrow{1.93\%} \mu^+\mu^-$	6.5×10^{-12}	...	0.06
	$\xrightarrow{2.2\times10^{-5}} 3^3P_0\gamma(78.7) \xrightarrow{0.0091\%} 1^3D_1\gamma(340.2) \xrightarrow{1.6\%} 1^3P_2\gamma(239.1) \xrightarrow{19.1\%} 1^3S_1\gamma(441.6) \xrightarrow{2.48\%} \mu^+\mu^-$	1.5×10^{-13}	...	...
	$\xrightarrow{2.2\times10^{-5}} 3^3P_0\gamma(78.7) \xrightarrow{0.0091\%} 1^3D_1\gamma(340.2) \xrightarrow{28\%} 1^3P_1\gamma(258.0) \xrightarrow{33.9\%} 1^3S_1\gamma(423.0) \xrightarrow{2.48\%} \mu^+\mu^-$	4.7×10^{-12}	...	...
	$\xrightarrow{2.2\times10^{-5}} 3^3P_0\gamma(78.7) \xrightarrow{0.0091\%} 1^3D_1\gamma(340.2) \xrightarrow{47.1\%} 1^3P_0\gamma(290.5) \xrightarrow{1.76\%} 1^3S_1\gamma(391.1) \xrightarrow{2.48\%} \mu^+\mu^-$	4.1×10^{-13}	...	...

TABLE XXVIII. The $2P$ decay chains, branching ratios and event estimates for LHCb Run II. These are based on producing 1.0×10^7 $\chi_{b2}(2P)$'s, 9.1×10^6 $\chi_{b1}(2P)$'s, 4.7×10^6 $\chi_{b0}(2P)$'s and 7.4×10^6 $h_b(2P)$'s as described in the text.

Parent	Decay chain	Combined BR	Events
2^3P_2	$\overset{1.2\%}{\to} 1^3D_3\gamma(96.5) \overset{91.0\%}{\to} 1^3P_2\gamma(256.0) \overset{19.1\%}{\to} 1^3S_1\gamma(441.6) \overset{2.48\%}{\to} \mu^+\mu^-$	5.2×10^{-5}	517
	$\overset{0.2\%}{\to} 1^3D_2\gamma(104.4) \overset{22\%}{\to} 1^3P_2\gamma(248.4) \overset{19.1\%}{\to} 1^3S_1\gamma(441.6) \overset{2.48\%}{\to} \mu^+\mu^-$	2.1×10^{-6}	21
	$\overset{0.2\%}{\to} 1^3D_2\gamma(104.4) \overset{74.7\%}{\to} 1^3P_1\gamma(267.3) \overset{33.9\%}{\to} 1^3S_1\gamma(423.0) \overset{2.48\%}{\to} \mu^+\mu^-$	1.2×10^{-5}	124
2^3P_1	$\overset{1.9\%}{\to} 1^3D_2\gamma(91.3) \overset{22\%}{\to} 1^3P_2\gamma(248.4) \overset{19.1\%}{\to} 1^3S_1\gamma(441.6) \overset{2.48\%}{\to} \mu^+\mu^-$	2.0×10^{-5}	180
	$\overset{1.9\%}{\to} 1^3D_2\gamma(91.3) \overset{74.7\%}{\to} 1^3P_1\gamma(267.3) \overset{33.9\%}{\to} 1^3S_1\gamma(423.0) \overset{2.48\%}{\to} \mu^+\mu^-$	1.2×10^{-4}	1100
	$\overset{0.80\%}{\to} 1^3D_1\gamma(100.8) \overset{1.6\%}{\to} 1^3P_2\gamma(239.1) \overset{19.1\%}{\to} 1^3S_1\gamma(441.6) \overset{2.48\%}{\to} \mu^+\mu^-$	6.1×10^{-7}	6
	$\overset{0.80\%}{\to} 1^3D_1\gamma(100.8) \overset{28\%}{\to} 1^3P_1\gamma(258.0) \overset{33.9\%}{\to} 1^3S_1\gamma(423.0) \overset{2.48\%}{\to} \mu^+\mu^-$	1.9×10^{-5}	174
	$\overset{0.80\%}{\to} 1^3D_1\gamma(100.8) \overset{47.1\%}{\to} 1^3P_0\gamma(290.5) \overset{1.76\%}{\to} 1^3S_1\gamma(391.1) \overset{2.48\%}{\to} \mu^+\mu^-$	1.6×10^{-6}	15
2^3P_0	$\overset{0.4\%}{\to} 1^3D_1\gamma(78.0) \overset{1.6\%}{\to} 1^3P_2\gamma(239.1) \overset{19.1\%}{\to} 1^3S_1\gamma(441.6) \overset{2.48\%}{\to} \mu^+\mu^-$	3.0×10^{-7}	1
	$\overset{0.4\%}{\to} 1^3D_1\gamma(78.0) \overset{28\%}{\to} 1^3P_1\gamma(258.0) \overset{33.9\%}{\to} 1^3S_1\gamma(423.0) \overset{2.48\%}{\to} \mu^+\mu^-$	9.4×10^{-6}	44
2^1P_1	$\overset{2.0\%}{\to} 1^1D_2\gamma(111.4) \overset{91.5\%}{\to} 1^1P_1\gamma(262.5) \overset{49\%}{\to} 1^1S_0\gamma(488.3) \overset{100\%}{\to} gg$	9.0×10^{-3}	6.6×10^4
	$\overset{48\%}{\to} 2^1S_0\ \gamma(257.7) \overset{100\%}{\to} gg$	0.48	3.6×10^6
	$\overset{22\%}{\to} 1^1S_0\ \gamma(825.8) \overset{100\%}{\to} gg$	0.22	1.6×10^6

Run I ~243 events for the decay chain $\chi(3P) \to \Upsilon(1S) \to \mu^+\mu^-$, ~371 for the $\Upsilon(2S)$ decay chain, and ~1030 for the $\Upsilon(3S)$ decay chain compared to the observed numbers of events of 329 ± 59, 121 ± 31 and 182 ± 23 respectively [34]. The agreement is reasonable for the $\Upsilon(1S)$ chain but becomes decreasingly so for the $\Upsilon(2S)$ and $\Upsilon(3S)$ chains. We assume this is due to decreasing photon detection efficiency as the photon energy goes down. Overall the agreement is not unreasonable considering the approximations used to obtain these values and our neglect of detector efficiencies and helps the reader judge the general reliability of our predictions for event rates.

In Table XXIX we summarize the event rates expected for the most promising decay chains. The $\chi_{b0}(3P)$ state is much broader and decays predominantly to light hadrons via gluon intermediate states with a small BR to $\gamma\Upsilon(1S)$ ($\sim 10^{-4}$) so it would be quite challenging to observe although it might be possible to observe via hadronic transitions to the 1^3P_2 state which subsequently undergoes a radiative transition to the 1^3S_1 state.

For both the $\chi_{b2}(3P)$ and $\chi_{b1}(3P)$ the decay chains to $\Upsilon(nS) \to \mu^+\mu^-$ where $n = 1, 2, 3$ give rise to the largest event rates and are the simplest to reconstruct so it is not surprising that these were the discovery channels. Run II should provide sufficient statistics to separately fit the $\chi_{b2}(3P)$ and $\chi_{b1}(3P)$ using these decay chains. Other decay chains are potentially interesting as they involve the undiscovered 2^3D_3, 2^3D_2, 2^3D_1, 1^3D_3, 1^3F_4 and 1^3F_3 $b\bar{b}$ states. However they generally have multiple photons in the final state making it difficult to reconstruct the initial particle. In addition, some of the photons in the decay chains are relatively low energy so could have low detection efficiencies. The one exception is $3^3P_1 \to 2^3D_1\gamma \to \mu^+\mu^-$. This final state is relatively clean but has a low combined BR. As we noted, we would not be surprised if our production rates are off by an order of magnitude so we do not rule out the possibility that the 2^3D_1 could be observed in this process.

We do not include decay chains for the $h_b(3P)$ state, with two exceptions, as we believe it would be very difficult to reconstruct in a hadronic environment for the following reasons. It decays predominantly to hadronic final states (~70% of the time) which would be difficult to identify in hadron collisions. The next largest BRs are to the $\eta_b(3S)$, $\eta_b(2S)$ and $\eta_b(1S)$. All of these decay almost 100% of the time to hadronic final states. The $\eta_b(3S)$ and $\eta_b(2S)$ have small BRs to $h_b(nP)$ and very small BRs to $\Upsilon(1S)$. While there are several hundred h_b's produced they would be difficult to see and the combined BR to $\Upsilon(1S) \to \mu^+\mu^-$ is too small to produce sufficient numbers to observe. We include the decay chain $h_b(3P) \to \eta_b(1S)\gamma \to gg$ as it might be possible to reconstruct the $h_b(3P)$ using the one final state photon and possibly simple η_b hadronic final states and likewise the decay chain $h_b(3P) \to h_b(1P) + \pi\pi \to \eta_b(1S)\gamma \to gg$ for the same reasons.

5. The 4P and 5P states

The $4P$ and $5P$ states are above $B\bar{B}$ threshold and have total widths of the order of tens of MeV so that BRs for radiative transitions are relatively small, $\mathcal{O}(10^{-4})$. However they undergo radiative transitions to $\Upsilon(nS)$ states which decay to $\mu^+\mu^-$ offering a clean final state to study. Our estimates for the expected number of events from these decay chains are given in Table XXX. While the number of

TABLE XXIX. 3^3P_J decay chains, branching ratios and event estimates for LHCb Run II. These are based on producing 9.9×10^6 $\chi_{b2}(3P)$'s, 7.9×10^6 $\chi_{b1}(3P)$'s, 3.5×10^6 $\chi_{b0}(3P)$'s and 7.3×10^6 $h_b(3P)$'s as described in the text.

Parent	Decay chain	Combined BR	Events
3^3P_2	$\overset{3.8\%}{\to} 3^3S_1\ \gamma(171.6) \overset{2.18\%}{\to} \mu^+\mu^-$	8.3×10^{-4}	8,240
	$\overset{1.8\%}{\to} 2^3S_1\ \gamma(492.9) \overset{1.93\%}{\to} \mu^+\mu^-$	3.5×10^{-4}	3,460
	$\overset{1.1\%}{\to} 1^3S_1\ \gamma(1013.8) \overset{2.48\%}{\to} \mu^+\mu^-$	2.7×10^{-4}	2,710
	$\overset{0.28\%}{\to} 1^3P_2\pi\pi \overset{19.1\%}{\to} 1^3S_1\gamma(441.6) \overset{2.48\%}{\to} \mu^+\mu^-$	1.3×10^{-5}	132
	$\overset{0.21\%}{\to} 1^3P_1\pi\pi \overset{33.9\%}{\to} 1^3S_1\gamma(423.0) \overset{2.48\%}{\to} \mu^+\mu^-$	1.8×10^{-5}	173
	$\overset{0.61\%}{\to} 2^3D_3\ \gamma(72.7) \overset{65.1\%}{\to} 2^3P_2\gamma(185.0) \overset{10.6\%}{\to} 2^3S_1\gamma(242.5) \overset{1.93\%}{\to} \mu^+\mu^-$	8.1×10^{-6}	80
	$\overset{0.61\%}{\to} 2^3D_3\ \gamma(72.7) \overset{65.1\%}{\to} 2^3P_2\gamma(185.0) \overset{7.0\%}{\to} 1^3S_1\gamma(776.5) \overset{2.48\%}{\to} \mu^+\mu^-$	6.9×10^{-6}	68
	$\overset{0.61\%}{\to} 2^3D_3\ \gamma(72.7) \overset{10\%}{\to} 1^3P_2\gamma(529.0) \overset{19.1\%}{\to} 1^3S_1\gamma(441.6) \overset{2.48\%}{\to} \mu^+\mu^-$	2.9×10^{-6}	29
	$\overset{0.61\%}{\to} 2^3D_3\ \gamma(72.7) \overset{6.7\%}{\to} 1^3F_4\gamma(96.7) \overset{100\%}{\to} 1^3D_3\gamma(200.9) \overset{91.0\%}{\to} 1^3P_2\gamma(256.0)$ $\overset{19.1\%}{\to} 1^3S_1\gamma(441.6) \overset{2.48\%}{\to} \mu^+\mu^-$	1.8×10^{-6}	18
	$\overset{0.019\%}{\to} 1^3D_3\gamma(350.0) \overset{91.0\%}{\to} 1^3P_2\gamma(256.0) \overset{19.1\%}{\to} 1^3S_1\gamma(441.6) \overset{2.48\%}{\to} \mu^+\mu^-$	8.2×10^{-7}	8
	$\overset{0.13\%}{\to} 2^3D_2\ \gamma(78.7) \overset{17\%}{\to} 2^3P_2\gamma(178.6) \overset{10.6\%}{\to} 2^3S_1\gamma(242.5) \overset{1.93\%}{\to} \mu^+\mu^-$	4.5×10^{-7}	4
	$\overset{0.13\%}{\to} 2^3D_2\ \gamma(78.7) \overset{17\%}{\to} 2^3P_2\gamma(178.6) \overset{7.0\%}{\to} 1^3S_1\gamma(776.5) \overset{2.48\%}{\to} \mu^+\mu^-$	3.8×10^{-7}	4
	$\overset{0.13\%}{\to} 2^3D_2\ \gamma(78.7) \overset{56.2\%}{\to} 2^3P_1\gamma(191.6) \overset{19.9\%}{\to} 2^3S_1\gamma(229.6) \overset{1.93\%}{\to} \mu^+\mu^-$	2.8×10^{-6}	28
	$\overset{0.13\%}{\to} 2^3D_2\ \gamma(78.7) \overset{56.2\%}{\to} 2^3P_1\gamma(191.6) \overset{9.2\%}{\to} 1^3S_1\gamma(764.3) \overset{2.48\%}{\to} \mu^+\mu^-$	1.7×10^{-6}	17
	$\overset{0.13\%}{\to} 2^3D_2\ \gamma(78.7) \overset{12\%}{\to} 1^3P_1\gamma(541.2) \overset{33.9\%}{\to} 1^3S_1\gamma(423.0) \overset{2.48\%}{\to} \mu^+\mu^-$	1.3×10^{-6}	13
	$\overset{0.13\%}{\to} 2^3D_2\ \gamma(78.7) \overset{6.6\%}{\to} 1^3F_3\gamma(93.7) \overset{89.3\%}{\to} 1^3D_2\gamma(189.2) \overset{74.7\%}{\to} 1^3P_1\gamma(267.3)$ $\overset{33.9\%}{\to} 1^3S_1\gamma(423.0) \overset{2.48\%}{\to} \mu^+\mu^-$	4.8×10^{-7}	5
3^3P_1	$\overset{7.2\%}{\to} 3^3S_1\ \gamma(159.8) \overset{2.18\%}{\to} \mu^+\mu^-$	1.6×10^{-3}	12,360
	$\overset{2.6\%}{\to} 2^3S_1\ \gamma(481.4) \overset{1.93\%}{\to} \mu^+\mu^-$	5.0×10^{-4}	3,950
	$\overset{1.1\%}{\to} 1^3S_1\ \gamma(1003.0) \overset{2.48\%}{\to} \mu^+\mu^-$	2.7×10^{-4}	2,150
	$\overset{0.75\%}{\to} 1^3P_2\pi\pi \overset{19.1\%}{\to} 1^3S_1\gamma(441.6) \overset{2.48\%}{\to} \mu^+\mu^-$	3.5×10^{-5}	278
	$\overset{0.48\%}{\to} 1^3P_1\pi\pi \overset{33.9\%}{\to} 1^3S_1\gamma(423.0) \overset{2.48\%}{\to} \mu^+\mu^-$	4.0×10^{-5}	317
	$\overset{0.40\%}{\to} 2^3D_1\ \gamma(74.7) \overset{5.3\times10^{-3}\%}{\to} \mu^+\mu^-$	2.1×10^{-7}	2
	$\overset{0.94\%}{\to} 2^3D_2\ \gamma(66.8) \overset{17\%}{\to} 2^3P_2\gamma(178.6) \overset{10.6\%}{\to} 2^3S_1\gamma(242.5) \overset{1.93\%}{\to} \mu^+\mu^-$	3.3×10^{-6}	26
	$\overset{0.94\%}{\to} 2^3D_2\ \gamma(66.8) \overset{17\%}{\to} 2^3P_2\gamma(178.6) \overset{7.0\%}{\to} 1^3S_1\gamma(776.5) \overset{2.48\%}{\to} \mu^+\mu^-$	2.8×10^{-6}	22
	$\overset{0.94\%}{\to} 2^3D_2\ \gamma(66.8) \overset{56.2\%}{\to} 2^3P_1\gamma(191.6) \overset{19.9\%}{\to} 2^3S_1\gamma(229.6) \overset{1.93\%}{\to} \mu^+\mu^-$	2.0×10^{-5}	158
	$\overset{0.94\%}{\to} 2^3D_2\ \gamma(66.8) \overset{56.2\%}{\to} 2^3P_1\gamma(191.6) \overset{9.2\%}{\to} 1^3S_1\gamma(764.3) \overset{2.48\%}{\to} \mu^+\mu^-$	1.2×10^{-5}	95
	$\overset{0.94\%}{\to} 2^3D_2\ \gamma(66.8) \overset{2\%}{\to} 1^3P_2\gamma(522.8) \overset{19.1\%}{\to} 1^3S_1\gamma(441.6) \overset{2.48\%}{\to} \mu^+\mu^-$	8.9×10^{-7}	7
	$\overset{0.94\%}{\to} 2^3D_2\ \gamma(66.8) \overset{12\%}{\to} 1^3P_1\gamma(541.2) \overset{33.9\%}{\to} 1^3S_1\gamma(423.0) \overset{2.48\%}{\to} \mu^+\mu^-$	1.1×10^{-5}	87
	$\overset{0.94\%}{\to} 2^3D_2\ \gamma(66.8) \overset{6.6\%}{\to} 1^3F_3\gamma(93.7) \overset{89.3\%}{\to} 1^3D_2\gamma(189.2) \overset{74.7\%}{\to} 1^3P_1\gamma(267.3)$ $\overset{33.9\%}{\to} 1^3S_1\gamma(423.0) \overset{2.48\%}{\to} \mu^+\mu^-$	3.5×10^{-6}	28
	$\overset{0.40\%}{\to} 2^3D_1\ \gamma(74.7) \overset{17\%}{\to} 2^3P_1\gamma(183.9) \overset{19.9\%}{\to} 2^3S_1\gamma(229.6) \overset{1.93\%}{\to} \mu^+\mu^-$	2.6×10^{-6}	21
	$\overset{0.40\%}{\to} 2^3D_1\ \gamma(74.7) \overset{17\%}{\to} 2^3P_1\gamma(183.9) \overset{9.2\%}{\to} 1^3S_1\gamma(764.3) \overset{2.48\%}{\to} \mu^+\mu^-$	1.6×10^{-6}	12
	$\overset{0.40\%}{\to} 2^3D_1\ \gamma(74.7) \overset{28.1\%}{\to} 2^3P_0\gamma(206.4) \overset{4.6\%}{\to} 2^3S_1\gamma(207.1) \overset{1.93\%}{\to} \mu^+\mu^-$	1.0×10^{-6}	8
	$\overset{0.40\%}{\to} 2^3D_1\ \gamma(74.7) \overset{28.1\%}{\to} 2^3P_0\gamma(206.4) \overset{0.9\%}{\to} 1^3S_1\gamma(743.1) \overset{2.48\%}{\to} \mu^+\mu^-$	2.5×10^{-7}	2
	$\overset{0.40\%}{\to} 2^3D_1\ \gamma(74.7) \overset{4.2\%}{\to} 1^3F_2\gamma(90.5) \overset{13.6\%}{\to} 1^3D_2\gamma(184.3) \overset{74.7\%}{\to} 1^3P_1\gamma(267.3$ $\overset{33.9\%}{\to} 1^3S_1\gamma(423.0) \overset{2.48\%}{\to} \mu^+\mu^-$	1.4×10^{-7}	1
3^3P_0	$\overset{0.054\%}{\to} 1^3P_2\pi\pi \overset{19.1\%}{\to} 1^3S_1\gamma(441.6) \overset{2.48\%}{\to} \mu^+\mu^-$	2.6×10^{-6}	9
3^1P_1	$\overset{4.3\%}{\to} 1^1S_0\ \gamma(1081.0) \overset{100\%}{\to} gg$	4.3×10^{-2}	3.1×10^5
	$\overset{1.7\%}{\to} 1^1P_1\pi\pi \overset{49\%}{\to} 1^1S_0\ \gamma(488.3) \overset{100\%}{\to} gg$	8.3×10^{-3}	6.0×10^4

TABLE XXX. 4^3P_J and 5^3P_J decay chains, branching ratios and event estimates for LHCb Run II. These are based on producing 9.7×10^6 $\chi_{b2}(4P)$'s, 7.4×10^6 $\chi_{b1}(4P)$'s, 3.1×10^6 $\chi_{b0}(4P)$'s, 8.2×10^6 $\chi_{b2}(5P)$'s, 5.7×10^6 $\chi_{b1}(5P)$'s and 2.2×10^6 $\chi_{b0}(5P)$'s as described in the text.

Parent	Decay chain	Combined BR	Events
4^3P_2	$\overset{0.012\%}{\to} 3^3S_1\ \gamma(433.9)\overset{2.18\%}{\to}\mu^+\mu^-$	2.6×10^{-6}	25
	$\overset{1.4\times10^{-3}\%}{\to} 2^3S_1\ \gamma(747.2)\overset{1.93\%}{\to}\mu^+\mu^-$	2.6×10^{-7}	3
	$\overset{5.0\times10^{-3}\%}{\to} 1^3S_1\ \gamma(1255.1)\overset{2.48\%}{\to}\mu^+\mu^-$	1.3×10^{-6}	12
4^3P_1	$\overset{0.013\%}{\to} 3^3S_1\ \gamma(424.3)\overset{2.18\%}{\to}\mu^+\mu^-$	2.7×10^{-6}	20
	$\overset{6.0\times10^{-4}\%}{\to} 2^3S_1\ \gamma(737.9)\overset{1.93\%}{\to}\mu^+\mu^-$	1.1×10^{-7}	1
	$\overset{3.3\times10^{-3}\%}{\to} 1^3S_1\ \gamma(1003.0)\overset{2.48\%}{\to}\mu^+\mu^-$	8.2×10^{-7}	6
4^3P_0	$\overset{6.4\times10^{-3}\%}{\to} 3^3S_1\ \gamma(411.8)\overset{2.18\%}{\to}\mu^+\mu^-$	1.4×10^{-6}	4
	$\overset{6.1\times10^{-4}\%}{\to} 1^3S_1\ \gamma(1234.8)\overset{2.48\%}{\to}\mu^+\mu^-$	1.5×10^{-7}	0.5
5^3P_2	$\overset{1\times10^{-4}\%}{\to} 3^3S_1\ \gamma(646.8)\overset{2.18\%}{\to}\mu^+\mu^-$	2.1×10^{-8}	0.2
	$\overset{2.5\times10^{-3}\%}{\to} 2^3S_1\ \gamma(953.7)\overset{1.93\%}{\to}\mu^+\mu^-$	4.8×10^{-7}	4
	$\overset{3.4\times10^{-3}\%}{\to} 1^3S_1\ \gamma(1451.3)\overset{2.48\%}{\to}\mu^+\mu^-$	8.4×10^{-7}	7
5^3P_1	$\overset{1.3\times10^{-3}\%}{\to} 2^3S_1\ \gamma(946.4)\overset{1.93\%}{\to}\mu^+\mu^-$	2.5×10^{-7}	1
	$\overset{1.4\times10^{-3}\%}{\to} 1^3S_1\ \gamma(1444.4)\overset{2.48\%}{\to}\mu^+\mu^-$	3.5×10^{-7}	2
5^3P_0	$\overset{3.0\times10^{-4}\%}{\to} 3^3S_1\ \gamma(629.9)\overset{2.18\%}{\to}\mu^+\mu^-$	6.5×10^{-8}	0.1
	$\overset{6.7\times10^{-4}\%}{\to} 2^3S_1\ \gamma(937.3)\overset{1.93\%}{\to}\mu^+\mu^-$	1.3×10^{-7}	0.3
	$\overset{4.1\times10^{-4}\%}{\to} 1^3S_1\ \gamma(1435.7)\overset{2.48\%}{\to}\mu^+\mu^-$	1.0×10^{-7}	0.2

expected events is small it is possible that our estimates are off by an order of magnitude. Also, our estimates are based on using LHCb event numbers and ATLAS and CMS with their different capabilities might be able to observe more events. Thus, for completeness we include estimates for both the $4P$ and $5P$ states. The most important message is that the higher energy and luminosity of LHC Run II could potentially observe some of the $4P$ and $5P$ states which would be an important test of models and lattice QCD results.

6. The 1D states

The production rate for the D-waves is significantly lower than that of P-waves. This is a consequence of the LDMEs going like $|R^{(l)}(0)|^2/M^{2l+2}$ so the production cross section is significantly suppressed by the mass factor in the denominator. The mass factor is simply a consequence of the dimensionality of the lth derivative of the wave function and will increasingly suppress the cross sections going to higher l multiplets.

Nevertheless, it is expected that the $1D$ states can be produced in sufficient quantity to be observed. There are three sources of the D states: direct production and from decay chains originating with the 3^3S_1 and 2^3P_J states. The decay chains and estimated number of events from direct production are given in Table XXXI. We estimate that direct production of the D-waves will yield $\sim$100 $\Upsilon_3(1D)$, $\sim$150 $\Upsilon_2(1D)$ and $\sim$50 $\Upsilon_1(1D)$ events. This is roughly comparable to the number of $3P$ events observed by LHCb. There are two differences. The $3P$ events were comprised of one photon and a $\mu^+\mu^-$ pair while the $1D$ events are generally comprised of two photons and a $\mu^+\mu^-$ pair making them more difficult to reconstruct. On the other hand, we can estimate the photon energies fairly accurately because the $\Upsilon_2(1D)$ mass has been measured. An exception is the $\Upsilon_1(1D)$ which can decay directly to a $\mu^+\mu^-$ final state. Unfortunately the BR appears to be too small to produce a sufficient number of events to find this state in this channel. On the other hand, as we have pointed out a number of times, our estimates can easily be off by an order of magnitude. In addition to direct production the $1D$ states will also be produced via transitions originating with 3^3S_1 and 2^3P_J. In fact, cascades originating from the 3^3S_1 contribute the largest number of events to the $2\gamma\mu^+\mu^-$ signal with roughly another 20% originating from 2^3P_J production. Specifically we expect $\sim$2700 events in $1^3D_3\to\gamma1^3P_2\to\gamma\gamma1^3S_1\to\gamma\gamma\mu^+\mu^-$, $\sim$6500 in $1^3D_2\to\gamma1^3P_1\to\gamma\gamma1^3S_1\to\gamma\gamma\mu^+\mu^-$ and $\sim$1200 in $1^3D_1\to\gamma1^3P_1\to\gamma\gamma1^3S_1\to\gamma\gamma\mu^+\mu^-$. Other decay chains will contribute to 1^3D_J production but they will have different photon energies so we only give estimates for the decay chains with the largest statistics.

TABLE XXXI. The $1D$ decay chains, branching ratios and event estimates for LHCb Run II and Belle II. For the pp column these are based on producing 2.0×10^4 $\Upsilon_3(1D)$'s and $\Upsilon_2(1D)$'s, 1.6×10^4 $\Upsilon_1(1D)$'s and 1.9×10^4 $\eta_{b2}(1D)$'s as described in the text. For the e^+e^- column these are based on 1.3×10^6 $\Upsilon_1(1D)$'s produced assuming $\sigma = 13$ pb and 100 fb^{-1} integrated luminosity.

Parent	Decay chain	Combined BR	Events pp	Events e^+e^-
1^3D_3	$\overset{91.0\%}{\to} 1^3P_2\gamma(256.0) \overset{19.1\%}{\to} 1^3S_1\gamma(441.6) \overset{2.48\%}{\to} \mu^+\mu^-$	4.3×10^{-3}	87	NA
	$\overset{0.74\%}{\to} 1^3S_1\pi^+\pi^- \overset{2.48\%}{\to} \mu^+\mu^-$	1.8×10^{-4}	4	NA
1^3D_2	$\overset{22\%}{\to} 1^3P_2\gamma(248.4) \overset{19.1\%}{\to} 1^3S_1\gamma(441.6) \overset{2.48\%}{\to} \mu^+\mu^-$	1.0×10^{-3}	20	NA
	$\overset{74.7\%}{\to} 1^3P_1\gamma(267.3) \overset{33.9\%}{\to} 1^3S_1\gamma(423.0) \overset{2.48\%}{\to} \mu^+\mu^-$	6.3×10^{-3}	126	NA
	$\overset{0.66\%}{\to} 1^3S_1\pi^+\pi^- \overset{2.48\%}{\to} \mu^+\mu^-$	1.6×10^{-4}	3	NA
1^3D_1	$\overset{1.6\%}{\to} 1^3P_2\gamma(239.1) \overset{19.1\%}{\to} 1^3S_1\gamma(441.6) \overset{2.48\%}{\to} \mu^+\mu^-$	7.6×10^{-5}	1	99
	$\overset{28\%}{\to} 1^3P_1\gamma(258.0) \overset{33.9\%}{\to} 1^3S_1\gamma(423.0) \overset{2.48\%}{\to} \mu^+\mu^-$	2.4×10^{-3}	38	3120
	$\overset{47.1\%}{\to} 1^3P_0\gamma(290.5) \overset{1.76\%}{\to} 1^3S_1\gamma(391.1) \overset{2.48\%}{\to} \mu^+\mu^-$	2.0×10^{-4}	3	260
	$\overset{0.40\%}{\to} 1^3S_1\pi^+\pi^- \overset{2.48\%}{\to} \mu^+\mu^-$	9.9×10^{-5}	2	129
	$\overset{3.93\times10^{-3}\%}{\to} \mu^+\mu^-$	3.9×10^{-5}	1	50
1^1D_2	$\overset{91.5\%}{\to} 1^1P_1\gamma(262.5) \overset{49\%}{\to} 1^1S_0\gamma(488.3) \overset{100\%}{\to} gg$	0.45	8550	NA
	$\overset{1.3\%}{\to} 1^1S_0\pi^+\pi^- \overset{100\%}{\to} gg$	1.3×10^{-2}	247	NA

We have also included the decay chains $1^3D_J \to 1^3S_1 + \pi^+\pi^- \to \mu^+\mu^-$ and $1^1D_2 \to 1^1S_0 + \pi^+\pi^- \to gg$ despite yielding few events as they offer a signal complementary to those involving photons.

Finally, we mention that the η_{b2} will decay predominantly via $\eta_{b2}(1D) \to \gamma h_b \to \gamma\gamma\eta_b(1S)$ with the $\eta_b(1S)$ decaying to hadrons. We do not see how the $\eta_{b2}(1D)$ can be reconstructed given the hadronic final state but perhaps experimentalists will come up with a clever approach that we have not considered.

7. The 2D and higher D-wave states

For the $2D$ states in Table XXXII, we focus on the simplest decay chains with two photons and a $\mu^+\mu^-$ pair in the final state which are most likely to be reconstructed. To estimate the number of expected events, we include contributions to the $\gamma\gamma\mu^+\mu^-$ final state from direct production and from decay chains originating from 3^3P_J production. There are a number of possible decay chains but the ones with the largest expected statistics are ~125 events for $2^3D_3 \to \gamma 2^3P_2 \to \gamma\gamma 2^3S_1 \to \gamma\gamma\mu^+\mu^-$, ~252 events for $2^3D_2 \to \gamma 2^3P_1 \to \gamma\gamma 2^3S_1 \to \gamma\gamma\mu^+\mu^-$ and ~37 events for $2^3D_1 \to \gamma 2^3P_1 \to \gamma\gamma 2^3S_1 \to \gamma\gamma\mu^+\mu^-$. In all cases more events are expected from 3^3P_J production than from direct $2D$ production.

For the $3D$ and $4D$ states we expect that each member of both multiplets will have of the order of 10^4 produced. However the predicted widths are $\mathcal{O}(100$ MeV) so the BRs for radiative transitions will be small. Thus, we only expect that they can be observed in $B\bar{B}$, $B\bar{B}^*$ or $B^*\bar{B}^*$ final states if they can be reconstructed with high enough efficiencies and separated from backgrounds.

8. The nF states

The production rate decreases quite dramatically for states with larger L as a consequence of our estimates which use Eq. (12) where the NR approximation of the cross section goes like the lth derivative of the wave function at the origin with the corresponding mass in the denominator needed for dimensional reasons. We only expect that ~200 for each of the $1F$ states will be produced. Once the BRs for the decay chains are included we expect that only 1 or fewer events will result. Considering experimental challenges in making these measurements we do not expect that the $1F$ states will be observed from direct production. Nevertheless, we include the dominant decay chains in Table XXXIII for completeness.

We do expect a small number of $1F$ states, ~28 1^3F_4's, ~44 1^3F_3's and ~2 1^3F_2, to be produced via radiative transitions originating with 3^3P_J and 2^3D_J states. Since there are 3γ's in the final state it is unlikely that the $1F$ states will be observed in hadron production.

We expect the $2F$ and $3F$ multiplets to be even more challenging to observe using radiative transition decay chains primarily because they are above $B\bar{B}$ threshold and are therefore broader, ranging from 2.8 MeV for the 2^3F_4 state to 88.6 MeV for the 2^3F_2 state. These states are very close to the $B\bar{B}$ and $B\bar{B}^*$ threshold and therefore are very sensitive to available phase space. If our mass predictions are too high it is possible that the total widths could be

TABLE XXXII. The $2D$ decay chains, branching ratios and event estimates for LHCb Run II. These are based on producing 3.4×10^4 $\Upsilon_3(2D)$'s, 3.1×10^4 $\Upsilon_2(2D)$'s, 2.4×10^4 $\Upsilon_1(2D)$'s and 2.9×10^4 $\eta_{b2}(2D)$'s as described in the text.

Parent	Decay chain	Combined BR	Events
2^3D_3	$\overset{65.1\%}{\to} 2^3P_2\gamma(185.0) \overset{10.6\%}{\to} 2^3S_1\gamma(242.5) \overset{1.93\%}{\to} \mu^+\mu^-$	1.3×10^{-3}	45
	$\overset{65.1\%}{\to} 2^3P_2\gamma(185.0) \overset{7.0\%}{\to} 1^3S_1\gamma(776.5) \overset{2.48\%}{\to} \mu^+\mu^-$	1.1×10^{-3}	38
	$\overset{10.3\%}{\to} 1^3P_2\gamma(529.0) \overset{19.1\%}{\to} 1^3S_1\gamma(441.6) \overset{2.48\%}{\to} \mu^+\mu^-$	4.9×10^{-4}	16
	$\overset{6.7\%}{\to} 1^3F_4\gamma(96.7) \overset{100\%}{\to} 1^3D_3\gamma(200.9) \overset{91.0\%}{\to} 1^3P_2\gamma(256.0) \overset{19.1\%}{\to} 1^3S_1\gamma(441.6) \overset{2.48\%}{\to} \mu^+\mu^-$	2.9×10^{-4}	10
2^3D_2	$\overset{17\%}{\to} 2^3P_2\gamma(178.6) \overset{10.6\%}{\to} 2^3S_1\gamma(242.5) \overset{1.93\%}{\to} \mu^+\mu^-$	3.5×10^{-4}	11
	$\overset{17\%}{\to} 2^3P_2\gamma(178.6) \overset{7.0\%}{\to} 1^3S_1\gamma(776.5) \overset{2.48\%}{\to} \mu^+\mu^-$	3.0×10^{-4}	9
	$\overset{56.2\%}{\to} 2^3P_1\gamma(191.6) \overset{19.9\%}{\to} 2^3S_1\gamma(229.6) \overset{1.93\%}{\to} \mu^+\mu^-$	2.1×10^{-3}	66
	$\overset{56.2\%}{\to} 2^3P_1\gamma(191.6) \overset{9.2\%}{\to} 1^3S_1\gamma(764.3) \overset{2.48\%}{\to} \mu^+\mu^-$	1.3×10^{-3}	39
	$\overset{12\%}{\to} 1^3P_1\gamma(541.2) \overset{33.9\%}{\to} 1^3S_1\gamma(423.0) \overset{2.48\%}{\to} \mu^+\mu^-$	1.0×10^{-3}	31
	$\overset{6.6\%}{\to} 1^3F_3\gamma(93.7) \overset{89.3\%}{\to} 1^3D_2\gamma(189.2) \overset{74.7\%}{\to} 1^3P_1\gamma(267.3) \overset{33.9\%}{\to} 1^3S_1\gamma(423.0) \overset{2.48\%}{\to} \mu^+\mu^-$	3.7×10^{-4}	11
2^3D_1	$\overset{5.28\times10^{-3}\%}{\to} \mu^+\mu^-$	5.3×10^{-5}	1
	$\overset{17\%}{\to} 2^3P_1\gamma(183.9) \overset{19.9\%}{\to} 2^3S_1\gamma(229.6) \overset{1.93\%}{\to} \mu^+\mu^-$	6.5×10^{-4}	16
	$\overset{28.1\%}{\to} 2^3P_0\gamma(206.4) \overset{4.6\%}{\to} 2^3S_1\gamma(207.1) \overset{1.93\%}{\to} \mu^+\mu^-$	2.5×10^{-4}	6
	$\overset{28.1\%}{\to} 2^3P_0\gamma(206.4) \overset{0.9\%}{\to} 1^3S_1\gamma(743.1) \overset{2.48\%}{\to} \mu^+\mu^-$	6.3×10^{-5}	2
	$\overset{4.2\%}{\to} 1^3F_2\gamma(90.5) \overset{13.6\%}{\to} 1^3D_2\gamma(184.3) \overset{74.7\%}{\to} 1^3P_1\gamma(267.3) \overset{33.9\%}{\to} 1^3S_1\gamma(423.0) \overset{2.48\%}{\to} \mu^+\mu^-$	3.6×10^{-5}	1
2^1D_2	$\overset{67.1\%}{\to} 2^1P_1\gamma(188.3) \overset{48\%}{\to} 2^1S_0\gamma(257.7) \overset{100\%}{\to} gg$	0.32	9280
	$\overset{67.1\%}{\to} 2^1P_1\gamma(188.3) \overset{22\%}{\to} 1^1S_0\gamma(825.8) \overset{100\%}{\to} gg$	0.15	4350
	$\overset{12\%}{\to} 1^1P_1\gamma(536.5) \overset{49\%}{\to} 1^1S_0\gamma(488.3) \overset{100\%}{\to} gg$	0.059	1710

significantly smaller leading to significantly larger BRs to the decay chains we have been focusing on. Nevertheless, given our expectations for the $1F$ states we do not feel it is likely that they would be discovered using radiative transitions. If the B and B^* mesons can be observed with high efficiencies the excited F-wave states might be observed in $B\bar{B}$ and $B\bar{B}^*$ final states.

The $3F$ multiplets are sufficiently above the $B\bar{B}$ and $B\bar{B}^*$ threshold that they are much broader. The only possibility that they might be observed would be in $B\bar{B}$, $B\bar{B}^*$ or $B^*\bar{B}^*$ final states.

9. The nG states

Even more so than the F-waves, the G-wave production cross sections are highly suppressed so we expect only $\mathcal{O}(1)$ mesons will be produced for each of the states in the G-wave multiplets in Run II which is far too small a number to have any hope of being seen.

B. At e^+e^- colliders

The question we wish to address in this section is whether previously unobserved states can be observed in e^+e^- collisions and outline how to do so. We will focus on 1^{--} states, the n^3S_1 and n^3D_1 states, since only 1^{--} states can be produced directly in e^+e^- collisions. To estimate the number of events requires a detailed Monte Carlo study that includes beam spread and initial state radiation which is beyond the scope of this work. Instead we will use cross sections derived from Belle and *BABAR* events along with integrated luminosities suggested for Belle II.

TABLE XXXIII. The $1F$ decay chains, branching ratios and event estimates for LHCb Run II. These are based on producing 166 $\chi_{b4}(1F)$'s, 163 $\chi_{b3}(1F)$'s, 147 $\chi_{b2}(1F)$'s and 158 $h_{b3}(1F)$'s as described in the text.

Parent	Decay chain	Combined BR	Events
1^3F_4	$\overset{100\%}{\to} 1^3D_3\gamma(184.9) \overset{91.0\%}{\to} 1^3P_2\gamma(256.0) \overset{19.1\%}{\to} 1^3S_1\gamma(441.6) \overset{2.48\%}{\to} \mu^+\mu^-$	4.3×10^{-3}	0.7
1^3F_3	$\overset{89.3\%}{\to} 1^3D_2\gamma(189.2) \overset{74.7\%}{\to} 1^3P_1\gamma(267.3) \overset{33.9\%}{\to} 1^3S_1\gamma(423.0) \overset{2.48\%}{\to} \mu^+\mu^-$	5.6×10^{-3}	1
1^3F_2	$\overset{82.4\%}{\to} 1^3D_1\gamma(194.1) \overset{28\%}{\to} 1^3P_1\gamma(258.0) \overset{33.9\%}{\to} 1^3S_1\gamma(423.0) \overset{2.48\%}{\to} \mu^+\mu^-$	1.9×10^{-3}	0.3
1^1F_3	$\overset{100\%}{\to} 1^1D_2\gamma(189.2) \overset{91.5\%}{\to} 1^1P_1\gamma(262.5) \overset{49\%}{\to} 1^1S_0\gamma(488.3) \overset{100\%}{\to} gg$	0.45	71

TABLE XXXIV. The 2^3D_1 decay chains, branching ratios and event estimates for Belle II. The event numbers are based on 2×10^6 $\Upsilon_3(2D)$'s produced assuming $\sigma = 18$ pb and 100 fb^{-1} integrated luminosity.

Parent	Decay chain	Combined BR	Events
2^3D_1	$\overset{5.28\times10^{-3}\%}{\rightarrow} \mu^+\mu^-$	5.3×10^{-5}	106
	$\overset{1\%}{\rightarrow} 2^3P_2\gamma(170.9) \overset{10.6\%}{\rightarrow} 2^3S_1\gamma(242.5) \overset{1.93\%}{\rightarrow} \mu^+\mu^-$	2.0×10^{-5}	40
	$\overset{1\%}{\rightarrow} 2^3P_2\gamma(170.9) \overset{7.0\%}{\rightarrow} 1^3S_1\gamma(776.5) \overset{2.48\%}{\rightarrow} \mu^+\mu^-$	1.7×10^{-5}	34
	$\overset{0.05\%}{\rightarrow} 1^3P_2\gamma(515.4) \overset{19.1\%}{\rightarrow} 1^3S_1\gamma(441.6) \overset{2.48\%}{\rightarrow} \mu^+\mu^-$	2.4×10^{-6}	5
	$\overset{17.2\%}{\rightarrow} 2^3P_1\gamma(183.9) \overset{19.9\%}{\rightarrow} 2^3S_1\gamma(229.6) \overset{1.93\%}{\rightarrow} \mu^+\mu^-$	6.6×10^{-4}	1320
	$\overset{17.2\%}{\rightarrow} 2^3P_1\gamma(183.9) \overset{9.2\%}{\rightarrow} 1^3S_1\gamma(764.3) \overset{2.48\%}{\rightarrow} \mu^+\mu^-$	3.9×10^{-4}	780
	$\overset{2.4\%}{\rightarrow} 1^3P_1\gamma(533.8) \overset{33.9\%}{\rightarrow} 1^3S_1\gamma(423.0) \overset{2.48\%}{\rightarrow} \mu^+\mu^-$	2.0×10^{-4}	400
	$\overset{28.1\%}{\rightarrow} 2^3P_0\gamma(206.4) \overset{4.6\%}{\rightarrow} 2^3S_1\gamma(207.1) \overset{1.93\%}{\rightarrow} \mu^+\mu^-$	2.5×10^{-4}	500
	$\overset{28.1\%}{\rightarrow} 2^3P_0\gamma(206.4) \overset{0.9\%}{\rightarrow} 1^3S_1\gamma(743.1) \overset{2.48\%}{\rightarrow} \mu^+\mu^-$	6.3×10^{-5}	126
	$\overset{7.7\%}{\rightarrow} 1^3P_0\gamma565.4) \overset{1.76\%}{\rightarrow} 1^3S_1\gamma(391.1) \overset{2.48\%}{\rightarrow} \mu^+\mu^-$	3.4×10^{-5}	68
	$\overset{4.2\%}{\rightarrow} 1^3F_2\gamma(90.5) \overset{14\%}{\rightarrow} 1^3D_2\gamma(184.3) \overset{74.7\%}{\rightarrow} 1^3P_1\gamma(267.3) \overset{33.9\%}{\rightarrow} 1^3S_1\gamma(423.0) \overset{2.48\%}{\rightarrow} \mu^+\mu^-$	3.7×10^{-5}	74
	$\overset{4.2\%}{\rightarrow} 1^3F_2\gamma(90.5) \overset{14\%}{\rightarrow} 1^3D_2\gamma(184.3) \overset{22\%}{\rightarrow} 1^3P_2\gamma(248.4) \overset{19.1\%}{\rightarrow} 1^3S_1\gamma(441.6) \overset{2.48\%}{\rightarrow} \mu^+\mu^-$	6.1×10^{-6}	12
	$\overset{4.2\%}{\rightarrow} 1^3F_2\gamma(90.5) \overset{0.35\%}{\rightarrow} 1^3D_3\gamma(176.5) \overset{91.0\%}{\rightarrow} 1^3P_2\gamma(256.0) \overset{19.1\%}{\rightarrow} 1^3S_1\gamma(441.6) \overset{2.48\%}{\rightarrow} \mu^+\mu^-$	6.3×10^{-7}	1
	$\overset{4.2\%}{\rightarrow} 1^3F_2\gamma(90.5) \overset{82.4\%}{\rightarrow} 1^3D_1\gamma(194.1) \overset{1.6\%}{\rightarrow} 1^3P_2\gamma(239.1) \overset{19.1\%}{\rightarrow} 1^3S_1\gamma(441.6) \overset{2.48\%}{\rightarrow} \mu^+\mu^-$	2.6×10^{-6}	5
	$\overset{4.2\%}{\rightarrow} 1^3F_2\gamma(90.5) \overset{82.4\%}{\rightarrow} 1^3D_1\gamma(194.1) \overset{28\%}{\rightarrow} 1^3P_1\gamma(258.0) \overset{33.9\%}{\rightarrow} 1^3S_1\gamma(423.0) \overset{2.48\%}{\rightarrow} \mu^+\mu^-$	8.1×10^{-5}	162
	$\overset{4.2\%}{\rightarrow} 1^3F_2\gamma(90.5) \overset{82.4\%}{\rightarrow} 1^3D_1\gamma(194.1) \overset{47.1\%}{\rightarrow} 1^3P_0\gamma(290.5) \overset{1.76\%}{\rightarrow} 1^3S_1\gamma(391.1) \overset{2.48\%}{\rightarrow} \mu^+\mu^-$	7.1×10^{-6}	14

TABLE XXXV. The 3^3D_1 decay chains and combined branching ratios. These are small enough that we do not expect enough events at Belle II for this state to be observed.

Parent	Decay chain	Combined BR
3^3D_1	$\overset{2.30\times10^{-6}\%}{\rightarrow} \mu^+\mu^-$	2.3×10^{-8}
	$\overset{5.6\times10^{-4}\%}{\rightarrow} 3^3P_2\gamma(168.6) \overset{3.8\%}{\rightarrow} 3^3S_1\gamma(171.6) \overset{2.18\%}{\rightarrow} \mu^+\mu^-$	4.6×10^{-9}
	$\overset{5.6\times10^{-4}\%}{\rightarrow} 3^3P_2\gamma(168.6) \overset{1.8\%}{\rightarrow} 2^3S_1\gamma(492.9) \overset{1.93\%}{\rightarrow} \mu^+\mu^-$	1.9×10^{-9}
	$\overset{9.2\times10^{-3}\%}{\rightarrow} 3^3P_1\gamma(180.4) \overset{7.2\%}{\rightarrow} 3^3S_1\gamma(159.8) \overset{2.18\%}{\rightarrow} \mu^+\mu^-$	1.4×10^{-7}
	$\overset{9.2\times10^{-3}\%}{\rightarrow} 3^3P_1\gamma(180.4) \overset{2.6\%}{\rightarrow} 2^3S_1\gamma(481.4) \overset{1.93\%}{\rightarrow} \mu^+\mu^-$	4.6×10^{-8}
	$\overset{9.2\times10^{-3}\%}{\rightarrow} 3^3P_1\gamma(180.4) \overset{1.1\%}{\rightarrow} 1^3S_1\gamma(1003.0) \overset{2.48\%}{\rightarrow} \mu^+\mu^-$	2.5×10^{-8}
	$\overset{1.35\times10^{-2}\%}{\rightarrow} 3^3P_0\gamma(196.2) \overset{0.31\%}{\rightarrow} 3^3S_1\gamma(144.0) \overset{2.18\%}{\rightarrow} \mu^+\mu^-$	9.1×10^{-9}
	$\overset{1.35\times10^{-2}\%}{\rightarrow} 3^3P_0\gamma(196.2) \overset{0.077\%}{\rightarrow} 2^3S_1\gamma(466.2) \overset{1.93\%}{\rightarrow} \mu^+\mu^-$	2.0×10^{-9}
	$\overset{1.35\times10^{-2}\%}{\rightarrow} 3^3P_0\gamma(196.2) \overset{0.01\%}{\rightarrow} 1^3S_1\gamma(988.5) \overset{2.48\%}{\rightarrow} \mu^+\mu^-$	3.3×10^{-10}
	$\overset{2\times10^{-5}\%}{\rightarrow} 2^3P_2\gamma(420.4) \overset{10.6\%}{\rightarrow} 2^3S_1\gamma(242.5) \overset{1.93\%}{\rightarrow} \mu^+\mu^-$	4.1×10^{-10}
	$\overset{2\times10^{-5}\%}{\rightarrow} 2^3P_2\gamma(196.2) \overset{7.0\%}{\rightarrow} 1^3S_1\gamma(776.5) \overset{2.48\%}{\rightarrow} \mu^+\mu^-$	3.5×10^{-10}
	$\overset{9.3\times10^{-4}\%}{\rightarrow} 2^3P_1\gamma(433.8) \overset{19.9\%}{\rightarrow} 2^3S_1\gamma(229.6) \overset{1.93\%}{\rightarrow} \mu^+\mu^-$	3.6×10^{-8}
	$\overset{9.3\times10^{-4}\%}{\rightarrow} 2^3P_1\gamma(433.8) \overset{9.2\%}{\rightarrow} 1^3S_1\gamma(764.3) \overset{2.48\%}{\rightarrow} \mu^+\mu^-$	2.1×10^{-8}
	$\overset{1.3\times10^{-4}\%}{\rightarrow} 1^3P_1\gamma(533.8) \overset{33.9\%}{\rightarrow} 1^3S_1\gamma(423.0) \overset{2.48\%}{\rightarrow} \mu^+\mu^-$	1.1×10^{-8}
	$\overset{2.7\times10^{-3}\%}{\rightarrow} 2^3P_0\gamma(454.9) \overset{4.6\%}{\rightarrow} 2^3S_1\gamma(207.1) \overset{1.93\%}{\rightarrow} \mu^+\mu^-$	2.4×10^{-8}
	$\overset{2.7\times10^{-3}\%}{\rightarrow} 2^3P_0\gamma(454.9) \overset{0.9\%}{\rightarrow} 1^3S_1\gamma(743.1) \overset{2.48\%}{\rightarrow} \mu^+\mu^-$	6.0×10^{-9}
	$\overset{5.7\times10^{-4}\%}{\rightarrow} 1^3P_0\gamma(806.1) \overset{1.76\%}{\rightarrow} 1^3S_1\gamma(391.1) \overset{2.48\%}{\rightarrow} \mu^+\mu^-$	2.5×10^{-9}
	$\overset{2.6\times10^{-3}\%}{\rightarrow} 2^3F_2\gamma(75.7) \overset{1.98\times10^{-2}\%}{\rightarrow} 2^3D_1\gamma(172.6) \overset{5.28\times10^{-3}\%}{\rightarrow} \mu^+\mu^-$	2.7×10^{-13}

We start with the $\Upsilon(3S)$ where we use the cross section of 4 nb based on Belle and *BABAR* measurements [102]. An integrated luminosity of $250\,\mathrm{fb}^{-1}$ would yield 10^9 $\Upsilon(3S)$'s, about a factor of 7 1/2 times the combined Belle-*BABAR* data set. We give estimates of number of events in Table XXVI based on this but the numbers can be easily rescaled for other integrated luminosities. We expect that $\mathcal{O}(10^3)$ 1^3D_J's will be produced via radiative transitions for each J value, which should be sufficient to identify each of the 1^3D_J states and measure and compare their masses to theoretical predictions.

The expectations are to accumulate several ab^{-1} of integrated luminosity at the $\Upsilon(4S)$. The cross section of $\sim$1 nb would yield several billion $\Upsilon(4S)$'s depending on the eventual integrated luminosity. We estimate the number of events given in Table XXVII assuming that 10^{10} $\Upsilon(4S)$'s will be produced based on $10\,\mathrm{ab}^{-1}$ of integrated luminosity but these numbers can easily be rescaled assuming different values of integrated luminosities. We expect sufficient events in the chains that proceed via the 3^3P_2 and 3^3P_1 so that these states should be observed in radiative decays of the $\Upsilon(4S)$. We do not expect that the 3^3P_0 will be observed in this manner. Another interesting possibility for studying the $3P$ states via radiative transitions from the $\Upsilon(4S)$ utilizes hadronic transitions from the $\Upsilon(3S)$ and $\Upsilon(2S)$ to $\Upsilon(2S)$ or $\Upsilon(1S)$ in the decay chain. This is experimentally very clean and would yield some tens of events for 3^3P_2 and 3^3P_1 intermediate states but only $\mathcal{O}(1)$ event for the 3^3P_0. This might be sufficient to resolve some of the J states. It would have been interesting to be able to observe the $2D$ states in radiative transitions originating with the $\Upsilon(4S)$ but this does not appear to be likely. Of all the 2^3D_J states the decay chain proceeding via the 2^3D_1 state will have the largest statistics although not sufficient to be observed considering the four photons in the decay chain.

It is unlikely that sitting on the $\Upsilon(5S)$ or $\Upsilon(6S)$ would produce enough bottomonium states via radiative transitions to be seen. This stems from the $\Upsilon(5S)$ and $\Upsilon(6S)$ having large total widths which leads to small BRs to e^+e^- and subsequently smaller production cross sections than the lower mass $^3S_1$ states. This also results in small BRs for photon decays. For the $\Upsilon(5S)$ the Belle Collaboration measures its e^+e^- production cross section to be 0.3 nb [102]. The radiative transition with the largest BR is to 4^3P_2 with $\mathrm{BR} = 1.6 \times 10^{-4}$ yielding $\sim 5 \times 10^3$ 4^3P_2's per $100\,\mathrm{fb}^{-1}$. From Table XXX the combined BRs for representative 4^3P_2 decay chains are $\mathcal{O}(10^{-6})$ so it is unlikely that $b\bar{b}$ states could be seen in decays originating from the $\Upsilon(5S)$ in e^+e^- collisions. We repeat the exercise for the $\Upsilon(6S)$. We assume an e^+e^- production cross section similar to that of the $\Upsilon(5S)$ although in fact it should be

TABLE XXXVI. The 4^3D_1 decay chains and combined branching ratios. These are small enough that we do not expect enough events at Belle II for this state to be observed.

Parent	Decay chain	Combined BR
4^3D_1	$\overset{3.04\times10^{-6}\%}{\to}\mu^+\mu^-$	3.0×10^{-8}
	$\overset{4\times10^{-5}\%}{\to}3^3P_2\gamma(392.7)\overset{3.8\%}{\to}3^3S_1\gamma(171.6)\overset{2.18\%}{\to}\mu^+\mu^-$	3.3×10^{-10}
	$\overset{4\times10^{-5}\%}{\to}3^3P_2\gamma(392.7)\overset{1.8\%}{\to}2^3S_1\gamma(492.9)\overset{1.93\%}{\to}\mu^+\mu^-$	1.4×10^{-10}
	$\overset{4\times10^{-5}\%}{\to}3^3P_2\gamma(392.7)\overset{1.1\%}{\to}1^3S_1\gamma(1003.0)\overset{2.48\%}{\to}\mu^+\mu^-$	1.1×10^{-10}
	$\overset{1.8\times10^{-3}\%}{\to}3^3P_1\gamma(404.2)\overset{7.2\%}{\to}3^3S_1\gamma(159.8)\overset{2.18\%}{\to}\mu^+\mu^-$	2.8×10^{-8}
	$\overset{1.8\times10^{-3}\%}{\to}3^3P_1\gamma(404.2)\overset{2.6\%}{\to}2^3S_1\gamma(481.4)\overset{1.93\%}{\to}\mu^+\mu^-$	9.0×10^{-9}
	$\overset{1.8\times10^{-3}\%}{\to}3^3P_1\gamma(404.2)\overset{1.1\%}{\to}1^3S_1\gamma(1003.0)\overset{2.48\%}{\to}\mu^+\mu^-$	4.9×10^{-9}
	$\overset{5.6\times10^{-3}\%}{\to}3^3P_0\gamma(419.6)\overset{0.31\%}{\to}3^3S_1\gamma(144.0)\overset{2.18\%}{\to}\mu^+\mu^-$	3.8×10^{-9}
	$\overset{5.6\times10^{-3}\%}{\to}3^3P_0\gamma(419.6)\overset{0.077\%}{\to}2^3S_1\gamma(466.2)\overset{1.93\%}{\to}\mu^+\mu^-$	8.3×10^{-10}
	$\overset{5.6\times10^{-3}\%}{\to}3^3P_0\gamma(419.6)\overset{0.01\%}{\to}1^3S_1\gamma(988.5)\overset{2.48\%}{\to}\mu^+\mu^-$	1.4×10^{-10}
	$\overset{2.1\times10^{-6}\%}{\to}2^3P_2\gamma(639.1)\overset{10.6\%}{\to}2^3S_1\gamma(242.5)\overset{1.93\%}{\to}\mu^+\mu^-$	4.3×10^{-11}
	$\overset{1\times10^{-4}\%}{\to}2^3P_1\gamma(652.3)\overset{19.9\%}{\to}2^3S_1\gamma(229.6)\overset{1.93\%}{\to}\mu^+\mu^-$	3.8×10^{-9}
	$\overset{1\times10^{-4}\%}{\to}2^3P_1\gamma(652.3)\overset{9.2\%}{\to}1^3S_1\gamma(764.3)\overset{2.48\%}{\to}\mu^+\mu^-$	2.3×10^{-9}
	$\overset{3.6\times10^{-4}\%}{\to}2^3P_0\gamma(672.9)\overset{4.6\%}{\to}2^3S_1\gamma(207.1)\overset{1.93\%}{\to}\mu^+\mu^-$	3.2×10^{-9}
	$\overset{3.6\times10^{-4}\%}{\to}2^3P_0\gamma(672.9)\overset{0.9\%}{\to}1^3S_1\gamma(743.1)\overset{2.48\%}{\to}\mu^+\mu^-$	8.0×10^{-10}
	$\overset{2.6\times10^{-4}\%}{\to}1^3P_1\gamma(986.0)\overset{33.9\%}{\to}1^3S_1\gamma(423.0)\overset{2.48\%}{\to}\mu^+\mu^-$	2.2×10^{-8}
	$\overset{1.0\times10^{-3}\%}{\to}1^3P_0\gamma1016.7)\overset{1.76\%}{\to}1^3S_1\gamma(391.1)\overset{2.48\%}{\to}\mu^+\mu^-$	4.4×10^{-9}

smaller due to its smaller BR to e^+e^-. For the $\Upsilon(6S)$ the largest BR is expected to be to the 3^3P_J states, $\mathcal{O}(10^{-5})$. However, in this case the combined BRs for some interesting $3P$ decay chains are $\mathcal{O}(10^{-4})$. Putting this together we expect ~ 0.5 event/100 fb^{-1} via the 3^3P_2 intermediate state. While still below an event rate needed to study these states it does offer some hope given the uncertainties in our assumption for the production cross section and with higher statistics.

Observation of the n^3D_1 states in e^+e^- collisions is interesting, even more so if they can be produced in sufficient numbers to see previously unobserved excited bottomonium states in their decays. Unfortunately the production cross section is proportional to the BR to e^+e^- which is roughly 3 orders of magnitude lower than for the S-wave states. The small number of signal events will also make it challenging to see the n^3D_1 states over backgrounds. Given these caveats we make a rough estimate of the number of n^3D_1 produced by multiplying the ratio of $nD/2S$ BRs to e^+e^- times the 2^3S_1 cross section to obtain the n^3D_1 production cross section. For the 1^3D_1 this gives ~ 13 pb. For 100 fb^{-1} of integrated luminosity we expect $\sim 1.3 \times 10^6$ 1^3D_1's to be produced. The expected number of events for several 1^3D_1 decay chains is given in Table XXXI. This will yield 50 events in $1^3D_1 \to \mu^+\mu^-$ but many more in radiative decay chains via intermediate $1P$ states.

In the same way as we estimated $\sigma(e^+e^- \to 1^3D_1)$ we obtain $\sigma(e^+e^- \to 2^3D_1) \sim 18$ pb. For 100 fb^{-1} of integrated luminosity we expect $\sim 2 \times 10^6$ 2^3D_1's produced. We use this number to estimate the number of events in the different decay chains given in Table XXXIV. With these assumptions it should be possible to observe the 2^3D_1. While the $\mu^+\mu^-$ mode may be the cleanest, other modes proceeding via radiative transition decay chains offer higher statistics, in particular decay chains proceeding by $1P$ and $2P$ intermediate states. More interesting is the possibility of observing the 1^3F_2 for the first time. The decay chain with the highest statistics proceeds via $1^3F_2 \to 1^3D_1 \to 1^3P_1$ which would also yield information on the 1^3D_1 state. One can easily scale our projected events up or down to reflect actual cross sections and integrated luminosities.

The $3D$ and $4D$ are above the $B\bar{B}$ threshold so have total widths $\mathcal{O}(100$ MeV) resulting in BR $\sim 10^{-8}$ and a cross section ~ 8 fb. For reasonable integrated luminosities and using the BRs for the 3^3D_1 and 4^3D_1 given in Tables XVI and XVIII we do not expect that the 3^3D_1 and 4^3D_1 states can be observed in e^+e^- collisions, as suggested by the results given in Tables XXXV and XXXVI.

VIII. SUMMARY

In this paper we calculated the properties of bottomonium mesons including masses, radiative transitions, annihilation decays, hadronic transitions and strong OZI allowed decays for states above threshold. These results were included in extensive tables with estimated BRs to different final states. While we are interested in how these predictions fare against experimental measurements as a test of our understanding in the context of the constituent quark model, the main objective of this work is to make predictions that can assist experimentalists in finding missing bottomonium states and measuring their properties.

We estimated the number of events expected in Run II of the LHC in the context of the LHCb experiment but they should also be relevant to the ATLAS and CMS experiments. We expect that significant numbers of $\chi_{b2}(3P)$ and $\chi_{b1}(3P)$ will be produced and decay via radiative transitions to the $\Upsilon(1S)$ and $\Upsilon(2S)$ which will subsequently decay to $\mu^+\mu^-$. Likewise we expect a large number of $\chi_{b2}(4P)$'s and $\chi_{b1}(4P)$'s to decay to $\Upsilon(3S)$. Thus, a promising search strategy for excited P-wave mesons is to reconstruct Υ's in $\mu^+\mu^-$ and look at the invariant mass distributions of the Υ's with one γ. We also expect that $\eta_b(3S)$ can be seen in this final state.

Turning to the D-waves, the 1^3D_3 and 1^3D_2 will undergo radiative transitions to the 1^3P_2 and 1^3P_1 respectively so they might be seen in final states with $\gamma\gamma\mu^+\mu^-$. Similarly, the $2D$ states will decay to $2^3P_{2,1}$ which decay to 2^3S_1. Thus, it might be possible to see most of the $1D$ and $2D$ spin triplet multiplets in the $\gamma\gamma\mu^+\mu^-$ final state. A challenge is that the photon energy for $2^3D_3 \to 2^3P_2$ is almost identical to that from the $2^3D_1 \to 2^3P_1$ transition so that one would need to be careful in looking at the invariant mass distributions of the final state.

For e^+e^- collisions, large numbers of 1^3D_J states will be produced by sitting on the $\Upsilon(3S)$ so it might be possible to resolve the three states and determine the splittings between members of the multiplets. Sitting on the $\Upsilon(4S)$ will produce $3^3P_{2,1}$ in radiative transitions. It should be possible to observe the 1^3D_1 and 2^3D_1 by an energy scan at the appropriate energy. Sitting on the 2^3D_1 resonance it might be possible to observe the 1^3F_2 via radiative transitions from the 2^3D_1.

The LHC experiments and Belle II hold the promise to increase our knowledge of bottomonium mesons. This improved knowledge will test the reliability of models of quarkonium physics. Lattice QCD is making ever more precise calculations of bottomonium mesons and it is important that these calculations be held to account by experiment. We expect that the phenomenological predictions presented in this paper will be a useful tool for experimentalists to do so.

ACKNOWLEDGMENTS

S. G. thanks Bryan Fulsom, Peter Lewis and Hassan Jawahery for helpful communications and discussions. S. G. thanks the Department of Physics University of Toronto, the Department of Physics and Astronomy University of Hawaii and TRIUMF for their hospitality where some of

this work was done. This research was supported in part by the Natural Sciences and Engineering Research Council of Canada under Grant No. 121209-2009 SAPIN.

APPENDIX: THE $^3P_0$ MODEL

The $^3P_0$ quark pair creation model [12,13,16,17,85] is used to calculate OZI allowed strong bottomonium decays. Given that details of the calculations such as phase conventions are important and not always clearly stated in the literature we summarize the details of the $^3P_0$ model to assist an interested reader in reproducing our results.

In the $^3P_0$ quark pair creation model [12,13,16,17,85], a $q\bar{q}$ pair is created from the vacuum in a $^3P_0$ state (the quantum numbers of the vacuum). The angular momentum and spin of the created $q\bar{q}$ pair are therefore $L_P = 1$, $S_P = 1$, and $J_P = 0$, so that $M_{L_P} = -M_{S_P} \equiv m$. The transition operator for $q\bar{q}$ pair creation can be written as

$$T = -3\gamma \sum_m \langle 11; m-m|00\rangle \sqrt{96\pi} \int d^3p_q d^3p_{\bar{q}} \delta^3(\vec{p}_q + \vec{p}_{\bar{q}}) \times \mathcal{Y}_{1m}\left(\frac{\vec{p}_q - \vec{p}_{\bar{q}}}{2}\right) \chi_{1-m} \phi_0 \omega_0 b_q^\dagger(\vec{p}_q) d_{\bar{q}}^\dagger(\vec{p}_{\bar{q}}) \quad \text{(A1)}$$

where $b_q^\dagger(\vec{p}_q)$ and $d_{\bar{q}}^\dagger(\vec{p}_{\bar{q}})$ are the creation operators for the quark and antiquark, respectively. The momenta of the created quark, $\vec{p}_q$, and the created antiquark, $\vec{p}_{\bar{q}}$, are integrated over all possible values, such that the delta function ensures that their total momentum is zero in their center-of-mass frame. The spin triplet state of the created $q\bar{q}$ pair is described by its spin wave function χ_{1-m} and the momentum-space distribution of the created pair is described by the solid harmonic, written in terms of the spherical harmonic as $\mathcal{Y}_{LM_L}(\vec{k}) \equiv |\vec{k}|^L Y_{LM_L}(\theta_k, \phi_k)$. The $SU(3)$ flavor singlet wave function of the created pair is $\phi_0 = \frac{1}{\sqrt{3}}(u\bar{u} + d\bar{d} + s\bar{s})$ and its color singlet wave function is ω_0. The overall factor of 3 in Eq. (A1) will cancel out when evaluating the color overlap. The factor of $\sqrt{96\pi}$ arises from the normalization and field theory conventions of Refs. [17,85,87]. The amplitude for quark-pair creation from the vacuum can therefore be described by a single free parameter, γ. Any differences in the constant factors that appear in Eq. (A1) simply result in a rescaling of the value of γ. For example, the value of γ used in Refs. [16,89] is larger than ours by a factor of $\sqrt{96\pi}$ due to the absence of this factor in their T operator.

The S-matrix for the meson strong decay $A \to BC$ is defined as

$$S \equiv I - 2\pi i \delta(E_f - E_i) T \quad \text{(A2)}$$

so that

$$\langle BC|T|A\rangle = \delta^3(\vec{p}_A - \vec{p}_B - \vec{p}_C) \mathcal{M}^{M_{J_A} M_{J_B} M_{J_C}} \quad \text{(A3)}$$

where, using the normalization from Refs. [17,85,87], the helicity amplitude is given by

$$\begin{aligned}\mathcal{M}^{M_{J_A} M_{J_B} M_{J_C}}(\vec{P}) = \gamma \sum & \langle L_A M_{L_A} S_A M_{S_A}|J_A M_{J_A}\rangle \langle L_B M_{L_B} S_B M_{S_B}|J_B M_{J_B}\rangle \langle L_C M_{L_C} S_C M_{S_C}|J_C M_{J_C}\rangle \\ & \times \langle 1m1-m|00\rangle \langle \chi^{14}_{S_B M_{S_B}} \chi^{32}_{S_C M_{S_C}} | \chi^{12}_{S_A M_{S_A}} \chi^{34}_{1-m}\rangle \\ & \times [\langle \phi_B^{14} \phi_C^{32}|\phi_A^{12}\phi_0^{34}\rangle I(\vec{P}, m_1, m_2, m_3) + (-1)^{1+S_A+S_B+S_C} \langle \phi_B^{32}\phi_C^{14}|\phi_A^{12}\phi_0^{34}\rangle I(-\vec{P}, m_2, m_1, m_3)] \end{aligned} \quad \text{(A4)}$$

where the sum is over $M_{L_A}, M_{S_A}, M_{L_B}, M_{S_B}, M_{L_C}, M_{S_C}$, and m. The two terms in the last factor correspond to the two possible diagrams. In the first diagram, quark 1 from meson A ends up in meson B and antiquark 2 from meson A ends up in meson C. In the second diagram, quark 1 from meson A ends up in meson C and antiquark 2 from meson A ends up in meson B. Indices 3 and 4 refer to the created quark and antiquark, respectively.

The momentum space integral for the first diagram is given by

$$I(\vec{P}, m_1, m_2, m_3) = \sqrt{96\pi} \int d^3p \mathcal{Y}_{1m}(\vec{p}) \psi_{n_A, L_A, M_{L_A}}(\vec{p} + \vec{P}) \psi^*_{n_B, L_B, M_{L_B}}\left(\vec{p} + \frac{m_3}{m_1 + m_3}\vec{P}\right) \psi^*_{n_C, L_C, M_{L_C}}\left(\vec{p} + \frac{m_3}{m_2 + m_3}\vec{P}\right) \quad \text{(A5)}$$

where m_1, m_2 and $m_3 = m_4$ are the constituent quark masses and we have taken $\vec{P} \equiv \vec{P}_B = -\vec{P}_C$ in the center-of-mass frame of A. To evaluate the spatial integral for the second diagram, we simply interchange $B \leftrightarrow C$, which amounts to making the replacement $m_1 \leftrightarrow m_2$ and $\vec{P} \to -\vec{P}$ in Eq. (A5), leading to the second term of Eq. (A4).

The techniques found in Appendix A of [103] were useful in simplifying and evaluating the spatial integrals. For the meson space wave functions, we use the momentum-space SHO wave functions, given by

$$\psi^{\rm SHO}_{nLM_L}(\vec{p}) = R^{\rm SHO}_{nL}(p) Y_{LM_L}(\theta_p, \phi_p) \quad \text{(A6)}$$

where the radial wave functions are given by

$$R^{\rm SHO}_{nL}(p) = \frac{(-1)^n(-i)^L}{\beta^{\frac{3}{2}}}\sqrt{\frac{2n}{\Gamma(n+L+\frac{3}{2})}} \times \left(\frac{p}{\beta}\right)^L L_n^{L+\frac{1}{2}}\left(\frac{p^2}{\beta^2}\right)e^{-p^2/(2\beta^2)} \quad \text{(A7)}$$

and $L_n^{L+\frac{1}{2}}(p^2/\beta^2)$ is an associated Laguerre polynomial. We use the SHO wave functions such that a meson with quantum numbers $n^{2S+1}L_J$ in spectroscopic notation uses $\psi^{\rm SHO}_{n-1,LM_L}$ for its momentum-space wave function. The values we use for the effective harmonic oscillator parameter, β, are listed in Tables I–III.

The color matrix element

$$\langle\omega_B^{14}\omega_C^{32}|\omega_A^{12}\omega_0^{34}\rangle = \langle\omega_B^{32}\omega_C^{14}|\omega_A^{12}\omega_0^{34}\rangle = \frac{1}{3} \quad \text{(A8)}$$

does not explicitly appear in Eq. (A4) since it cancels the overall factor of 3 from Eq. (A1).

The flavor matrix element can be easily found by writing the flavor wave functions of mesons A, B and C and that of the created quark pair as 5×5 matrices with rows indicating the quark flavor (u,d,s,c,b) and columns indicating the antiquark flavor $(\bar{u},\bar{d},\bar{s},\bar{c},\bar{b})$. For example, the flavor wave function for the created $q\bar{q}$ pair is

$$\phi_0 = \frac{1}{\sqrt{3}}(u\bar{u}+d\bar{d}+s\bar{s}) = \frac{1}{\sqrt{3}}\begin{pmatrix}1&0&0&0&0\\0&1&0&0&0\\0&0&1&0&0\\0&0&0&0&0\\0&0&0&0&0\end{pmatrix}. \quad \text{(A9)}$$

The flavor overlaps for each of the two terms in Eq. (A4) are therefore given by

$$\langle\phi_B^{14}\phi_C^{32}|\phi_A^{12}\phi_0^{34}\rangle = {\rm Tr}[\phi_A^\top\phi_B\phi_0^\top\phi_C] \quad \text{(A10)}$$

$$\langle\phi_B^{32}\phi_C^{14}|\phi_A^{12}\phi_0^{34}\rangle = {\rm Tr}[\phi_A^\top\phi_C\phi_0^\top\phi_B]. \quad \text{(A11)}$$

The spin matrix elements for the first and second diagrams are written in terms of the Wigner $9j$ symbols [104] as

$$\langle\chi^{14}_{S_BM_{S_B}}\chi^{32}_{S_CM_{S_C}}|\chi^{12}_{S_AM_{S_A}}\chi^{34}_{1-m}\rangle = (-1)^{1+S_C}\sqrt{3(2S_A+1)(2S_B+1)(2S_C+1)} \times\sum_{S,M_S}\langle S_BM_{S_B}S_CM_{S_C}|SM_S\rangle\langle S_AM_{S_A}1-m|SM_S\rangle\begin{Bmatrix}\frac{1}{2}&\frac{1}{2}&S_A\\\frac{1}{2}&\frac{1}{2}&1\\S_B&S_C&S\end{Bmatrix} \quad \text{(A12)}$$

$$\langle\chi^{32}_{S_BM_{S_B}}\chi^{14}_{S_CM_{S_C}}|\chi^{12}_{S_AM_{S_A}}\chi^{34}_{1-m}\rangle = (-1)^{1+S_A+S_B+S_C}\langle\chi^{14}_{S_BM_{S_B}}\chi^{32}_{S_CM_{S_C}}|\chi^{12}_{S_AM_{S_A}}\chi^{34}_{1-m}\rangle, \quad \text{(A13)}$$

where the spin matrix element for the second diagram was obtained using an alternative definition for the $9j$ symbols that couple the quarks differently [104]. This expression, given in Eq. (A13), was used to simplify Eq. (A4).

Using the Jacob-Wick formula [105,106], the helicity amplitudes $\mathcal{M}^{M_{J_A}M_{J_B}M_{J_C}}$, given by Eq. (A4), are converted to partial wave amplitudes $\mathcal{M}^{LS}$ via

$$\mathcal{M}^{LS}(P) = \frac{\sqrt{4\pi(2L+1)}}{2J_A+1}\sum_{M_{J_B},M_{J_C}}\langle L0SM_{J_A}|J_AM_{J_A}\rangle\langle J_BM_{J_B}J_CM_{J_C}|SM_{J_A}\rangle\mathcal{M}^{M_{J_A}M_{J_B}M_{J_C}}(P\hat{z})|_{M_{J_A}=M_{J_B}+M_{J_C}} \quad \text{(A14)}$$

where $\vec{S}=\vec{J}_B+\vec{J}_C$ and $\vec{J}_A=\vec{L}+\vec{S}$ such that

$$|J_B-J_C|\le S\le J_B+J_C \quad \text{(A15)}$$

$$|J_A-S|\le L\le J_A+S \quad \text{(A16)}$$

and the outgoing momentum of meson B, $\vec{P}\equiv P\hat{z}$, is chosen to lie along the $\hat{z}$-axis in the center-of-mass frame of meson A so that the helicities and angular momentum projections are related by $M_{J_B}=\lambda_B$, $M_{J_C}=-\lambda_C$ and $M_{J_A}=M_{J_B}+M_{J_C}=\lambda_B-\lambda_C$. This on-shell momentum is conveniently written in terms of the masses of mesons A, B and C as

$$P=\frac{\sqrt{[M_A^2-(M_B+M_C)^2][M_A^2-(M_B-M_C)^2]}}{2M_A}. \quad \text{(A17)}$$

Using relativistic phase space, as described in Refs. [16,85], the partial width for a given partial wave amplitude is given by

$$\Gamma^{LS} = 2\pi P \mathcal{S} \frac{E_B E_C}{M_A} |\mathcal{M}^{LS}|^2 \tag{A18}$$

where $E_B = \sqrt{M_B^2 + P^2}$, $E_C = \sqrt{M_C^2 + P^2}$, and $\mathcal{S}$ is a symmetry factor given by

$$\mathcal{S} = \frac{1}{1+\delta_{BC}} = \begin{cases} \frac{1}{2} & \text{if } B \text{ and } C \text{ are identical} \\ 1 & \text{otherwise} \end{cases}. \tag{A19}$$

Finally, the strong decay width for a given decay mode of meson A is just the sum of its partial widths:

$$\Gamma = \sum_{L,S} \Gamma^{LS}. \tag{A20}$$

The calculations of the strong decay widths, as outlined in this section, were performed using the Mathematica software package, version 7.0 [107].

[1] G. Aad *et al.* (ATLAS Collaboration), Observation of a New χ_b State in Radiative Transitions to $\Upsilon(1S)$ and $\Upsilon(2S)$ at ATLAS, Phys. Rev. Lett. **108**, 152001 (2012).

[2] A. Chisholm, Measurements of the χ_c and χ_b quarkonium states in pp collisions with the ATLAS experiment, Report No. CERN-THESIS-2014-071.

[3] A. G. Drutskoy, F.-K. Guo, F. J. Llanes-Estrada, A. V. Nefediev, and J. M. Torres-Rincon, Hadron physics potential of future high-luminosity B-factories at the $\Upsilon(5S)$ and above, Eur. Phys. J. A **49**, 7 (2013).

[4] R. Lewis and R. M. Woloshyn, Higher angular momentum states of bottomonium in lattice NRQCD, Phys. Rev. D **85**, 114509 (2012).

[5] R. Lewis and R. M. Woloshyn, Excited upsilon radiative decays, Phys. Rev. D **84**, 094501 (2011).

[6] R. Lewis and R. M. Woloshyn, More about excited bottomonium radiative decays, Phys. Rev. D **86**, 057501 (2012).

[7] R. J. Dowdall, C. T. H. Davies, T. Hammant, and R. R. Horgan (HPQCD Collaboration), Bottomonium hyperfine splittings from lattice nonrelativistic QCD including radiative and relativistic corrections, Phys. Rev. D **89**, 031502 (2014).

[8] N. Brambilla, S. Eidelman, B. K. Heltsley, R. Vogt, G. T. Bodwin, E. Eichten, A. D. Frawley, A. B. Meyer *et al.*, Heavy quarkonium: Progress, puzzles, and opportunities, Eur. Phys. J. C **71**, 1534 (2011).

[9] C. Patrignani, T. K. Pedlar, and J. L. Rosner, Recent results in bottomonium, Annu. Rev. Nucl. Part. Sci. **63**, 21 (2013).

[10] E. Eichten, S. Godfrey, H. Mahlke, and J. L. Rosner, Quarkonia and their transitions, Rev. Mod. Phys. **80**, 1161 (2008).

[11] S. Godfrey and N. Isgur, Mesons in a relativized quark model with chromodynamics, Phys. Rev. D **32**, 189 (1985).

[12] L. Micu, Decay rates of meson resonances in a quark model, Nucl. Phys. **B10**, 521 (1969).

[13] A. Le Yaouanc, L. Oliver, O. Pene, and J. C. Raynal, Naive quark pair creation model of strong interaction vertices, Phys. Rev. D **8**, 2223 (1973).

[14] T. Barnes and S. Godfrey, Charmonium options for the X(3872), Phys. Rev. D **69**, 054008 (2004).

[15] S. Godfrey, Testing the nature of the $D_{sJ}^*(2317)^+$ and $D_{sJ}(2463)^+$ states using radiative transitions, Phys. Lett. B **568**, 254 (2003).

[16] H. G. Blundell and S. Godfrey, The $\xi(2220)$ reexamined: Strong decays of the 1^3F_2 and 1^3F_4 $s\bar{s}$ mesons, Phys. Rev. D **53**, 3700 (1996).

[17] T. Barnes, S. Godfrey, and E. S. Swanson, Higher charmonia, Phys. Rev. D **72**, 054026 (2005).

[18] S. Godfrey and K. Moats, $D_{sJ}^*(2860)$ mesons as excited D-wave $c\bar{s}$ states, Phys. Rev. D **90**, 117501 (2014).

[19] S. Godfrey, High spin mesons in the quark model, Phys. Rev. D **31**, 2375 (1985).

[20] S. Godfrey and N. Isgur, Isospin violation in mesons and the constituent quark masses, Phys. Rev. D **34**, 899 (1986).

[21] S. Godfrey, Spectroscopy of B_c mesons in the relativized quark model, Phys. Rev. D **70**, 054017 (2004).

[22] S. Godfrey, Properties of the charmed P-wave mesons, Phys. Rev. D **72**, 054029 (2005).

[23] B. Aubert *et al.* (*BABAR* Collaboration), Observation of a Narrow Meson Decaying to $D_s^+\pi^0$ at a Mass of 2.32-GeV/c^2, Phys. Rev. Lett. **90**, 242001 (2003).

[24] D. Besson *et al.* (CLEO Collaboration), Observation of a narrow resonance of mass 2.46 GeV/c^2 decaying to $D_s^{*+}\pi^0$ and confirmation of the $D_{sJ}^*(2317)$ state, Phys. Rev. D **68**, 032002 (2003); **75**, 119908(E) (2007).

[25] P. Krokovny *et al.* (Belle Collaboration), Observation of the $D_{sJ}(2317)$ and $D_{sJ}(2457)$ in B Decays, Phys. Rev. Lett. **91**, 262002 (2003).

[26] S.-K. Choi *et al.* (Belle Collaboration), Observation of a Narrow Charmoniumlike State in Exclusive $B^\pm \to K^\pm\pi^+\pi^- J/\psi$ Decays, Phys. Rev. Lett. **91**, 262001 (2003).

[27] S. Godfrey and S. L. Olsen, The exotic XYZ charmonium-like mesons, Annu. Rev. Nucl. Part. Sci. **58**, 51 (2008).

[28] S. Godfrey, Topics in hadron spectroscopy in 2009, arXiv:0910.3409.

[29] E. Braaten, Theoretical interpretations of the XYZ mesons, arXiv:1310.1636.

[30] F. De Fazio, New spectroscopy of heavy mesons, *Proc. Sci.*, HQL2012 (2012) 001 [arXiv:1208.4206].

[31] E. J. Eichten, K. Lane, and C. Quigg, Charmonium levels near threshold and the narrow state $X(3872) \to \pi^+\pi^- J/\psi$, Phys. Rev. D **69**, 094019 (2004).

[32] K. A. Olive *et al.* (Particle Data Group Collaboration), Review of particle physics, Chin. Phys. C **38**, 090001 (2014).

[33] R. Aaij *et al.* (LHCb Collaboration), Measurement of the $\chi_b(3P)$ mass and of the relative rate of $\chi_{b1}(1P)$ and $\chi_{b2}(1P)$ production, J. High Energy Phys. 10 (2014) 88.

[34] R. Aaij *et al.* (LHCb Collaboration), Study of χ_b meson production in p p collisions at $\sqrt{s} = 7$ and 8 TeV and observation of the decay $\chi_b(3P) \to \Upsilon(3S)\gamma$, Eur. Phys. J. C **74**, 3092 (2014).

[35] W. Kwong and J. L. Rosner, D wave quarkonium levels of the upsilon family, Phys. Rev. D **38**, 279 (1988).

[36] P. del Amo Sanchez *et al.* (*BABAR* Collaboration), Observation of the $\Upsilon(1^3D_J)$ bottomonium state through decays to $\pi^+\pi^-\Upsilon(1S)$, Phys. Rev. D **82**, 111102 (2010).

[37] T. Skwarnicki, CLEO results on transitions in heavy quarkonia, arXiv:hep-ex/0505050.

[38] A. Grant and J. L. Rosner, Dipole transition matrix elements for systems with power law potentials, Phys. Rev. D **46**, 3862 (1992).

[39] S. Godfrey and J. L. Rosner, Production of the $\eta_b(\mathrm{nS})$ states, Phys. Rev. D **64**, 074011 (2001); **65**, 039901(E) (2002).

[40] B. Aubert *et al.* (*BABAR* Collaboration), Observation of the Bottomonium Ground State in the Decay $\Upsilon(3S) \to \gamma\eta_b$, Phys. Rev. Lett. **101**, 071801 (2008); **102**, 029901(E) (2009).

[41] V. A. Novikov, L. B. Okun, M. A. Shifman, A. I. Vainshtein, M. B. Voloshin, and V. I. Zakharov, Charmonium and gluons, Phys. Rep. **41**, 1 (1978).

[42] F. Daghighian and D. Silverman, Relativistic formulation of the radiative transitions of charmonium and b quarkonium, Phys. Rev. D **36**, 3401 (1987).

[43] J. Ferretti, G. Galat, and E. Santopinto, Quark structure of the $X(3872)$ and $\chi_b(3P)$ resonances, Phys. Rev. D **90**, 054010 (2014).

[44] D. Ebert, R. N. Faustov, and V. O. Galkin, Properties of heavy quarkonia and B_c mesons in the relativistic quark model, Phys. Rev. D **67**, 014027 (2003).

[45] T. Wei-Zhao, C. Lu, Y. You-Chang, and C. Hong, Bottomonium states versus recent experimental observations in the QCD-inspired potential model, Chin. Phys. C **37**, 083101 (2013).

[46] A. Pineda and J. Segovia, Improved determination of heavy quarkonium magnetic dipole transitions in potential nonrelativistic QCD, Phys. Rev. D **87**, 074024 (2013).

[47] T. Appelquist and H. D. Politzer, Heavy Quarks and e^+e^- Annihilation, Phys. Rev. Lett. **34**, 43 (1975).

[48] A. DeRujula and S. L. Glashow, Is Bound Charm Found? Phys. Rev. Lett. **34**, 46 (1975).

[49] M. Chanowitz, Comment on the decay of $\psi(3.1)$ into even-G- parity states, Phys. Rev. D **12**, 918 (1975).

[50] R. Barbieri, R. Gatto, and R. Kögerler, Calculation of the annihilation rate of P wave quark-antiquark bound states, Phys. Lett. **60B**, 183 (1976).

[51] R. Barbieri, R. Gatto, and E. Remiddi, Singular binding dependence in the hadronic widths of 1^{++} and 1^{+-} heavy quark antiquark bound states, Phys. Lett. **61B**, 465 (1976).

[52] R. Barbieri, G. Curci, E. d'Emilio, and E. Remiddi, Strong radiative corrections to annihilations of quarkonia in QCD, Nucl. Phys. **B154**, 535 (1979).

[53] W. Kwong, P. B. Mackenzie, R. Rosenfeld, and J. L. Rosner, Quarkonium annihilation rates, Phys. Rev. D **37**, 3210 (1988).

[54] E. S. Ackleh and T. Barnes, Two photon widths of singlet positronium and quarkonium with arbitrary total angular momentum, Phys. Rev. D **45**, 232 (1992).

[55] E. S. Ackleh, T. Barnes, and F. E. Close, Two photon helicity selection rules and widths for positronium and quarkonium states with arbitrary angular momenta, Phys. Rev. D **46**, 2257 (1992).

[56] G. Belanger and P. Moxhay, Three gluon annihilation of D wave quarkonium, Phys. Lett. B **199**, 575 (1987).

[57] L. Bergström and P. Ernström, Decays of D-wave quarkonium states into ggg and γgg, Phys. Lett. B **267**, 111 (1991).

[58] R. W. Robinett and L. Weinkauf, Covariant formalism for F-wave quarkonium production and annihilation: Application to ${}^3F_J \to gg$ decays, Phys. Rev. D **46**, 3832 (1992).

[59] A. Bradley and A. Khare, QCD correction to the leptonic decay rate of D wave vector mesons, Z. Phys. C **8**, 131 (1981).

[60] T. M. Yan, Hadronic transitions between heavy quark states in quantum chromodynamics, Phys. Rev. D **22**, 1652 (1980).

[61] Y. P. Kuang and T. M. Yan, Predictions for hadronic transitions in the $b\bar{b}$ system, Phys. Rev. D **24**, 2874 (1981).

[62] Y. P. Kuang, S. F. Tuan, and T. M. Yan, Hadronic transitions and ${}^1P_1$ states of heavy quarkonia, Phys. Rev. D **37**, 1210 (1988).

[63] Y. P. Kuang and T. M. Yan, Hadronic transitions of D wave quarkonium and $\Psi(3770) \to J/\Psi\pi\pi$, Phys. Rev. D **41**, 155 (1990).

[64] J. L. Rosner, Prospects for detection of $\Upsilon(1D) \to \Upsilon(1S)\pi\pi$ via $\Upsilon(3S) \to \Upsilon(1D) + X$, Phys. Rev. D **67**, 097504 (2003).

[65] M. B. Voloshin and V. I. Zakharov, Measuring Quantum-Chromodynamic Anomalies in Hadronic Transitions between Quarkonium States, Phys. Rev. Lett. **45**, 688 (1980).

[66] V. A. Novikov and M. A. Shifman, Comment on the $\psi' \to J/\psi\pi\pi$ decay, Z. Phys. C **8**, 43 (1981).

[67] B. L. Ioffe and M. A. Shifman, The decays $\psi';' \to J/\psi + \pi^0(\eta)$ and quark masses, Phys. Lett. **95B**, 99 (1980).

[68] M. B. Voloshin, Yad. Fiz. **43**, 1571 (1986) [Hadronic transitions from $\Upsilon(3S)$ to 1 P wave singlet bottomonium level, Sov. J. Nucl. Phys. **43**, 1011 (1986)].

[69] M. B. Voloshin, The enhancement of the decay $\Upsilon(1D) \to \eta\Upsilon(1S)$ by the axial anomaly in QCD, Phys. Lett. B **562**, 68 (2003).

[70] P. Ko, Search for η_c' and $h_c({}^1P_1)$ states in the e^+e^- annihilations, Phys. Rev. D **52**, 1710 (1995).

[71] P. Moxhay, Hadronic transitions of D-wave quarkonium, Phys. Rev. D **37**, 2557 (1988).

[72] P. Ko, On the branching ratio of $\Upsilon(1D) \to \Upsilon(1S)\pi\pi$, Phys. Rev. D **47**, 208 (1993).

[73] Y. P. Kuang, QCD multipole expansion and hadronic transitions in heavy quarkonium systems, Front. Phys. China **1**, 19 (2006).
[74] S. Godfrey and J. L. Rosner, Production of singlet P wave $c\bar{c}$ and $b\bar{b}$ states, Phys. Rev. D **66**, 014012 (2002).
[75] J. L. Rosner *et al.* (CLEO Collaboration), Observation of $h_c(^1P_1)$ State of Charmonium, Phys. Rev. Lett. **95**, 102003 (2005).
[76] P. Rubin *et al.* (CLEO Collaboration), Observation of the $^1P_1$ state of charmonium, Phys. Rev. D **72**, 092004 (2005).
[77] J. P. Lees *et al.* (*BABAR* Collaboration), Evidence for the $h_b(1P)$ meson in the decay $\Upsilon(3S) \to \pi^0 h_b(1P)$, Phys. Rev. D **84**, 091101 (2011).
[78] H. Severini *et al.* (CLEO Collaboration), Observation of the Hadronic Transitions $\chi_{b1,2}(2P) \to \omega\Upsilon(1S)$, Phys. Rev. Lett. **92**, 222002 (2004).
[79] E. J. Eichten and C. Quigg, Mesons with beauty and charm: Spectroscopy, Phys. Rev. D **49**, 5845 (1994).
[80] K. Chen *et al.* (Belle Collaboration), Observation of Anomalous $\Upsilon(1S)\pi^+\pi^-$ and $\Upsilon(2S)\pi^+\pi^-$ Production near the $\Upsilon(5S)$ Resonance, Phys. Rev. Lett. **100**, 112001 (2008).
[81] J. Segovia, D. R. Entem, and F. Fernandez, Puzzles in hadronic transitions of heavy quarkonium with two pion emission, Phys. Rev. D **91**, 014002 (2015).
[82] A. Ali, C. Hambrock, and M. J. Aslam, A Tetraquark Interpretation of the BELLE Data on the Anomalous $\Upsilon(1S)\pi^+\pi^-$ and $\Upsilon(2S)\pi^+\pi^-$ Production near the $\Upsilon(5S)$ Resonance, Phys. Rev. Lett. **104**, 162001 (2010); **107**, 049903 (2011).
[83] A. Ali, C. Hambrock, and S. Mishima, Tetraquark-Based Analysis and Predictions of the Cross Sections and Distributions for the Processes $e^+e^- \to \Upsilon(1S)(\pi^+\pi^-, K^+K^-, \eta\pi^0)$ near $\Upsilon(5S)$, Phys. Rev. Lett. **106**, 092002 (2011).
[84] D. Y. Chen, J. He, X. Q. Li, and X. Liu, Dipion invariant mass distribution of the anomalous $\Upsilon(1S)\pi^+\pi^-$ and $\Upsilon(2S)\pi^+\pi^-$ production near the peak of $\Upsilon(10860)$, Phys. Rev. D **84**, 074006 (2011).
[85] E. S. Ackleh, T. Barnes, and E. S. Swanson, On the mechanism of open-flavor strong decays, Phys. Rev. D **54**, 6811 (1996).
[86] J. Ferretti and E. Santopinto, Higher mass bottomonia, Phys. Rev. D **90**, 094022 (2014).
[87] J. Segovia, D. R. Entem, and E. Fernandez, Scaling of the $^3P_0$ strength in heavy meson decays, Phys. Lett. B **715**, 322 (2012).
[88] D. Ebert, R. N. Faustov, and V. O. Galkin, Strong decays of vector mesons to pseudoscalar mesons in the relativistic quark model, Phys. Lett. B **744**, 1 (2015).
[89] H. G. Blundell, Meson properties in the quark model: A look at some outstanding problems, arXiv:hep-ph/9608473.
[90] F. E. Close and E. S. Swanson, Dynamics and decay of heavy-light hadrons, Phys. Rev. D **72**, 094004 (2005).
[91] G. T. Bodwin, E. Braaten, and G. P. Lepage, Rigorous QCD analysis of inclusive annihilation and production of heavy quarkonium, Phys. Rev. D **51**, 1125 (1995); **55**, 5853(E) (1997).
[92] A. K. Likhoded, A. V. Luchinsky, and S. V. Poslavsky, Production of χ_b-mesons at LHC, Phys. Rev. D **86**, 074027 (2012).
[93] H. Han, Y. Q. Ma, C. Meng, H. S. Shao, Y. J. Zhang, and K. T. Chao, $\Upsilon(nS)$ and $\chi_b(nP)$ production at hadron colliders in nonrelativistic QCD, arXiv:1410.8537.
[94] A. Ali, C. Hambrock, and W. Wang, Hadroproduction of $\Upsilon(nS)$ above $B\bar{B}$ thresholds and implications for $Y_b(10890)$, Phys. Rev. D **88**, 054026 (2013).
[95] G. Aad *et al.* (ATLAS Collaboration), Measurement of upsilon production in 7 TeV pp collisions at ATLAS, Phys. Rev. D **87**, 052004 (2013).
[96] S. Chatrchyan *et al.* (CMS Collaboration), Measurement of the $\Upsilon(1S)$, $\Upsilon(2S)$, and $\Upsilon(3S)$ cross sections in pp collisions at $\sqrt{s} = 7$ TeV, Phys. Lett. B **727**, 101 (2013).
[97] I. Adachi *et al.* (Belle Collaboration), First Observation of the P-wave Spin-Singlet Bottomonium States $h_b(1P)$ and $h_b(2P)$, Phys. Rev. Lett. **108**, 032001 (2012).
[98] G. Bonvicini *et al.* (CLEO Collaboration), First observation of a $\Upsilon(1D)$ state, Phys. Rev. D **70**, 032001 (2004).
[99] S. Godfrey and J. L. Rosner, Production of the D wave $b\bar{b}$ states, Phys. Rev. D **64**, 097501 (2001); **66**, 059902(E) (2002).
[100] J. P. Lees *et al.* (*BABAR* Collaboration), Bottomonium spectroscopy and radiative transitions involving the $\chi_{bJ}(1P, 2P)$ states at *BABAR*, Phys. Rev. D **90**, 112010 (2014).
[101] V. M. Abazov *et al.* (D0 Collaboration), Observation of a narrow mass state decaying into $\Upsilon(1S) + \gamma$ in $p\bar{p}$ collisions at $\sqrt{s} = 1.96$ TeV, Phys. Rev. D **86**, 031103 (2012).
[102] A. J. Bevan *et al.* (*BABAR* and Belle Collaborations), The physics of the B factories, Eur. Phys. J. C **74**, 3026 (2014).
[103] W. Roberts and B. Silvestre-Brac, General method of calculation of any hadronic decay in the $^3P_0$ model, Few-Body Syst. **11**, 171 (1992).
[104] A. de-Shalit and I. Talmi, *Nuclear Shell Theory* (Academic Press, New York, 1963).
[105] M. Jacob and G. C. Wick, On the general theory of collisions for particles with spin, Ann. Phys. (N.Y.) **7**, 404 (1959).
[106] J. D. Richman, An experimenter's guide to the helicity formalism, Technical Note CALT-68-1148, California Institute of Technology, 1984.
[107] Wolfram Research, Inc., Mathematica, Version 7.0, Wolfram Research, Inc., Champaign, Illinois, 2007.